Title

Phospholipid lateral diffusion in model membranes investigated with nuclear spin-lattice relaxation in the rotating frame

Author

Fisher, Ross W.

Publication Date

1979

Peer reviewed|Thesis/dissertation

PHOSPHOLIPID LATERAL DIFFUSION IN MODEL MEMBRANES INVESTIGATED WITH NUCLEAR SPIN-LATTICE RELAXATION IN THE ROTATING FRAME

by

Ross W. Fisher

B.S., University of California Berkeley 1974

DISSERTATION

Submitted in partial satisfaction of the requirements for the degree of

DOCTOR OF PHILOSOPHY

in

PHARMACEUTICAL CHEMISTRY

in the

GRADUATE DIVISION

of the

UNIVERSITY OF CALIFORNIA

San Francisco

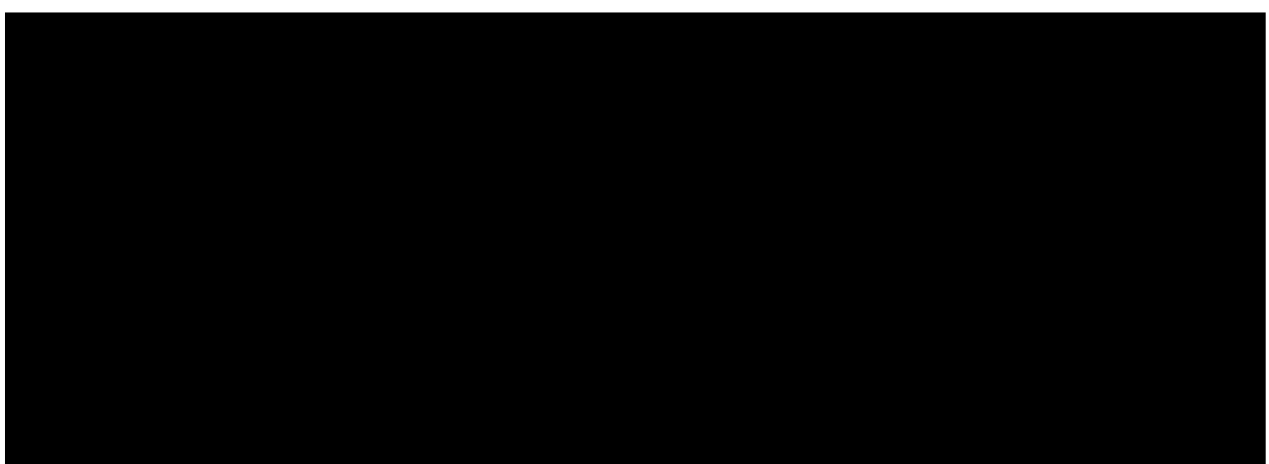

Date University Librarian

Degree Conferred: APR 1 1979

ACKNOWLEDGEMENTS

I would like to express my deepest appreciation to Dr. T. L. James for his supervision, friendship and guidance in helping me design a challenging and exciting problem, and to Dr. G. B. Matson for his time and effort spent helping with the design and modification of the instrumentation.

I also wish to thank my wife Judith for her support and patience and my parents for their constant interest throughout this work. These factors have been important to me.

My gratitude is extended to Alan Deese and Dr. E. A. Dratz at the University of California, Santa Cruz for their time, effort and generosity in providing the retinal rod outer segment membranes and lipids extracted from these membranes for the biomembrane experiments done in this work.

I am also endebted to Ms. Maureen Fowler for the excellent illustrations she made for this dissertation.

ABSTRACT

A novel proton nuclear magnetic resonance (NMR) investigation of molecular dynamics within phospholipid model membranes is described. The radiofrequency dependence of the rotating frame nuclear spin-lattice relaxation rate ($1/T_{1\rho}^{-1}$) is utilized for the direct determination of the lateral diffusion coefficient (D, cm^2/sec) of phospholipids in model membrane systems. Preliminary results from a study of diffusion in a biomembrane (retinal rod outer segment (ROS) membranes) using this unique method are also reported.

It has been shown that a frequency dependence of the spin-lattice relaxation rate, T_1^{-1} in the Zeeman field and $T_{1\rho}^{-1}$ in the rotating frame, arises when dipolar intermolecular interactions due to the relative translation of the spins on adjacent molecules provide the predominant mechanism promoting relaxation. With the theory of intermolecular relaxation due to translational diffusion, it is possible to use the dependence of the experimentally determined rotating frame relaxation rate $1/T_{1\rho}$ on the rotating frame angular frequency (ω_1) to calculate directly the lateral diffusion coefficient as a quantitative parameter of phospholipid translational mobility. This approach offers advantages

lacking in the techniques previously applied to the study of diffusion in model and biomembrane systems, as it employs the spins of the molecules studied as intrinsic probes and it alleviates the need for estimates of correlation times and molecular geometries in the calculation of the diffusion coefficient.

Experiments based on the temperature and frequency dependence of $1/T_{1\rho}$ as well as partial substitution with perdeuterated phospholipids indicate that intermolecular dipolar relaxation is indeed significant for the phospholipid systems. A linear dependence of $1/T_{1\rho}$ on the square root of the applied radiofrequency ($\omega_1^{1/2}$) was observed for the systems under consideration. The spin-locking pulsed NMR experiment was employed to measure the rotating frame spin-lattice relaxation rate for a variety of unsonicated phospholipid-D_2O multilamellar dispersions. The effects of such factors as phospholipid-to-D_2O ratio (concentration effects), phospholipid hydrocarbon chain length, phospholipid polar headgroup composition, and the presence of unsaturation in the hydrocarbon chains on molecular dynamics were investigated. Another advantage of this novel technique for studying phospholipid diffusion is demonstrated by the results for diffusion in phospholipid bilayers below the gel-to-liquid crystalline phase transition temperature indicating that its capabilities extend into the gel phase without the severe problems associated with the conventional magnetic resonance techniques. The potential applicability

of this method to biomembrane systems is illustrated by the results derived from a study of diffusion in the ROS membranes and lipids extracted from these membranes.

In addition to the experimental results of this valuable new approach to diffusion studies is a discussion of some of the instrumentation. A description of the NMR probe designed for these experiments is given and the modification of the Spin-Lock CPS-2 pulsed NMR spectrometer is discussed.

TABLE OF CONTENTS

LIST OF FIGURES

LIST OF TABLES

ABBREVIATIONS AND TERMINOLOGY

NMR	nuclear magnetic resonance
ESR	electron spin resonance
PFGSE	pulsed field gradient spin echo
DLPC	dilauroylphosphatidylcholine
DMPC	dimyristoylphosphatidylcholine
DPPC	dipalmitoylphosphatidylcholine
DSPC	distearoylphosphatidylcholine
DOPC	dioleoylphosphatidylcholine
DPPE	dipalmitoylphosphatidylethanolamine
PE	phosphatidylehtanolamine
DPC	didihydrosterculoylphosphatidylcholine
EYL	egg yolk lecithin
ROS	(retinal) rod outer segment
T_C	Chapman or gel-to-liquid crystalline phase transition temperature
H_o	applied dc magnetic field (gauss)
H_1	rotating frame (spin-locking) field (gauss)
H_{loc}	local dipolar field
ω	"omega"
ω_o	Larmor precession frequency (rad/sec)
ω_1	rotating frame angular frequency (rad/sec)
γ	"gamma" proton gyromagnetic ratio
N	resonant spin density (spins/cc)
π	"pi"
$\hbar$	Planck's constant divided by 2π

σ	"sigma" closest approach distance for adjacent molecules
T_1	longitudinal or spin-lattice relaxation time
T_2	transverse or spin-spin relaxation time
$T_{1\rho}$	rotating frame spin-lattice relaxation time
ρ	"rho"
τ, τ_j	"tau" correlation time, time between diffusive jumps
ν_j	"nu" diffusive jump frequency
Ω	"large omega" ohms
VIM	vector impedance meter
$\langle r^2 \rangle$	root mean squared jump distance

---

gel phase The phase in a lyotropic (water containing) phospholipid system, below the temperature at which the mesomorphic or liquid crystalline mesophase is initiated (see section 1 in Chapter 2).

CHAPTER 1

PHOSPHOLIPID MODEL MEMBRANE SYSTEMS

1.1. Introduction.

During the 1970's we have witnessed a vast increase of knowledge in the field of membrane biology and chemistry. The primary motivation behind these developments is the underlying importance of the various cell membranes and their components in biomedical research and in the practice of medicine. The specific requirements imposed upon membranes by the variety of tissues in an organism are reflected in the tremendous variation in membrane complexity. However, in spite of this diversity, nearly all membranes maintain fundamental similarities in basic structure and function. Membranes play the role of a barrier, allowing the compartmentalization necessary for physical separation of the many processes which concertedly work together as the biochemical basis of life. Not only is the membrane a barrier, but it is also an architectural framework housing the many valves, gates and switches responsible for controlling the environments adjacent to this barrier. The membrane as the "architectural framework" is not necessarily passive, as its dynamic nature may influence or be

influenced by the "devices" it houses. Alterations in cellular or extracellular conditions may change the physical state of the membrane which, consequently, may effect some change in one or more of the "devices" embedded in it; or the membrane may undergo some change in response to the activation or deactivation of one of these specialized "devices". Therefore, understanding the structural and functional integrity of membranes should provide insight into homeostatic mechanisms.

1.2. The fluid mosaic membrane model.

As early as 1925 information was obtained regarding the structuring of membrane lipids. Gorter and Grendel's (1) surface area experiments implied that the lipids of the erythrocyte membrane most likely exist as a bilayer. Since that time, the concept of the basic membrane structure existing predominantly as a phospholipid bilayer has gained acceptance as an experimentally proven hypothesis. The generally accepted picture is that the lipid chains of opposing monolayers of the amphipathic phospholipid molecules form a non-polar hydrophobic "core" region within the bilayer between the polar hydrophilic "headgroup" regions on either side of the hydrocarbon core. Despite advances in characterization of the structural features in membranes, the clarity of the membrane picture is clouded by the variety of components constituting the system and all of their ensuing

interactions.

Proteins, the second major component of membranes, are believed to be primarily responsible for membrane function (acting as the valves, gates and switches mentioned previously). Membrane structure and the protein-lipid interactions have attracted considerable research interest. Models of how the membrane proteins are integrated into the bilayer's phospholipid framework have been hypothesized by Davson and Danielli (2) and by Singer and Nicolson (3). Protein components are known to be submerged either wholly or in part (similar to an iceberg) in the phospholipid matrix. Hydrophobic regions of the protein are associated with the bilayer's hydrocarbon core while hydrophilic regions could be found extending into the cytoplasmic reaches or extracellular space around the membrane. Figure 1-1 depicts this generally accepted fluid mosaic model for biological membranes. The many membrane events of physical and biochemical significance spawned by this fluid mosaic model include the potential for lateral phase separations (lipid clustering), clustering of functionally related proteins, and transmission of information <u>via</u> the lateral motion of other components on the membrane surface (as in the case of chemotaxis and cell recognition).

A simplified description of the biological membrane system such as this is rather deceiving since every aspect of the system (composition, structure, interaction of its

FIGURE 1-1

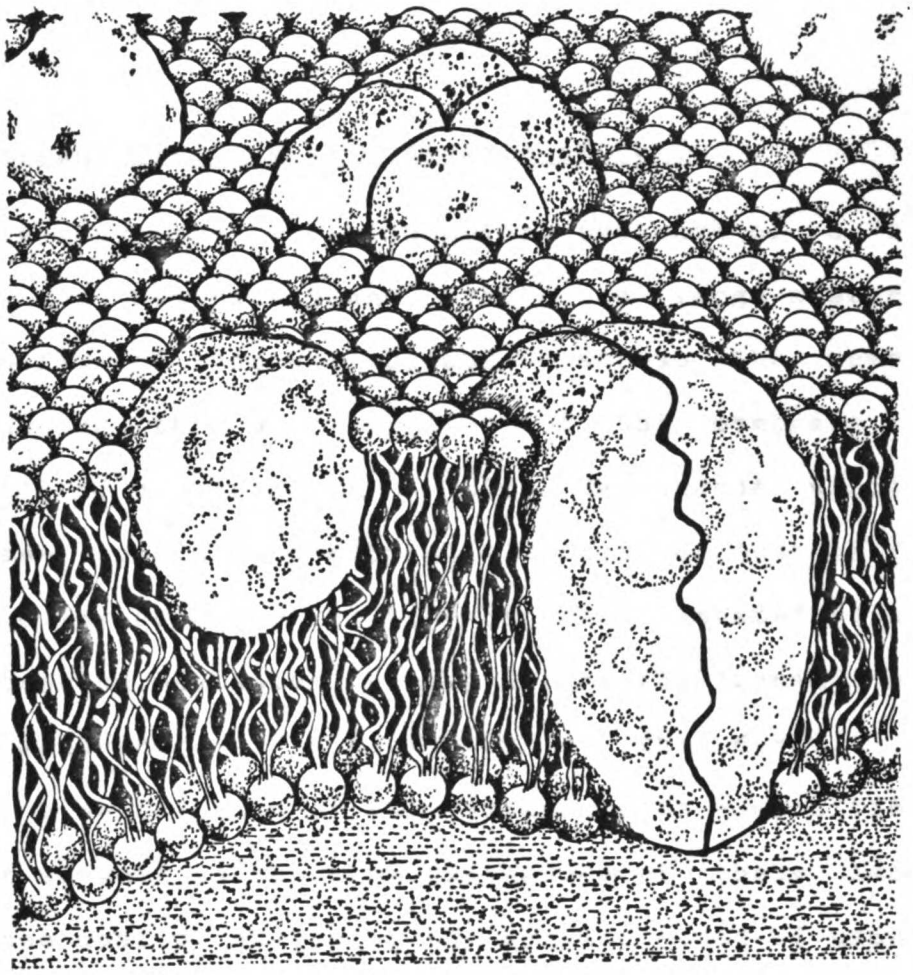

Figure 1-1: An artistic depiction of the fluid mosaic model of a membrane, consisting of a fluid hydrocarbon core sandwiched between the polar headgroup layers with the proteins either partially or wholly emersed in the phospholipid matrix. Redrawn from Cell Membranes (4).

own components, interaction of the membrane with its environment and the effects of physicochemical parameters on the membrane system) still has many features which remain elusive.

1.3. Membrane fluidity and 'dynamic state'.

While many important biochemical pathways of a living organism are membrane-bound events, a large number also require a flux of ions and molecules across the membrane. In discussing the participation of the membrane in the maintenance of homeostasis, a time dependence associated with these specialized molecular activities must be found. Just as we may describe the time-dependent "state" of a system in quantum mechanics, we may define the "dynamic state" of the membrane. A description of the dynamic state includes a description of the instantaneous composition and structure as well as the time dependence of these factors. Towards the goal of analyzing the dynamic state of membranes comprehensively, appropriate observables must be found. In biochemical or functional terms, observables may include specific activities of membrane components (e.g., enzymes, receptors, etc.), membrane surface potentials, or chemical gradients across a membrane. In physical chemical terms, there are observables such as phase transition temperature[1] or solubility of membrane-soluble agents. Membrane

[1] See chapter 2.

fluidity, another variable, is a descriptive term which is found in the literature. However, no experiment exists in which the value of "F" (the fictitious fluidity factor) may be determined. Fluidity is a contrived or hypothetical observable whose origin is in molecular dynamics. Within molecular dynamics, however, experimental techniques are capable of measuring a number of observables related to fluidity. The sum of the many molecular and sub-molecular motions are ultimately responsible for the fluidity of a membrane, where each particular type of motion may be assigned some observable. The lateral self-diffusion coefficient (D, cm^2/sec) is one such dynamic parameter which is understood to represent the lateral mobility of a molecule parallel to the plane of a membrane's surface. In an attempt to gain more insight into the dynamic state of the membrane system, it is the goal of this work to investigate the lateral diffusion coefficient of phospholipid molecules in model membrane systems and in a biological membrane.

The remainder of this introductory chapter serves two purposes. The first is to justify the use of model membrane systems for subsequent experiments, and the second is to illustrate the particular applicability of the new technique we have employed for determining diffusion coefficients for improving our understanding of the dynamic state of membranes.

1.4. Model vs biomembranes.

To justify employing model membrane systems in the primal stages of work intended to explore the physics and biochemistry of natural membrane systems, a logical course is to compare factors relating to the dynamic state of both the model and biomembranes. X-ray diffraction studies, analysis of neutron scattering data and differential scanning calorimetric experiments on aqueous lecithin and natural membrane dispersions have provided excellent evidence supporting the structural and organizational theories that phospholipids form the lamellar framework of membranes[2]. The organization of hydrated egg yoke lecithin (EYL) and an EYL/cholesterol mixture in the characteristic lamellar structure consisting of a hydrocarbon core between the polar headgroup regions of these molecular sandwiches is demonstrated in Figure 1-2 as electron density profiles obtained from X-ray diffraction experiments (5). Furthermore, X-ray diffraction data show that within this hydrocarbon core corresponding to the low central regions in Figure 1-2, the motional freedom over all of the chains is somewhat constrained presumably due to molecular packing restrictions. That the order towards the terminal methyl group is affected greatly by the presence of cholesterol is made apparent by inspection of Figure 1-2. In a similar study, Wilkins *et al* (6) using *Mycoplasma laidlawii* membranes,

---

[2] A discussion of the physical properties of liquid crystals as they pertain to membranes is found in Chapter 2, Section 1.

FIGURE 1-2

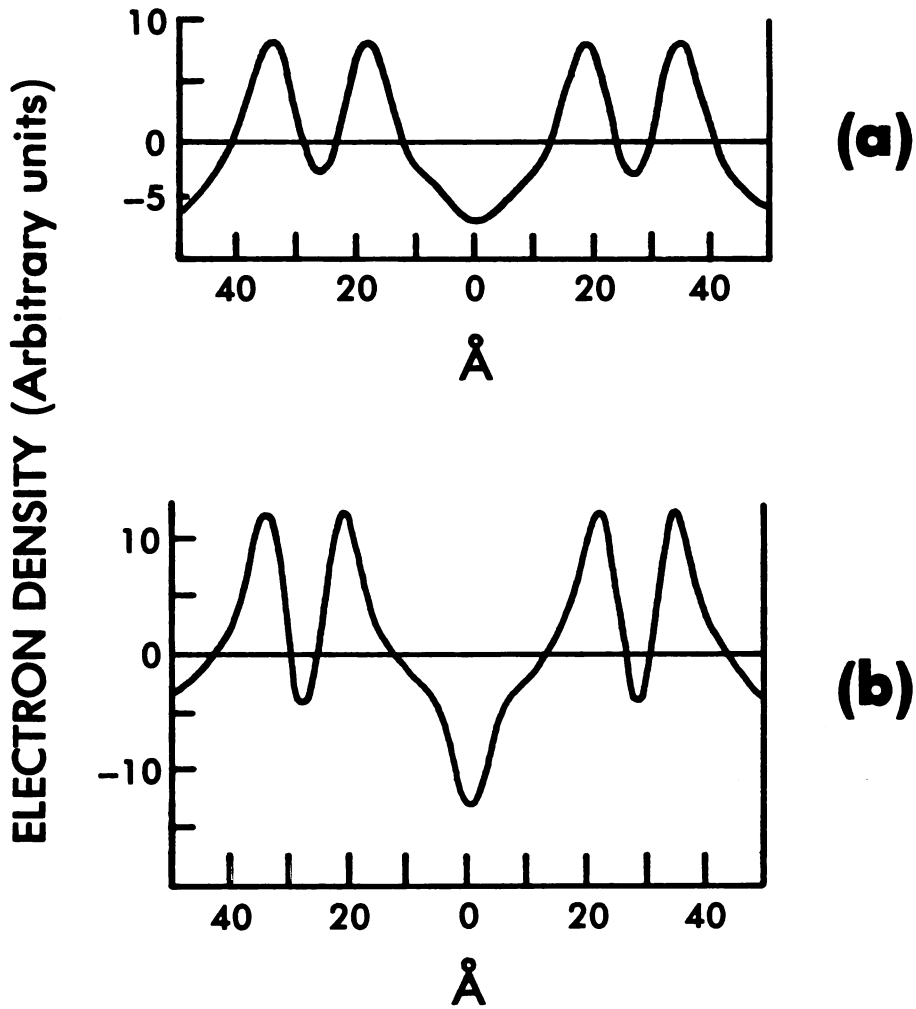

Figure 1-2: Electron density profiles as synthesized from the X-ray diffraction data of Levine and Wilkins (5): (a) EYL, 21% water; (b) EYL/cholesterol, 22% water.

hemoglobin-free erythrocyte ghosts, nerve-ending plasma membranes and Escherichia coli plasma membranes found the X-ray diffraction bands in accord with the earlier simple bilayer results, providing further evidence that the biomembrane includes the elementary bilayer structure as determined in the case of synthetic lipid systems.

Additional support for a lamellar structure of the lipid molecules for both model systems and biological membranes is found in the neutron scattering experiments reported by Schoenborn (7,8). Neutron scattering appears to be a useful approach to the study of these membrane systems (except for the scarcity of available equipment and limitations in the magnitude in the energy flux available for the experiment). Because the phenomenon is due to nuclear factors and is not electronic in nature, large differences arise in the relative scattering parameters for different nuclei, even for isotopes of a given nucleus. Either by substituting deuterium for hydrogen in a membrane lipid molecule, or by varying the ratio of heavy to normal water, assignment of densities in terms of the spatial arrangement of nuclei within the bilayer is permitted. Dipalmitoyl lecithin (DPPC) in DPPC/cholesterol systems was examined in this manner, yielding calculated density results in excellent agreement with Figure 1-2, giving an even better resolution of the water layer between the polar headgroups of adjacent bilayers (7,8). This method will certainly become of more interest as the protein component in membranes is

studied, for it will allow resolution of small areas with differing densities such as the lipid region surrounding a protein.

The differential scanning calorimetric experiments of Reinert and Steim (9) on the viable organism Mycoplasma laidlawii show a phase transition which is matched in temperature range and endothermicity for both the whole membranes extracted from this system and the lipids extracted from these membranes. Except for a transition due to protein denaturation, all the observed transitions were reversible and reproducible as is true for artificial bilayer systems. The cells were cultured on a substrate such that about 70% of the membranes lipids' fatty acid content was palmitate. Therefore the coincidence of the endothermic transition with the known transition for phospholipid systems composed of DPPC lamellar systems is excellent evidence for the existence of lamellar structure in the biological membrane system. Enthalpies associated with the phase transition for the lipids of whole membranes and for the extracted lipids (i.e., in the absence of protein) were found to be very similar (ratio = 0.9 ± 0.1) adding more credance to the argument that a lamellar bilayer forms the structural basis for biomembranes as well as model membrane systems.

Spectral parameters from electron spin resonance (ESR) experiments are sensitive to the environmental effects on an electron spin's motion in a spin-labeled molecule used as a

probe in a sample membrane system. Results of ESR experiments in which lecithin molecules labeled at various positions along the fatty acid lipid chain with N-oxyl-4',4'-dimethyloxazolidine as a paramagnetic probe were incorporated in aqueous lecithin model membrane dispersions have been interpreted as arising from rapid anisotropic motions of this probe due to the anisotropic intra-chain reorientations along the fatty-acyl chains of the lecithin molecules in the bilayer (10). Order parameters, calculated from the ESR spectra, decrease as the label's position on the chain approaches the methyl terminus and, therefore, the center of the bilayer. They further report analogous trends in the order parameter for spin-labeled fatty acids incorporated in the membrane of unmyelinated walking leg axon nerve fiber of Homarus americanus (Maine lobster), again indicating the illustrative role of the model system. The data is certainly in accord with the following profile of membranes: a fluid-like hydrocarbon core with increasing motional freedom towards the terminal methyl groups at the center of the bilayer. It is apparent that the similarities in the structural aspects of the model and biomembranes' dynamic state are well founded in that the results of all the above experiments are mirrored in each type of membrane system considered.

Allied with the architectural foundation of membranes is the composition of the membranes. In fact, the integrity and capacity of a membrane to perform its specific function

or functions are reflected by the quantity and particular assortment of molecular species present. For example, the myelin membrane of nerves is primarily an insulator which is reflected in the small protein-to-lipid ratio. Mitochondrial inner membrane, where biochemical events intimately involved with respiration are the main function, has a large protein-to-lipid ratio with a large variety of proteins (11). Grouping the membranes' components into only two categories (i.e., protein or lipid) imposes only a superficial view as to how the molecular content of a membrane and the resulting specialization of that membrane are connected with its dynamic state. The diversity in protein and lipid molecules found in membranes is considerable as must be the effects each has on the dynamic state.

Alterations in physicochemical and biophysical properities are now considered when the membrane is altered or subjected to abnormal physical stress. Permeability, involving the passive diffusion of a substance across a barrier, will undoubtedly be sensitive to the internal dynamic state of the barrier. De Gier et al (12) studied the temperature dependence of the permeability to glycerol and erythritol of liposomes whose phospholipid composition was varied in chain length, presence and quantity of chain unsaturation, chain composition within one phospholipid molecule, and presence of cholesterol. Their experiments revealed that those factors which resulted in increased membrane fluidity also resulted in increased permeability, in accord with earlier

results from studies on the temperature dependence of the permeability of erythrocyte ghosts to nonelectrolytes.

Anesthesia, in all probability, is attributable to the membrane bilayer's hydrocarbon core playing host to a variety of small lipid soluble molecules and the subsequently redefined dynamic state within the membrane. Exactly how anesthetic-mediated effects relate to the various surgical planes of anesthesia remains to be answered unequivocally. However, the alterations of a membrane's normal state, while under the influence of an anesthetic agent, provide insight into the dynamic state of a membrane system by virtue of the comparable effects produced and observed in model and natural membrane systems. Several instances follow in which parallel experiments have been performed on natural and model membranes which support the model membrane's reliability as a predictive system.

Bilayers in dimyristoyl lecithin (DMPC) and DPPC vesicles were shown to undergo physical changes, the rate of molecular diffusion in the bilayer increasing (presumably due to decreases in the phase transition temperature) when some lipid-soluble general anesthetic molecules were introduced into the system (13). Proton nuclear magnetic resonance (NMR) studies showed an increased lipid resonance intensity which was interpreted to be caused by a lowering of the phase transition temperature leading to a greater amount of motionally unrestricted lipid. Diffusion rates determined using fluorescence decay experiments with

fluorescent probes in the bilayer, indicated a more rapid diffusion in the presence of anesthetic. Samples derived from red cell ghosts and sarcoplasmic reticulum membranes yielded similar fluorescence decay results, and NMR results from experiments with the sarcoplasmic reticulum system paralleled those from the model membrane vesicles (13).

The molecule TEMPO (2,2,6,6-tetramethylpiperidine-1-oxyl), being lipid-soluble and possessing an unpaired electron spin was found to be a good ESR probe of the motional state within the hydrocarbon core of artificial phospholipid bilayer systems and in several varieties of excitable biomembrane preparations when used in low enough concentrations to rule out appreciable electron spin-spin interactions between neighboring probe molecules (14). The solubility of the TEMPO probe in the hydrocarbon portion of the bilayer, as monitored by the ESR spectrum, was found to increase two- to five-fold when the membrane was also host to the local anesthetic tetracaine, for both artificial phospholipid vesicles and an excitable membrane from the walking leg nerve fiber of a Maine lobster (14).

Elevated hydrostatic pressure is an antagonist to the anesthetized state of a membrane. This pressure reversing effect on anesthesia also illustrates the parallel between biological and model membrane systems. Pressure reversal of anesthesia has been demonstrated in the classical tadpole experiment (15) and also with newts (16). The latter workers also evaluated the effects of elevated pressure on

liposomes subjected to several anesthetics. The anesthetics alone increased the liposomes' permeability to K^+ and Rb^+ ions. If the system was then pressurized to about 150 atm, initial permeability to the particular ions was re-established. The correspondence between the liposome system and the biological system (newts in this case) is that the anesthetic concentration used in the liposome experiments equaled the threshold concentration for inhibition of the righting reflex in newts, and the pressure necessary to reverse this inhibition was about 150 atm. Experiments with erythrocyte membranes show how anesthetics, in concentrations equivalent to the minimum alveolar concentration (MAC) suitable for surgery, create an anti-hemolytic effect in the erythrocytes (17 and references therein). As anesthetic-induced membrane expansion, responsible for the anti-hemolytic effects, is most likely to be the phenomenon antagonized by elevated pressure, some interesting calculations have been done.

Corresponding to surgical anesthetic concentrations is an increase in the erythrocyte membrane area of 0.4%. This is surprisingly in agreement with the change in membrane area calculated when the membrane is compressed by an applied pressure equal to the pressure which produces a reversal of the anesthetic effects. Thus, in the realm of experimental information derived from anesthetics' interactions with biological and model membrane systems, an elegant analogy has developed between the two systems.

In conclusion, phospholipid bilayer models provide an opportunity for the researcher to design a system to meet the special requirements of a particular experiment aimed at answering a specific question about the biological counterpart of the model system.

1.5. Lateral diffusion studies on model and biomembranes.

Lateral diffusion of membrane components has received much attention in the last decade in order to comprehend in greater detail the temporal nature of the membrane's dynamic state. The foremost *a priori* restrictions imposed upon such investigations is that the methods used must necessarily involve a time scale coincident with that of the dynamic state observables to be monitored. Magnetic resonance spectroscopy satisfies this condition and has been employed in the measurement of the diffusion rates of molecules in membrane systems and as a general tool for probing the molecular dynamics of membrane bilayers using both the nuclear spin resonance and electron spin resonance condition as an experimental basis. Proton NMR spin-spin relaxation times of certain lipid resonances have been used to estimate a lower limit for the diffusion coefficient in DPPC vesicles (18). Wade (19) has determined the lateral self-diffusion coefficient for oriented lecithin bilayers using the pulsed field gradient spin echo (PFGSE) proton NMR experiment. The nature of the fluidity of several membrane systems has been

investigated and estimates of the diffusion coefficient of spin-labeled probes incorporated into various membrane systems have been obtained with ESR experiments (20-22). Optical spectroscopic techniques have also achieved some success in diffusion studies employing fluorescence probes in membrane systems (23-25). A brief summary follows of the significant investigations reporting values of diffusion coefficients for various lipid molecules in membrane systems.

1.6. ESR.

ESR spectroscopy has been applied to the problem of determining lateral diffusion rates in model and natural membranes by monitoring the spectral properties of "spin-labeled" probes inserted into the membrane system under investigation. Typically, the spin-label consists of a nitroxide group, with an unpaired pi electron, attached to a phospholipid analog. The ESR lineshape of the nitroxide probe is influenced by the molecular motions available to the probe which are ultimately influenced by the molecular structure and dynamics of its surrounding environment. Interaction between the unpaired electron spins of adjacent probes may occur, providing spectral characteristics such as changes in the hyperfine splittings, g-factor and absorption intensities, from which information about molecular dynamics can be extracted.

Träuble and Sackmann (20), in a series of ESR experiments, studied the structure and behavior of DPPC model membrane systems above and below the liquid crystalline phase transition temperature using a spin-labeled steroid. The collision rate of the paramagnetic spin probes affects the ESR line shape *via* spin exchange interactions. In their approach, spin exchange frequencies, determined as a function of temperature and steroid concentration from experimental and computer-simulated spectra, were applied to a diffusion model developed to incorporate the exchange parameter. They reported a lateral diffusion coefficient of approximately 1×10^{-8} cm^2/sec for an androstane spin-label in DPPC bilayers just above the phase transition temperature.

Devaux and McConnell (21) studied lateral diffusion using another ESR line shape analysis based on the interactions between the unpaired electron spins of oxyloxazolidine rings attached to the choline nitrogen atom of DPPC molecules inserted into oriented multilamellar systems of EYL and didihydrosterculoyl phosphatidylcholine (DPC). A concentrated "spot" of the spin-labeled DPPC probe was placed in the host phospholipid multilayers and the ESR spectrum recorded at intervals of time until the spectrum representing the completely randomized or dilute spin probe was obtained. Spectra calculated with diffusion related parameters for varying concentrations of the spin-label probe were compared with the experimental spectra for deter-

mining the diffusion coefficient. For the spin-labeled DPPC molecule embedded in DPC multilayers, a lateral diffusion coefficient of (1.8 ± 0.6) X 10^{-8} cm^2/sec at 25°C was reported.

Scandella et al (22) have also investigated the diffusion of a spin-label probe in both EYL/cholesterol bilayer vesicles and in vesicles made from rabbit sarcoplasmic reticulum membranes. Spin-label collision rates, determined in terms of the electron spin exchange contribution to the concentration broadening of the ESR spectra, were used for calculating diffusion coefficients. Lateral diffusion rates demonstrated very little change with temperature in EYL/cholesterol bilayers (e.g., ranging from D = (1.5 ± 0.2) X 10^{-7} cm^2/sec at 40°C to (2.0 ± 0.15) X 10^{-7} cm^2/sec at 70°C) while in sarcoplasmic reticulum membrane vesicles values calculated for D ranged from D = (7.5 ± 2) X 10^{-8} cm^2/sec at 40°C to 1.2 X 10^{-7} cm^2/sec at 70°C. It was subsequently reported (26) that a spin-labeled phosphatidyl ethanolamine (PE) probe diffuses in the EYL/cholesterol vesicles at a rate very close to that of a DPPC probe in that system.

1.7. NMR.

The absorption of energy in the radiofrequency range by a nuclear spin system in a large constant external magnetic field induces transitions between the nuclear energy levels

and thus perturbs the populations of the spin system. The return of the spin system to equilibrium is modulated by the intra- and intermolecular motions of the molecules housing the spin system under observation. Thus, as the nuclear spin analog to ESR, NMR proves to be a valuable investigative tool for studying molecular dynamics. NMR, however, offers an advantage because the nuclear spins within a membrane's molecules are intrinsic probes.

The large number of monographs and volumes covering the formalism of nuclear induction and nuclear spin relaxation (27-30) supersede such a discussion here. For now it is sufficient to provide only a brief description of the relationship between molecular motion and nuclear spin relaxation.

When relaxation is due to dipolar interactions between the individual nuclear magnetic moments of a spin system, it is possible to compute the effect of the local magnetic fields, h, on the net magnetic moment, M, of the spin system

$$\begin{aligned}\vec{\mathbf{h}} \times \vec{\mathbf{M}} = {} & (h_y M_z - h_z M_y)\hat{\mathbf{i}} \\ & + (h_z M_x - h_x M_z)\hat{\mathbf{j}} \\ & + (h_x M_y - h_y M_x)\hat{\mathbf{k}}\end{aligned} \qquad [1]$$

where

$$\vec{\mathbf{h}} = h_x\hat{\mathbf{i}} + h_y\hat{\mathbf{j}} + h_z\hat{\mathbf{k}} \qquad [2]$$

and

$$\vec{M} = M_x\hat{i} + M_y\hat{j} + M_z\hat{k} \qquad [3]$$

Longitudinal, T_1 or nuclear spin-lattice relaxation, which occurs after the absorption of radiofrequency energy, involves re-establishment of the nuclear spins to their equilibrium occupation of energy states in the presence of the applied constant magnetic field H_o (which arbitrarily defines the z axis of our coordinate system). Longitudinal relaxation is promoted by the h_x and h_y, but not the h_z, local field components. The loss of phase coherence or distribution of spin energy solely within the spin system, T_2, transverse or nuclear spin-spin relaxation is also a consequence of the h_x and h_y components but is singularly affected by h_z. Eq [4] and Figure 1-3 summarize the relationships between the local field components and the T_1 and T_2 relaxation processes.

$$\left.\begin{array}{l} h_{x'} \rightarrow M_{y'},\ M_{z'} \rightarrow T_1,\ T_2 \\ h_{y'} \rightarrow M_{x'},\ M_{z'} \rightarrow T_1,\ T_2 \\ h_{z'} \rightarrow M_{x'},\ M_{y'} \rightarrow T_2 \end{array}\right\} \qquad [4]$$

These relations actually describe the events while observing the system in the rotating frame, obtained simply by transforming the laboratory frame of reference with the operator ω_o, along the z (laboratory frame) axis as illustrated in eq [5]

$$\left.\begin{array}{l} z \rightarrow z' = z \\ x \rightarrow x'(\omega_o) \\ y \rightarrow y'(\omega_o) \end{array}\right\} \qquad [5]$$

FIGURE 1-3

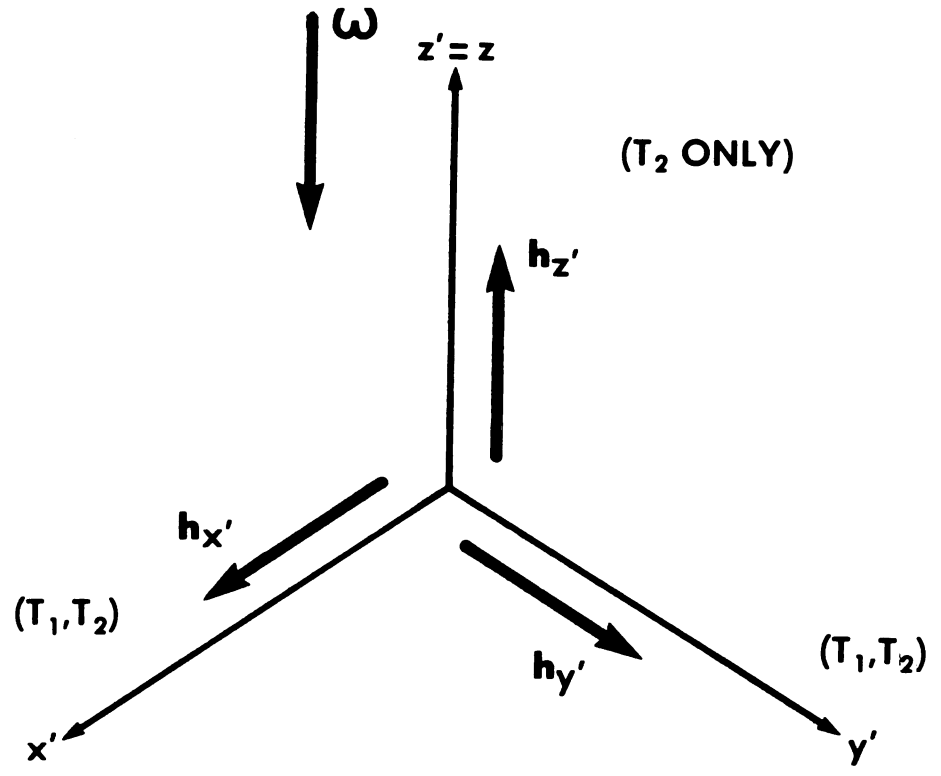

Figure 1-3: The rotating frame of reference and the relaxation processes affected by the respective local magnetic field vectors.

Nuclear spin relaxation is a consequence of the interaction of the fluctuating local magnetic fields with the nuclear dipole moments. Fluctuations in these interactions are influenced by the motional state of the molecules in the sample. Particular molecular motions yield Fourier frequency components in the power spectrum which provide efficient nuclear spin relaxation (e.g., those near ω_o, the Larmor or nuclear precession frequency). Fourier components exist which are effective for both T_1 and T_2 processes; other components significantly affect T_2 relaxation only.

The dependence on motional frequency, expressed in terms of the rotational correlation time τ_c of the nuclear spin relaxation time, is exemplified for the case of intramolecular relaxation in Figure 1-4. More rapid motions are characterized by shorter correlation times.

In the first attempt to study lateral diffusion in phospholipid model membrane systems with NMR, Kornberg and McConnell (32) gained only a qualitative picture indicating that diffusive motions of phospholipids in vesicles must be occurring with a frequency greater than 3×10^3 sec^{-1}. Although they did not report a value, simple diffusion theory may be used to estimate a lower limit for the diffusion coefficient from the limiting jump frequency. Assuming a value of $\sigma = 8$Å (33) for the distance of closest approach of neighboring molecules, a lower limit of 4.8×10^{-12} cm^2/sec is calculated for the diffusion coefficient from eq [6] (33)

FIGURE 1-4

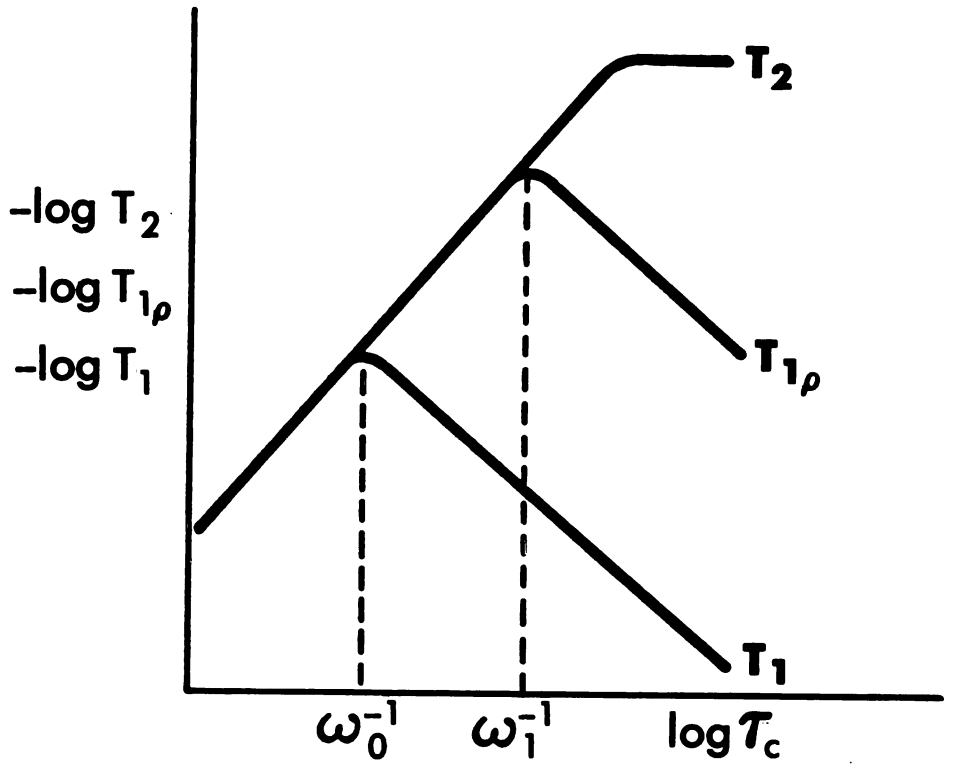

Figure 1-4: Theoretical curves illustrating the T_1, T_2 and $T_{1\rho}$ relaxation rates' dependence on correlation time for intramolecular dipolar relaxation. From James (30).

$$\tau_{jump} = \frac{\sigma^2}{4D} \qquad [6]$$

Experimentally, line broadening of the choline N-methyl proton resonance in DPC vesicles was monitored as a function of DPPC spin-label probe concentration to determine the residence time of nearest neighbors and, consequently, the diffusional motion frequency. The limiting value of the diffusion coefficient is smaller by several orders of magnitude than the diffusion coefficients reported in the more quantitative approaches to be described. This may reflect the inability of this technique to single out diffusion as the prevailing mode through which paramagnetic line broadening of the N-methyl resonances occurs.

Arguing that intermolecular dipolar relaxation due to translational diffusion is the dominant mechanism for relaxation of the terminal methyl and choline N-methyl proton resonances of phospholipid molecules in sonicated vesicles, Lee _et al_ (18) were able to evaluate a lower limit for the diffusion coefficients of membrane lipids from proton NMR linewidth measurements. Their argument requires proof that intermolecular relaxation is due to the relative translation of the lecithin molecules in the bilayer as opposed to rotational motions or other molecular excursions. As will be discussed later this is of primary concern for the method upon which this dissertation is based. Lee _et al_ (18) concluded that an intermolecular contribution is important for the methyl proton relaxation rate by comparison with ^{13}C

relaxation results (^{13}C will be relaxed by attached protons). Deuterium dilution experiments gave further evidence of intermolecular contributions to the spin-lattice relaxation rates and to the linewidths, at least for the N-methyl and terminal methyl groups in lecithin vesicles. From ^{13}C longitudinal relaxation rates the proton intramolecular contribution $(1/T_1)_{intra}$ may be estimated, thus enabling calculation of the intermolecular contribution $(1/T_1)_{inter}$ by eq [7]

$$\left[\frac{1}{T_1}\right]_{OBS} = \left[\frac{1}{T_1}\right]_{INTRA} + \left[\frac{1}{T_1}\right]_{INTER} \qquad [7]$$

In view of the proton T_1 value of 0.84 sec for the terminal methyl group in DPPC vesicles and the estimate for the intramolecular contribution of approximately 4 sec, the overall relaxation rate is indeed dominated by the intermolecular contribution of approximately 1.06 sec. Their assessment of diffusion coefficients arises from the theory for dipolar intermolecular relaxation due to translational diffusion (34,35). The correlation time associated with the translational motion of the relaxing spins may be related to the diffusion coefficient by the relationship

$$\tau_c = \left[\frac{1}{5}d^2 + \frac{1}{12}\langle r^2\rangle\right]\frac{1}{D} \qquad [8]$$

where σ is the distance of closest approach of two nuclei on different molecules and $\langle r^2\rangle$ is the mean-squared jump

distance. Assuming a jump distance of 5Å, correlation times calculated from T_2 data (36) yield a diffusion coefficient of 9.5 X 10^{-9} cm^2/sec in EYL at 20°C. It should be pointed out that the value found for D is very dependent on the assumed jump distance and distance of closest approach.

Headgroup phosphate linewidths and residual second moments derived from high resolution ^{31}P NMR experiments with EYL and DPPC vesicles were used by Cullis (37) to calculate the lateral diffusion of these phospholipids in vesicles. Glycerol was added to the systems to retard vesicular tumbling such that the vesicular rotational contribution to the diffusion term in eq [9] was eliminated, i.e., $D_R << D_t$ such that $D = D_t + D_R \rightarrow D_t$

$$\frac{1}{T_2} = \frac{M_2 a^2}{6\left[\frac{k T}{8 \pi \eta a} + D_t\right]} + C \qquad [9]$$

Diffusion coefficients were estimated over a wide range of temperatures for both systems. At 45°C the diffusion coefficient in DPPC vesicles is about 2.5 X 10^{-8} cm^2/sec and in the EYL vesicles at 50°C, D = 2.6 X 10^{-8} cm^2/sec. Of special interest is that this technique allows the measurement of diffusion below the gel to liquid crystalline phase transition giving, for example, at 35°C a diffusion coefficient of 1 X 10^{-9} cm^2/sec in DPPC vesicles. This is in agreement with our $T_{1\rho}$ work[3] and represents one of the few

[3]See Chapter 4.

measurements in the gel phase so far reported. The order of magnitude change in diffusion rate for the DPPC system appears to occur during the temperature range, just below the gel-to-liquid crystalline transition, associated with the endothermic pre-transition which is observed in calorimetric experiments on these bilayer systems. Despite the agreement of these results with other reports on diffusion coefficient measurements, little discussion is given as to the correctness of separating the diffusion term into the translational and rotational components as is done to arrive at eq [9].

The experiments mentioned above indirectly produce diffusion coefficients. NMR spin echo experiments potentially may provide a direct monitor of molecular diffusion. Unfortunately, because of incomplete averaging of dipolar interactions due to the anisotropic molecular motions within a bilayer, diffusion studies have not been altogether successful in membranes. The PFGSE experiments on membranes push the technique's capabilities to their limit. For unsonicated lecithin dispersions, transverse relaxation is dominated by the residual dipolar coupling, swamping any diffusion contribution; thus the experiment cannot be done in this case unless all the bilayers are oriented at an angle of 54.7° (the magic angle) with respect to the magnetic field direction; this orientation minimizes residual dipolar interactions. For sonicated phospholipid vesicles in PFGSE experiments, the diffusion monitored is that of the

whole vesicles and not the lateral diffusion of the phospholipid in the vesicles' bilayer (38).

Lindblom et al (39) report a lateral diffusion coefficient of 2.1 X 10^{-8} cm^2/sec for the ternary system of dilauroyl lecithin (DLPC), sodium cholate and D_2O using the PFGSE experiment. The PFGSE experiment is successfully applied to the cubic mesophase of such systems since molecular motions are sufficiently isotropic to permit a respectable degree of motional narrowing. The extension to a diffusion coefficient for the lamellar phase is purely the result of approximations based on the assumption that the phospholipid molecules "feel" the same immediate environment in both the lamellar and cubic phases. There is however, surprising agreement in these results and other published values for diffusion coefficients in model and natural membrane systems.

Lindblom and Wennerström (40) later employed magic angle orientation of their samples in order to perform the conventional PFGSE experiment. Interestingly, this more direct method yields a diffusion coefficient roughly an order of magnitude faster, D = 1.2 X 10^{-7} cm^2/sec, than the method involving several assumptions and the presence of a third component.

Wade (19) has also used ordered multilayers and magic angle orientation with the PFGSE experiments on several phospholipid systems. His results are also an order of magnitude faster than the values for diffusion coefficients in

systems studied by ESR and other NMR techniques, ranging between 1 and 7 X 10^{-7} cm^2/sec for DLPC, DMPC and DPPC.

1.8. Fluorescence.

Diffusion in membranes has been investigated with several fluorescence spectroscopic techniques either by incorporating a fluorophore into one of the membrane molecules or by using a membrane-soluble fluorophore which is foreign to the system. The results are summarized here for comparative purposes. Fahey *et al* (23) found for DPPC at 47°C, D = 1.1 X 10^{-7} cm^2/sec and using two different probes in EYL measured diffusion coefficients of 1.7 and 2.4 X 10^{-7} cm^2/sec at 26°C and 24°C respectively. In the plasma membrane of L-6 myoblast cells, at 23°C, the diffusion coefficient of the lipid component is 9 X 10^{-9} cm^2/sec while that of the protein is 2 X 10^{-10} cm^2/sec (24). Wu *et al* (25) report a value of D = 4 X 10^{-8} cm^2/sec in EYL at 25°C. They also studied two other phospholipid systems; DMPC in which D = 5.5 X 10^{-8} cm^2/sec at 30°C and DPPC, where D = 7 X 10^{-8} cm^2/sec at 45°C. In these last two systems the diffusion coefficient was observed to decrease by two orders of magnitude at temperatures below the phase transition temperature.

1.9. Inadequacies of existing approaches.

Two reviews (41,42) present an overview of lateral diffusion in membranes, model and natural, as studied by ESR, NMR and fluorescence spectroscopy. It is apparent that no method for determining diffusion coefficients in membranes has gained general acceptance due to technical and experimental limitations and because of the potential perturbation of the membrane system by foreign probes or the estimates and approximations needed when calculating the diffusion coefficient from the experimental results. Some of the major problems regarding the existing techniques are: (a) The experimental phospholipid system most closely simulating the natural membrane bilayer is that of unsonicated phospholipid dispersions or ordered multilayers as it has been suggested that vesicle curvature affects lamellar packing and thus the phospholipids' motions. However, the high resolution NMR spectra required for the techniques discussed in this chapter are unobtainable with unsonicated dispersions. Also as mentioned with respect to the PFGSE experiments magic angle orientation is necessary when using these ordered multilayers. This is an extreme when it comes to experimental difficulty. (b) The use of extrinsic probes yields the diffusion coefficient of the probe and hence only an estimate for the rate of diffusion of the inherent membrane molecules. The uncertainty as to what perturbing effects the probe has on the dynamic state of the host molecules also exists (43). (c) Many of the methods involve

the use of approximations. When assumptions about molecular geometries and motional time scales are employed, the final evaluation of a diffusion coefficient can be, at its best, only an estimate.

1.10. A brighter future.

Burnett and Harmon have shown that in a viscous system such as glycerol, if certain conditions prevail, vida infra, the diffusion coefficient may be determined directly from NMR relaxation data (44). If intermolecular dipolar relaxation due to translational diffusion gives rise to a significant contribution to the spin-lattice relaxation rate in the Zeeman field or stationary frame ($1/T_1$) or in the spin-locking field or rotating frame ($1/T_{1\rho}$), a radiofrequency dependence exists from which the self-diffusion coefficient may be obtained directly. The initial goal of this work was to determine the usefulness of this technique for determining the lateral diffusion rates of phospholipid molecules in model membrane bilayers. Our feasibility studies did, in fact, prove this method to be successful for the measurement of phospholipid lateral diffusion rates, thus obtaining a new probe of the molecular dynamics within model membrane systems.

This dissertation describes a study of diffusion in membranes as a probe of the dynamic structure and shows how various conditions affect lateral diffusion within the

membrane bilayer. Proton NMR is used, thus monitoring an intrinsic membrane probe in unsonicated phospholipid dispersions and in a biomembrane. Spin-lattice relaxation rates in the rotating frame were obtained as a function of frequency, temperature, concentration and composition yielding diffusion coefficients which are calculated from strictly measurable quantities.

As indicated in this introductory chapter, many scientists have spent considerable time and effort in contributing to a description of the dynamic state of membranes. The work described here is notable for the experimental approach we have used in studying diffusion, which permits the phospholipid diffusion coefficients to be obtained directly from experimentally determined parameters and without the addition of an extrinsic probe.

CHAPTER 2

FUNDAMENTAL CONSIDERATIONS

2.1. Intermediate States of Molecular Order.

Temperature-pressure phase diagrams delineate the boundaries separating the solid, liquid and gaseous phases of a substance. For any given values of pressure and temperature, the existance of a crystalline solid (potentially one of several polymorphic crystalline phases), an amorphous solid, an isotropic liquid or the gaseous phase depends on the balance between the net attractive intermolecular forces and the thermal energy within the system. At constant pressure, above the triple point pressure, increasing temperature typically gives the sequence of transitions: SOLID → LIQUID → VAPOR. In some instances, molecules possessing some configurational asymmetry (usually involving a low ratio of width to length) and often a relatively polar region may pass from the crystalline solid to an intermediate paracrystalline or liquid crystalline mesophase before passing into the isotropic liquid phase. These anisotropic partially ordered mesophases are a result of thermal energy weakening the attractive intermolecular forces in the crystalline lattice. Remaining attractive forces maintain some

of the order present in the solid crystalline lattice.

Three principle thermotropic mesophases may be formed: the smectic, nematic and cholesteric mesophases as shown in Figure 2-1 (45-47). Characteristic of each of these mesophases is a particular axial alignment providing configurations with minimum interaction energy between the hydrophobic regions and hydrophilic regions of each molecule. Some substances may yield more than one mesophase upon raising the temperature (enantiotropic) while some mesophases are formed only upon supercooling of the isotropic liquid (monotropic). In the latter case, a second mesophase may occur with changes in temperature in either direction. Figure 2-2 illustrates these two processes schematically; however, combinations of these transitions may give rise to more complex schemes.

Penetration of a solvent into the crystalline lattice is another mechanism whereby the cohesive intermolecular interactions responsible for maintaining the lattice integrity may be diminished. Weakening of the crystal lattice's intermolecular forces due to the solvent-solute interactions results once again, for certain substances, in a phase transition to a mesophase intermediate to the solid and isotropic liquid phase of the binary system. Such phase behavior, i.e., resulting from variation in the solvent to solute ratio, is termed lyotropic mesomorphism. The amphipathic biological lipids offer an excellent example of this lyotropic mesomorphic behavior. The primary lyotropic

FIGURE 2-1

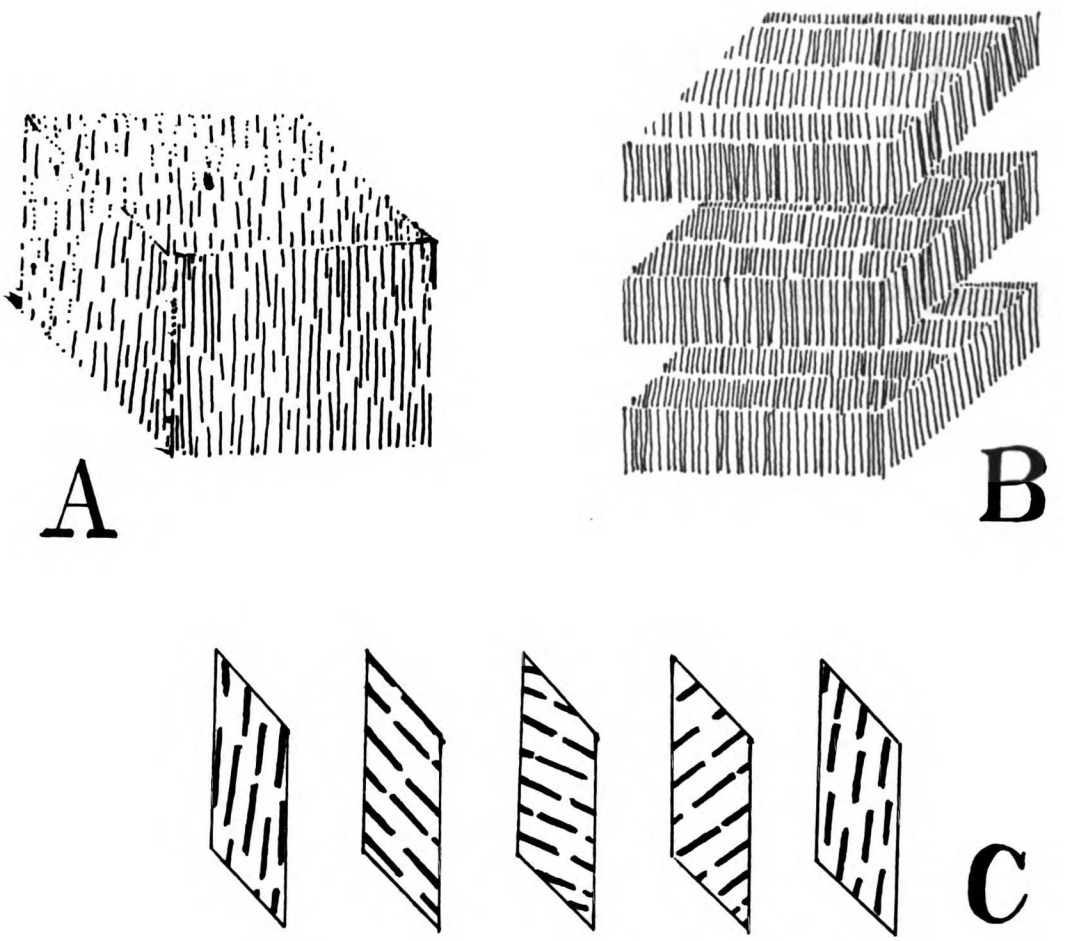

Figure 2-1: Line drawings of the three primary thermotropic mesophases. The lines represent the long molecular axis, illustrating the relation of the molecular asymmetry to the long range order of each liquid crystalline phase: (A) Nematic, (B) Smectic, (C) Cholesteric.

FIGURE 2-2

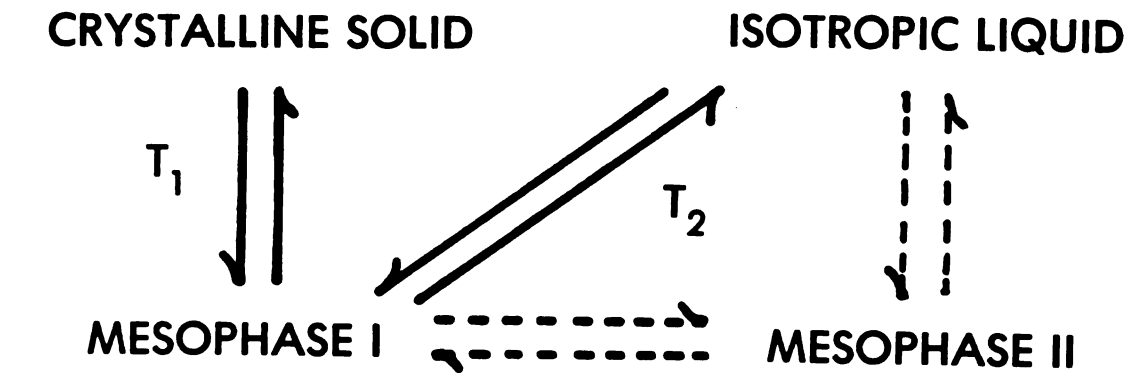

ENANTIOTROPIC MESOMORPHISM

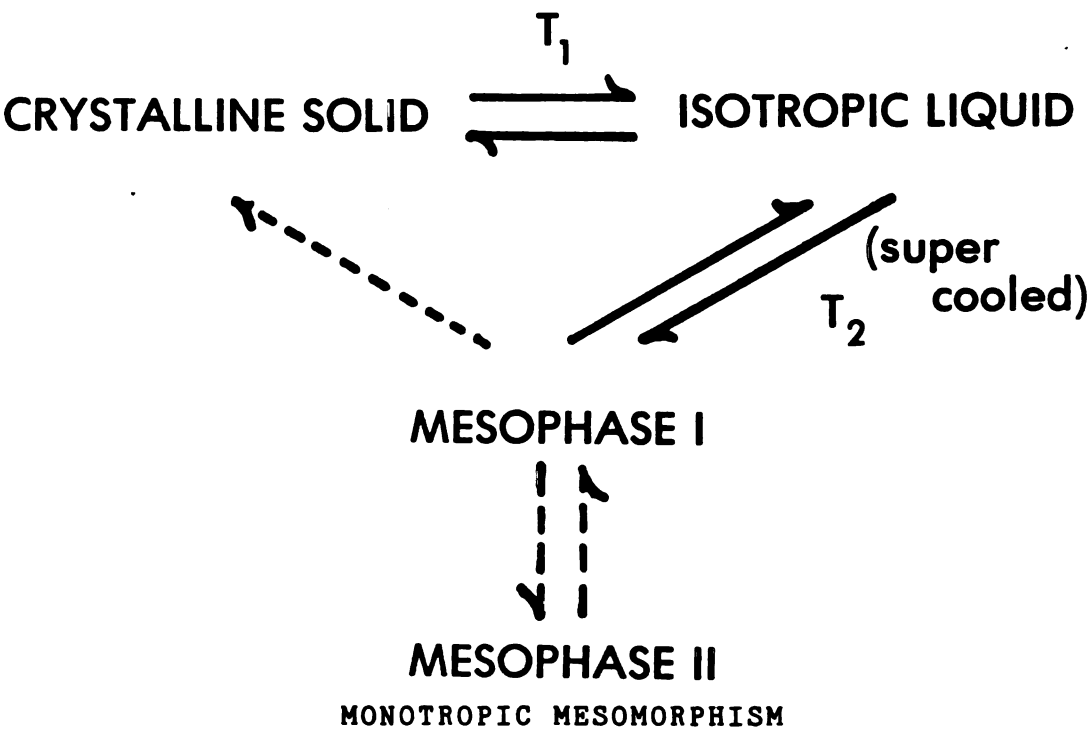

MONOTROPIC MESOMORPHISM

mesophases, determined as a function of water concentration and temperature, for these systems are the lamellar (smectic), hexagonal and cubic phases (47-54). Sketches of these phases are given in Figure 2-3.

Further discussion of lyotropic mesomorphism is confined to the phospholipid molecules of interest in this dissertation: (dilauroyl (12C) DLPC, 1,2-diacyl-sn-glycero-3-phosphocholines dimyristoyl (14C) DMPC, dipalmitoyl (16C) DPPC, distearoyl (18C) DSPC and dioleoyl (18:1 cis) DOPC) and the 16 carbon analog of the 1,2-diacyl-sn-glycero-3-phosphoethanolamine series, dipalmitoyl phosphatidylethanolamine DPPE. The structures of these molecules are shown in Figure 2-4.

Anhydrous phospholipids exhibit thermotropic mesomorphism as well as lyotropic mesomorphism when water is present (54-56). The relative positions of the solid-to-liquid crystalline thermotropic phase transition and gel-to-liquid crystalline[4] phase transition temperatures (for a system with a given water concentration) are influenced similarly by some certain factors. A decrease in hydrocarbon chain length or an increase in degree of unsaturation are found to lower the transition temperature, cis double bonds effecting a greater lowering of the transition temperature than trans double bonds (55).

[4] To be discussed shortly.

FIGURE 2-3

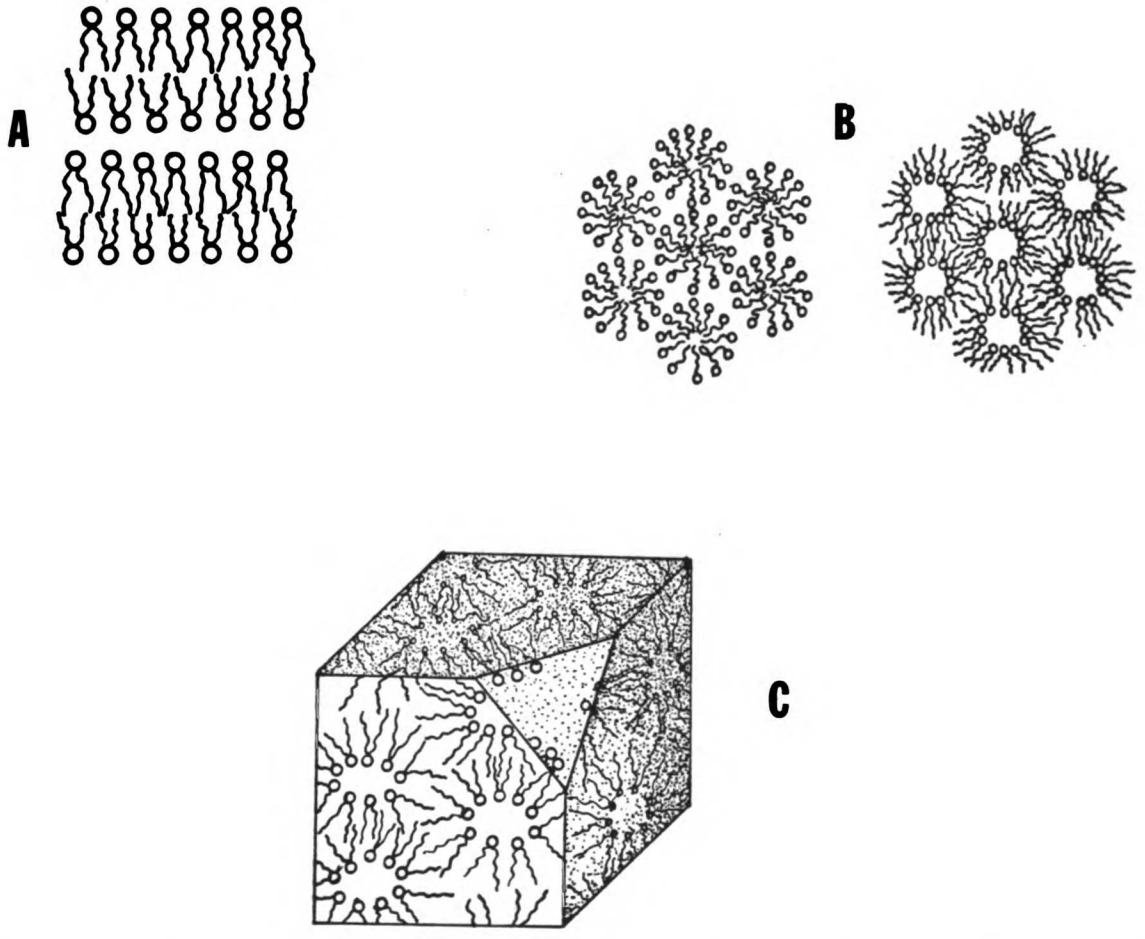

Figure 2-3: Drawings of the three primary lyotropic mesophase structures obtained with the binary phospholipid-water systems: (A) Lamellar (smectic), (B) Hexagonal (two forms), H_I-oil in water type, and H_{II}-water in oil type, (C) Cubic. The predominant hexagonal phase for the diacylated phospholipids is of the type water in oil.

FIGURE 2-4

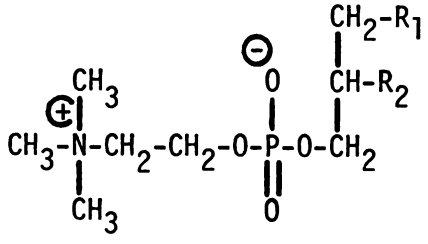

R_1, R_2 = Lauric acid, Myristic acid, Palmitic acid, Stearic acid and Oleic acid

1,2-DIACYL-sn-GLYCERO-3-PHOSPHOCHOLINES

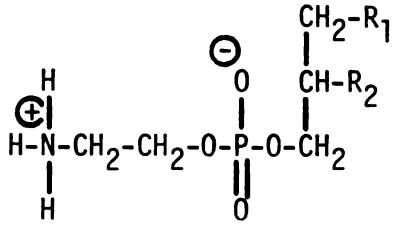

R_1, R_2 = Palmitic acid

1,2-DIPALMITOYL-sn-GLYCERO-3-PHOSPHOETHANOLAMINE

The phase diagram for the water-DPPC system given in Figure 2-5 is representative of the behavior of the phosphatidylcholines studied in this work, where the concentration c is expressed as weight % of the phospholipid. The gel-to-liquid crystalline transition (heavy line in Figure 2-5) temperature or (Chapman transition temperature) T_C signifies two important physical phenomena. For a given amount of water, it represents the minimum temperature necessary for penetration of the anhydrous crystalline lattice by the water molecules. The first thermotropic transition for anhydrous DPPC is at 90°C (on the left axis of the phase diagram). The phase diagram illustrates the large effect the addition of water has in lowering the transition temperature to the lower-limiting value of T_C at 41°C (the Krafft temperature) obtained at high water content.

The bimolecular lamellae of the smectic liquid crystalline phase, in which the hydrocarbon chains enjoy to a certain degree the disorder found in liquid paraffins, occupy the major portion of the phase diagram of the binary lecithin-water system (for the homogeneous chain lecithins) (56) including the water concentration and temperature ranges of biological interest. Hexagonal and cubic mesophases (see Figure 2-3) evolve at much higher temperature and at water concentrations bordering the anhydrous limit of the phase diagram (50). The long range order of the anhydrous solid crystalline lecithin is the two dimensional bimolecular lamellar lattice with the hexagonally-packed,

FIGURE 2-5

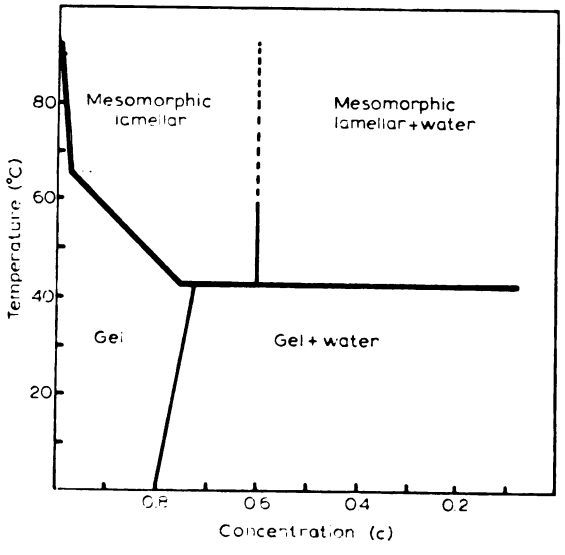

Figure 2-5: Temperature-concentration phase diagram for the DPPC-water system. From Chapman et al (56).

saturated hydrocarbon chains rigid and extending in the all-trans configuration (57) from the firmly positioned polar headgroups. When present, the involvement of water molecules is with the hydrophilic choline headgroups in the inter-lamellar channels. Calorimetric experiments have indicated that approximately 20% (by weight) of water is actually bound to the DPPC headgroup (56), or ten molecules of water per headgroup; above T_c up to 40% is accomodated in this channel region before two phases appear whereas below T_c (in the gel phase) some of this "channel water" is excluded, the amount depending upon the temperature. The polar headgroup determines the amount of bound water in these systems, the hydrocarbon chain length or degree of unsaturation have no influence on this property (54). Phospholipids bearing a net electrical charge such as the acidic phopholipids will take up additional amounts of water before separation into two phases as the channels are enlarged due to interlamellar repulsion by the charged headgroups (50,56). It is interesting to note that egg lecithin also shows a maximum hydration close to that of DPPC (50,56). The gel phase is, strictly speaking, not a liquid crystalline phase because the hydrocarbon chains possess a degree of order similar to that found in the crystalline solid lattice. However, it has been termed by some the smectic B phase as opposed to the smectic A phase found above the T_c line on the phase diagram (58). Hydration of the polar headgroups promotes a weakening of their intermolecular

associations, transmitting a greater degree of disorder to the hydrocarbon chains. Above the phase transition temperature thermal enhancement of this disorder occurs, the chains adopting a perpendicular orientation to the lamellar plane (smectic A phase), while below T_c the lack of thermal energy leads to the energetically preferred conformation of the chains oriented at an angle of 58° with respect to the bilayer plane (smectic B phase) (59). In some cases this gel phase may be metastable and may end up as a coagel in which water has been excluded forming small crystalline domains suspended in an aqueous environment. The overall structure, however, is constrained to be of the lamellar type for both the gel and coagel phases. With respect to this elementary picture of hydration of these lamellar systems, there are some physical parameters of particular interest (46). On increasing the water content up to the point where two phases exist, the interfacial surface area per molecule increases and the thickness of the bilayer decreases. Below T_c, the lamellar repeat distance increases with increasing water content until the one-phase two-phase equilibrium is reached. At T_c, an appreciable shrinkage occurs. While above T_c, it expands again until the boundary marking the existance of two phases is reached.

The lyotropic behavior of the homologous series C12 to C18 and the C18:1 analog is similar to that demonstrated in Figure 2-5 for DPPC. The main differences arise from the effect of chain length and the presence of unsaturation on

the transition temperature T_C such that the family of phase diagrams would be shifted along the temperature axis according to their relative Krafft temperatures. These temperatures are (54): DSPC (58°C), DPPC (41°C), DMPC (23°C), DLPC (0°C), and DOPC (-22°C). This trend in limiting-transition-temperature as a function of chain length or unsaturation is comparable to the variation in fatty acid capillary melting point behavior for the analogous family of fatty acids. Thus, chain length and unsaturation have a profound effect on the transition temperature. One phenomenon of unclear significance associated with the transition between the gel-to-liquid crystal transition is a "pre-transition", a small endothermic phenomenon, found several degrees below the T_C. It has been attributed to a conformational change in the phosphate headgroup which may be related to the difference in channel hydration above and below the T_C and to the differences between the smectic A and smectic B structural forms, (i.e., the reorientation of the chains from a tilted to perpendicular configuration with respect to the bilayer plane).

The phase behavior described above is for 1,2-diacyl-sn-glycero-3-phosphocholines with homogeneous lipid chains. When heterogeneity occurs, either due to variance in chain length within one molecule or differing degrees of unsaturation between the two chains, the lyotropic mesomorphism becomes much more complex and the structural variants of each principle phase multiply (50). Two examples in Figure

2-6 serve to illustrate this point. Note that the hexagonal phase appears at lower temperatures and higher water content for some natural phospholipid systems.

1,2-dipalmitoyl-sn-glycero-3-phosphoethanolamine also exhibits thermotropic and lyotropic mesomorphic behavior. In contrast to the lecithins, however, it does not remain zwitterionic over the full pH range which gives DPPE a more complex phase diagram. The phase transition to the liquid crystalline state for completely hydrated DPPE occurs 22 degrees higher than its choline analog, i.e., at 63°C (60). Although egg yolk phosphatidylethanolamine (PE) has been studied (52), a complete analysis of the synthetic PE phase diagram has not been made available. In view of the likely similarity between the hydrocarbon chains of egg yolk lecithin and PE the phase diagram for egg yolk lecithin can be viewed as a reference point. PE appears to form a hexagonal phase, cylinders of water channels or of the type water in oil, over a larger region than is found for either egg yolk lecithin or the homogeneous chain phosphatidylcholines. The hexagonal phase coexists with the lamellar phase at least in the range of 25°C to 35°C but at 55°C, between .96 < c (wt. % DPPE) < .79, only the hexagonal phase exists. The lamellar phase can be formed exclusively at a pH of 6.0 in 145mM KCl (54), but is otherwise most likely found at higher water content and above T_c.

Classification of the physical state of these liquid crystalline systems can be taken one step further. When the

FIGURE 2-6

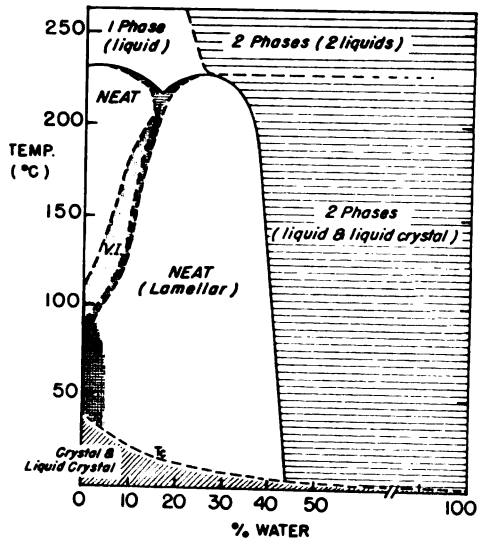

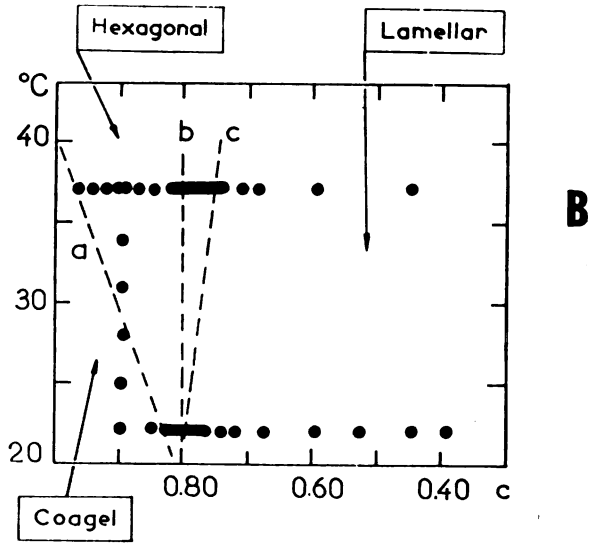

Figure 2-6: Binary phase diagrams for water and (A) egg lecithin (49); and (B) phospholipid isolated form beef brain extract (48).

phospholipid in the presence of sufficient water is above the transition temperature T_c and is mechanically agitated it spontaneously forms concentric multilamellar liposome structures (54,61). These are large spherical domains, heterogeneous in overall size ranging from 0.5μ to 20μ in diameter with approximately 150,000 molecules per liposome. Application of ultrasonic irradiation transforms these liposomes into smaller spheres yielding, in the limit of long sonication time, single bilayer vesicles of approximately 200Å - 500Å diameter and containing about 2000 - 3000 molecules per vesicle distributed asymmetrically with a greater proportion of the molecules on the outside of the bilayer vesicle.

Of interest to this work are the unsonicated dispersions of large lamellar domains which do not present the curvature effects on lattice packing found in the smaller vesicles (62,63). The multilamellar dispersions offer an excellent system for studies of translational diffusion in the plane of the phospholipid bilayer.

2.2. Translational diffusion and the frequency dependence of nuclear spin-lattice relaxation.

Nuclear spin relaxation may be accomplished *via* several modes of electromagnetic interactions. Dipolar coupling of the spins modulated by the relative intermolecular motions provides the basis for the diffusion measurements performed and described in this dissertation.

Intramolecular dipolar spin-lattice relaxation has been described in detail (27). It is well known that under motional narrowing conditions, *i.e.*, $\omega^2\tau^2 << 1$, where ω is the Larmor angular frequency and τ is the correlation time for the motion causing relaxation, there is no frequency dependence of the spin-lattice relaxation rates $(1/T_1)_{INTRA}$. In fact, for the case of like spins, the spin-lattice and spin-spin relaxation rates $(1/T_1)$ and $(1/T_2)$ and the spin-lattice relaxation rate in the rotating frame $(1/T_{1\rho})$, in the motional narrowing region, all reduce to a simple monotonic function of τ such that

$$\left[\frac{1}{T_1}\right]_{INTRA} = \left[\frac{1}{T_2}\right]_{INTRA} + \left[\frac{1}{T_{1\rho}}\right]_{INTRA} \qquad [1]$$

Treatment of intermolecular dipolar relaxation, being diffusion-model dependent, is more complex (27,31,34). Under the motional narrowing conditions the intermolecular spin-lattice relaxation rate $(1/T_1)_{INTER}$, which occurs as a result of the relative translational motion of the molecules

comprising the system, has been shown to be related to the self-diffusion coefficient (27):

$$\left[\frac{1}{T_1}\right]_{INTER} = \frac{2\pi N \gamma^4 \hbar^2}{5\sigma D} \qquad [2]$$

where N is the spin density, γ is the gyromagnetic ratio for the nucleus being observed, σ is the molecular diameter, D is the diffusion coefficient and $\hbar$ is Planck's constant divided by 2π.

Bloembergen et al (BPP) (31) arrived at a similar expression for intermolecular spin-lattice relaxation resulting from translational diffusion of nearest neighbors. Torrey (34) pursued the problem of nuclear spin-lattice relaxation via translational diffusion. He employed random walk theory which gives rise to explicit relationships between the detailed events associated with the diffusion process and nuclear spin relaxation. The value in such an approach is that the diffusion coefficient is obtained as well as parameters such as jump time and root mean square flight distance. Treatment of the diffusional effects on spin-lattice relaxation in these two cases, however, was incomplete. The BPP approach accounts for only the nearest neighbor interactions which immediately removes any frequency dependence from the relaxation rate. This may be correct only when the condition $\omega^2\tau^2 << 1$ holds, but should there be contributions from even the "next-to-nearest"

neighbors the quantity $\omega^2\tau^2$ may indeed become comparable to unity. Harmon and Muller (64) extended Torrey's random walk approach by including a suitable radial distribution function in the expressions used in calculating the correlation functions and thus in the evaluation of the spectral densities. This addition allows a more realistic description of the system and essentially provides a greater sensitivity to the contributing motions. Apparently, "feeling" the presence of these "not-so-near" neighbors can show profound differences in the relaxation rates. Furthermore, they show that in the low frequency limit, if a series expansion of the appropriate frequency terms in the spectral density is performed and all but the leading terms of the resulting expansion neglected, the intermolecular spectral density "rolls off" with increasing frequency in the region $\omega < 1/\tau$. Thus if the overall spin-lattice relaxaton rate is dominated by intermolecular effects, the relaxaton rates exhibit a frequency dependence in the extreme narrowing region in contrast with the case for intramolecular relaxation.

For spin 1/2 systems, the relaxation rate $(1/T_1)_{INTER}$ is (64)

$$\left[\frac{1}{T_1}\right]_{INTER} = \frac{2\pi N \gamma^4 \hbar^2}{5\sigma D}\left[1 + A(\langle r^2, \sigma\rangle) - B\left[\frac{\omega\sigma^2}{D}\right]^{1/2}\right] \qquad [3]$$

with $\langle r^2 \rangle$ being the mean squared jump distance, A and B representing numerical constants and the other symbols are

as described above. Evaluation of the only frequency-dependent term of eq [3] in terms of jump diffusion parameters shows that the size of ω becomes important when the time between diffusive jumps, τ, becomes comparable to the Larmor period:

$$\left[\frac{\omega\,\sigma^2}{D}\right]^{1/2} = \left[\omega\,\tau\,\frac{6\,\sigma^2}{\langle r^2\rangle}\right]^{1/2} \qquad [4]$$

The parameters of eq [4] are as described above, and τ, the mean time between diffusive jumps, can be used as a correlation time for the diffusive motion causing relaxation. It is apparent from eq [3] that measurements of the spin-lattice relaxation rate as a function of frequency can lead to a determination of the diffusion coefficient.

Diffusion in viscous or low temperature systems will involve motions on a much slower time scale. Consequently, with respect to utilizing the frequency dependent term arising in the expression for the relaxation rate, it is advantageous to measure the spin-lattice relaxation time in the rotating frame ($T_{1\rho}$) as a function of $\omega_1 (=\gamma H_1)$, the angular frequency for the applied radiofrequency field H_1. Typically ω_1 is more than three orders of magnitude smaller than $\omega_0 (=\gamma H_0)$, the Larmor precessional frequency in the laboratory reference frame. Two significant advantages arise when using the applied radiofrequency field H_1 to provide the smaller field in which the spin system is allowed to undergo

relaxation. Technically, the convenience and practicality in varying the strength of the applied radiofrequency field H_1 by far exceed the efforts associated with varying the stationary magnetic field H_o. Secondly, because of signal-to-noise considerations, by Curie's Law it is preferable to observe the nuclear resonance condition and initiate the experiment with the spin system in the presence of as large a stationary magnetic field as possible. In the experiments to be described, the "spin-locking" method was used (65). The macroscopic magnetization of the spin system is initially prepared in the presence of the large externally applied dc magnetic field H_o. The spin system is subsequently subjected to and monitored in the field H_{eff} in the rotating reference frame which is no longer H_o but in fact, when on resonance, becomes equal to H_1, the applied radiofrequency field. To understand how the rotating frame experiment provides the basis for using the readily variable field H_1, the following explanation is given.

If the z axis of the laboratory reference frame is defined by the direction of the constant external magnetic field $\vec{H}_o$, the effective field may be written in vector notation as

$$\vec{H}_{eff} = H_o \mathbf{k} \qquad [5]$$

and the equation describing the net motion of the spin system is simply

$$\frac{d\vec{M}}{dt} = \gamma\vec{M} \times \vec{H}_o = \gamma\vec{M} \times \vec{H}_{eff} \qquad [6]$$

where $H_o = H_{eff}$ and M is the magnetization vector for the spin system in the field H_o. If, however, the reference frame is given an angular velocity, ω, the equation of motion is transformed to

$$\frac{d\vec{M}}{dt} = \frac{\partial\vec{M}}{\partial t} + \vec{\omega} \times \vec{M} \qquad [7]$$

Appropriate substitution and rearrangement yields

$$\frac{\partial\vec{M}}{\partial t} = \gamma\vec{M} \times \left[\vec{H}_o + \frac{\vec{\omega}}{\gamma}\right] = \gamma\vec{M} \times \vec{H}_{eff} \qquad [8]$$

similar to eq [6] where the quantity $(H_o + \omega/\gamma)$ is now the effective field. The ω/γ term is a Corealis field or fictitious field evolving from the angular transformation. If an oscillating field H_1 synchronous with the rotating reference frame is applied perpendicularly to the z axis (which in the rotating frame maintains its laboratory frame identity), the effective field becomes

$$\vec{H}_{eff} = H_{1_x}\hat{i} + H_{1_y}\hat{j} + \left[H_o + \frac{\omega}{\gamma}\right]\hat{k} \qquad [9]$$

It is then apparent that choice of an appropriate rotating

frame angular frequency, i.e., such that $\omega = -\gamma H_o$, and suitable orientation of H_1 in the x'y' plane, e.g., along the x' axis (this is arbitrary for purposes of this discussion), the resulting effective field magnitude is

$$\left| H_{eff} \right| = \left| H_1 \right| \qquad [10]$$

Eq [10] should be qualified by stating that the condition $H_1 > H_{loc}$ must be satisfied, where H_{loc} is the local dipolar field strength. The incorporation of this transformation into the experimental design is discussed in Chapter three.

According to Burnett and Harmon (44), for intermolecular dipole-dipole spin-lattice relaxation in the rotating frame,

$$\frac{1}{T_{1\rho}} = C\,\omega_1^{1/2} + \frac{1}{T_2} \qquad [11]$$

where the constant C contains the diffusion coefficient and $1/T_2$ is the spin-spin or transverse relaxation rate such that $1/T_2 = 1/T_{1\rho}$ in the limit of $\omega_1 = 0$. Taking the derivative of eq [11] with respect to $\omega_1^{1/2}$, a quantitative expression is obtained which relates experimentally determined parameters to the diffusion coefficient

$$\frac{d\left[\frac{1}{T_{1\rho}}\right]}{d\left[\omega_1^{1/2}\right]} = \frac{-\sqrt{2}\,\gamma^4 \hbar^2 \pi N}{20\,D^{3/2}} \qquad [12]$$

Treatment of the system in terms of a weak collision theory model (66) such that many diffusive jumps are required to relax the spin system, or expressed another way $\tau \ll T_{1\rho}$, satisfies the limitation on ω_1 that $H_1 > H_{loc}$.

The above theory is based on isotropic diffusion in three dimensions and is not directly applicable to the system in which we are interested. Using a simple argument based on random walk theory (67), the lateral diffusion coefficient may be obtained for the case of translation in two dimensions only (diffusion in the plane of a phospholipid bilayer) by a minor modification of eq [12].

The sensitivity of the frequency dependent spectral density term is intimately related to the size of the Larmor period ($T=2\pi/\omega$) and the correlation time for the diffusional jump motions (taken to be the time τ between diffussive jumps). It is convenient then to use the Larmor period to define a segment of time T over which diffusion of a spin may occur. After this time T a spin will have associated with it in any arbitrary direction a mean squared displacement

$$\langle s^2 \rangle = 2D'T \qquad [13]$$

where D' is the diffusion coefficient for isotropic diffusion in one dimension. Adding the degrees of freedom necessary to construct a two and then a three dimensional system

the mean squared displacement is related to the diffusion coefficients for isotropic diffusion in two and three dimensions, respectively,

$$2\langle s^2 \rangle = 4 D'' T \qquad [14]$$

$$3\langle s^2 \rangle = \langle r^2 \rangle = 6 D''' T \qquad [15]$$

where D'' and D''' are the diffusion coefficients for isotropic diffusion in two and three dimensional systems respectively. In eq [15] the mean squared displacement is replaced, for three dimensional isotropic diffusion, by the mean squared jump distance $\langle r^2 \rangle$. In defining the problem of spin relaxation due to translational molecular motions, the extent of the relaxation is assumed invariant to the dimensionality of the system, i.e., the spin "knows" only that it is being influenced by the dipolar fields of neighboring molecules but is unaware as to whether the motions are parallel or perpendicular to the plane in which it sits. In contradistinction, the respective diffusion coefficients are inherently products of the dimensionality of the spin system and therefore reflect whether isotropic diffusion in two or three dimensions is involved. Thus if diffuson is isotropic in three dimensions, the net displacement or mean squared jump distance in the defined period of time T is 6D'''T. If, however, the diffusion is two dimensionally isotropic

the resulting relaxation in the period of time T is expected to be the same and thus the net displacement must also be the same but it is expressed as 4D''T. Equating these two representations of the net displacement yields the relations

$$4D''T = 6D'''T \qquad [16]$$

$$D'' = 3/2\,D''' \qquad [17]$$

where D'' is the diffusion coefficient for isotropic diffusion in a two dimensional system. Thus, substitution of the two dimensional diffusion coefficient D'' into eq [12] and eliminating the primes, eq [18] relates the frequency dependence of the spin-lattice relaxation rate in the rotating frame to the diffusion coefficient appropriate for a two dimensionally isotropic system:

$$\frac{d\left[\frac{1}{T_{1\rho}}\right]}{d\left[\omega_1^{1/2}\right]} = \frac{-3\sqrt{3}\,\gamma^4\hbar^2\,\pi\,N}{40\,D^{3/2}} \qquad [18]$$

Equation [18] will find practical utility[5] in that measurements of the rotating frame spin-lattice relaxation rate as a function of the radiofrequency strength H_1 ($=\omega_1/\gamma$) will yield directly the two-dimensional (or lateral) diffusion coefficient in phospholipid bilayer systems as long as an estimate of the spin density N of a sample can be made.

---

[5] See Chapter 4.

CHAPTER 3

EXPERIMENTAL CONSIDERATIONS

3.1. Chemicals and principal materials.

The source and other pertinent information for the phospholipids studied are as follows. Dipalmitoyl DL-α-phosphatidylcholine (DPPC), grade I, crystalline synthetic (approximately 99% pure), Lot 103C-2790-1; Dimyristoyl L-α-phosphatidylcholine (DMPC), crystalline synthetic (approximately 98% pure), Lot 66C-01881; Dioleoyl L-α-phosphatidylcholine (DOPC), in chloroform solution (20mg/ml), (approximately 98% pure), Lot 116C-8111; and L-α-phosphatidyl-L-serine (PS), from bovine brain extract, in chloroform-methanol (95:5) solution, Lot 28C-8365 were obtained through the Sigma Chemical Co. of St. Louis, MO, and used without further purification. L-α-lecithin, β-γ-dipalmitoyl (DPPC), grade A synthetic, Lot 501926; L-α-lecithin, β-γ-dilauroyl (DLPC), grade A synthetic, Lot 740092; and L-α-lecithin, β-γ-distearoyl (DSPC), grade A synthetic, Lot 740123 were obtained through Calbiochem, San Diego, CA and used without further purification. Di(perdeutero-palmitoyl) phosphatidylcholine (DPPC-d_{62}) was purchased in sealed ampoules from Lipid Specialties of

Boston, MA, as a solution in 15% chloroform and 85% benzene, Lots H-2-001 and 003. These, also were used without further purification steps. Aldrich-Diaprep Inc. deuterium oxide (D_2O), 100 atom%, Gold Label, was used in the preparation of all samples. The only exception being the use of 99.8% D_2O in the initial exchange stages with the bovine rod outer segment membranes. Prepurified nitrogen gas was used in all instances. Mallinckrodt Analytical Reagent grade chloroform ($CHCl_3$) was used in all preparative steps. Crystalline nickle chloride ($NiCl_2$), used as a NMR relaxation time standard solution, was taken from the laboratory shelf and dried to constant weight after recrystallizing from twice distilled water.

Bovine rod outer segment (ROS) membranes and extracted lipids from these membranes were kindly provided by Dr. Ed Dratz and Alan Deese from the University of California, Santa Cruz.

NMR experiments were also performed on a sample containing DPPC/DPPC-d_{62} in a 50-50 weight composition ratio loaned to us by Dr. S. I. Chan at the California Institute of Technology, Pasadena, CA.

NMR sample tubes were constructed from ordinary 5mm O.D. glass tubing with an I.D. of 3.38mm.

3.2. NMR sample tube design.

Specially constricted 5mm NMR tubes are available commercially from the Wilmad Glass Co., Inc., Buena, NJ. However, these were found to be extremely susceptible to breakage at the constriction when centrifuged.

Glass tubing was cut into sections of approximately 20cm in length, cleaned in chromic acid cleaning solution, and rinsed thoroughly with twice distilled water. When dry, an oxygen-natural gas blowpipe was used to seal one end of the tube and to form a constriction with a throat of from 1.5 to 2.5mm at a point 6 to 7 cm from the sealed end of the tube. Structural integrity was insured by making the outside diameter of the glass around the constriction as nearly as possible the same as for the rest of the tube, i.e., 5mm.

When the tubes were ready for sealing, a vacuum line was attatched to the open end and heat applied evenly around the tube's circumference from 5 to 6cm above the constriction. The vacuum inside the tube enhanced the sealing process by collapsing the tube walls. Throughout the sealing process the portion of the tube below the constriction (where the sample is located) was emersed in an ice bath to prevent heating of the sample.

3.3. Preparation of phospholipid dispersions.

The commercial phospholipid samples and extracted lipids from ROS membranes were prepared according to the following scheme. The crystalline phospholipids were dissolved in a minimal amount of analytical reagent grade chloroform and the solution transfered to preweighed sample tubes. Phospholipids received as organic solvent solutions were crystallized by evaporating the solvent with a stream of nitrogen gas and redissolved in a minimal amount of analytical reagent grade chloroform and then transfered to preweighed sample tubes. The bulk solvent was evaporated from the sample tubes by directing a jet of prepurified nitrogen over the surface of the solution through an extruded glass capillary inserted into the sample tube. When all visible traces of solvent were removed the sample tube was evacuated to 0.1-0.01 mm Hg at 70°-90°C for 14-16 hours to remove any traces of solvent left after the evaporative process. To minimize the possible oxidation of samples containing lipid chain unsaturation, these samples were not subjected to the higher temperatures during the vacuum process. The tubes were then re-weighed, the appropriate quantity of D_2O was micropipetted into the sample tube, the tubes were re-weighed for accurate concentration determination, nitrogen was flushed through the tube and the tubes were sealed under house vacuum as described in the previous section. At no time were the samples subjected to prolonged exposure to the atmosphere.

The shipping solvent was stripped from the DPPC-d_{62} and the resulting crystalline solid redissolved in chloroform. Samples containing deuterated phospholipid were prepared by dissolving the appropriate amount of normal DPPC in the DPPC-d_{62}/chloroform solution. The rest of this preparation for the deuterated phospholipid samples parallels the above description except the samples were left at room temperature while under vacuum.

The ROS membranes were obtained as a suspension in 99.8% D_2O under an argon atmosphere. At all subsequent stages of preparation a nitrogen atmosphere was layered over the ROS membranes and the D_2O was deoxygenated with prepurified nitrogen gas. The suspension was centrifuged using a SS-34 rotor in a Sorvall® RC-5B Refrigerated Superspeed Centrifuge at 18,000 rpm for approximately 1.5 hours at 5°C. The clear D_2O was removed from the centrifuge tube and the ROS membrane pellet was resuspended in a fresh quantity of D_2O. This was done three times with 99.8% D_2O and three times with 100% D_2O. After the third pelleting in 100% D_2O, the material was freeze-dried three times, resuspending each time with 100% D_2O. After the final freeze-drying step the resuspended ROS membranes were pelleted once more, the supernate discarded and the pellet transfered to a Wilmad 507pp NMR tube. The tube was flushed with nitrogen and the cap securely placed and sealed on the tube with parafilm.

Homogeneous multilamellar dispersions of all the commercial phospholipids were prepared by centrifuging the

samples through the constriction in the sealed sample tube at least 9-10 times while maintaining the sample above the phase transition temperature. This mechanical agitation is required to expedite the hydration of the phospholipids in the high concentration range used in these experiments. The centrifugation procedure was carried out prior to each experiment to insure the homogeneity of the lamellar dispersions.

An opaque-to-solid white looking substance below the phase transition temperature and a translucent-to-clear looking substance above the phase transition temperature is seen upon visual inspection of the resulting multilamellar dispersions. Their consistancy appears to be much like Vaseline® petroleum jelly.

3.4. Instrumentation.

The collective proton resonance of the model membrane systems was monitored at 44.376 MHz using a modified coherent pulse CPS-2 pulsed NMR spectrometer and PGS-2 pulse programmer built by Spin-Lock Electronics Ltd. of Canada in conjunction with a JEOL model 4H-100 electromagnet and power supply operated at 10.419 kGauss. Visual inspection of the NMR signal was made on a Tektronix 465 oscilloscope. Variable temperature capability was supplied by a JEOL model JES-VT-3 temperature controller enabling the use of a constant temperature within $\pm 0.5^{\circ}C$ as monitored by a Fluke

2100A digital thermometer equipped with a copper-constantin thermocouple. Liquid nitrogen was used with the temperature control apparatus for attaining temperatures below 30°C. Air velocity in the probe was rapid enough to allow temperature equilibration of the samples at the extreme temperatures used within 5-7 minutes. The NMR free induction decay (FID) was sampled with a Princeton Applied Research CW-1 boxcar integrator and the resulting output read on a Hewlett-Packard model 3034A digital voltmeter to three significant figures. A schematic diagram of the equipment configuration is shown in Figure 3-1.

3.5. Spectrometer modification and probe design.

Modification of the Spin Lock CPS-2 44.376 MHz NMR spectrometer and a new probe design were necessary. The areas demanding attention were: (1) Impedance matching of the spectrometer transmitter output stage and the tuned resonant circuit in the probe to attain optimal power transmission. (2) Optimization of the electronic characteristics of the probe design for maximal signal-to-noise attainment. (3) Design and construction of a probe with efficient temperature control features.

3.5.1. Impedance matching. The goal of the spectrometer modification was to deliver an output impedance of 50 ohms purely resistive impedance ($50\Omega\angle 0^{\circ}$), where the phase angle (resistance phase angle) is the amount by which the voltage

FIGURE 3-1

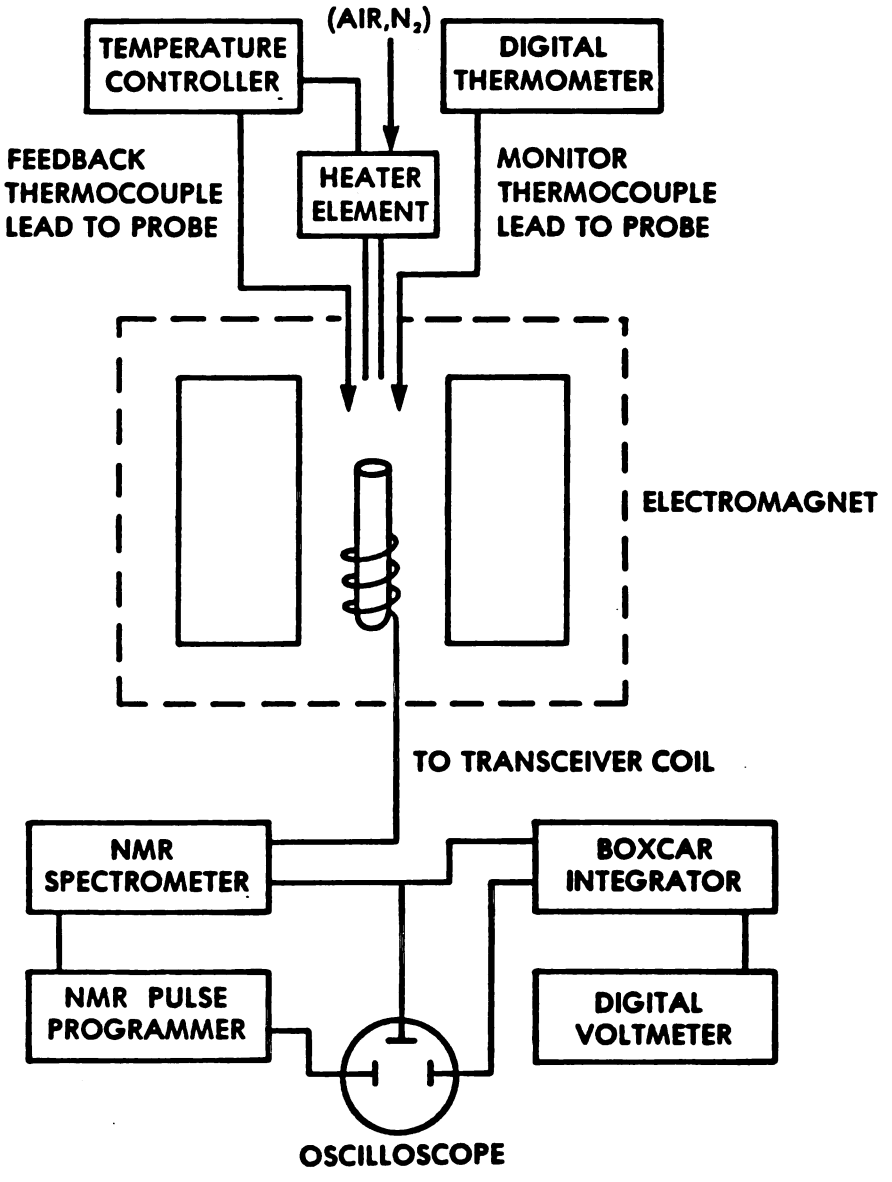

Figure 3-1: Block diagram of the NMR and accessory instrumentation used.

lags or leads the current, i.e., whether the reactance is of a capacitive or inductive nature respectively. If 50Ω coaxial cable is used between the transmitter and probe (and assuming the probe is designed to "look at" 50Ω∠0°, i.e., a 50Ω input impedance) the cable does not contribute to the tuning of the resonant circuitry in the probe. The schematic diagram for the output stage of the transmitter is shown in Figure 3-2.

Three major alterations of the "old" output stage were made to arrive at the configuration of Figure 3-2. It was necessary to replace the coil at the point where the radiofrequency signal is inductively coupled into the output stage from the "push-pull" type power amplification stage. The design of this inductor, L_1 in Figure 3-2, to yield the approproiate resistance and inductance was essentially a "trial and error" process rather than a theoretically-based approach. Second, it was necessary to "tune" the circuits with the appropriate capacitance, C_1 in Figure 3-2, to give the transmitter tuning capacitor on the spectrometer a sensitive range of operation. The third modification was the addition of a 50Ω test circuit which can be switched into operation at any time to assure that maximum radiofrequency power is in fact being achieved, or to preset the transmitter's output impedance to 50Ω if it has been detuned. The test circuit tuning is accomplished by observing a radiofrequency signal fed out of an observe channel of the spectrometer and adjusting the transmitter tuning knob to

FIGURE 3-2

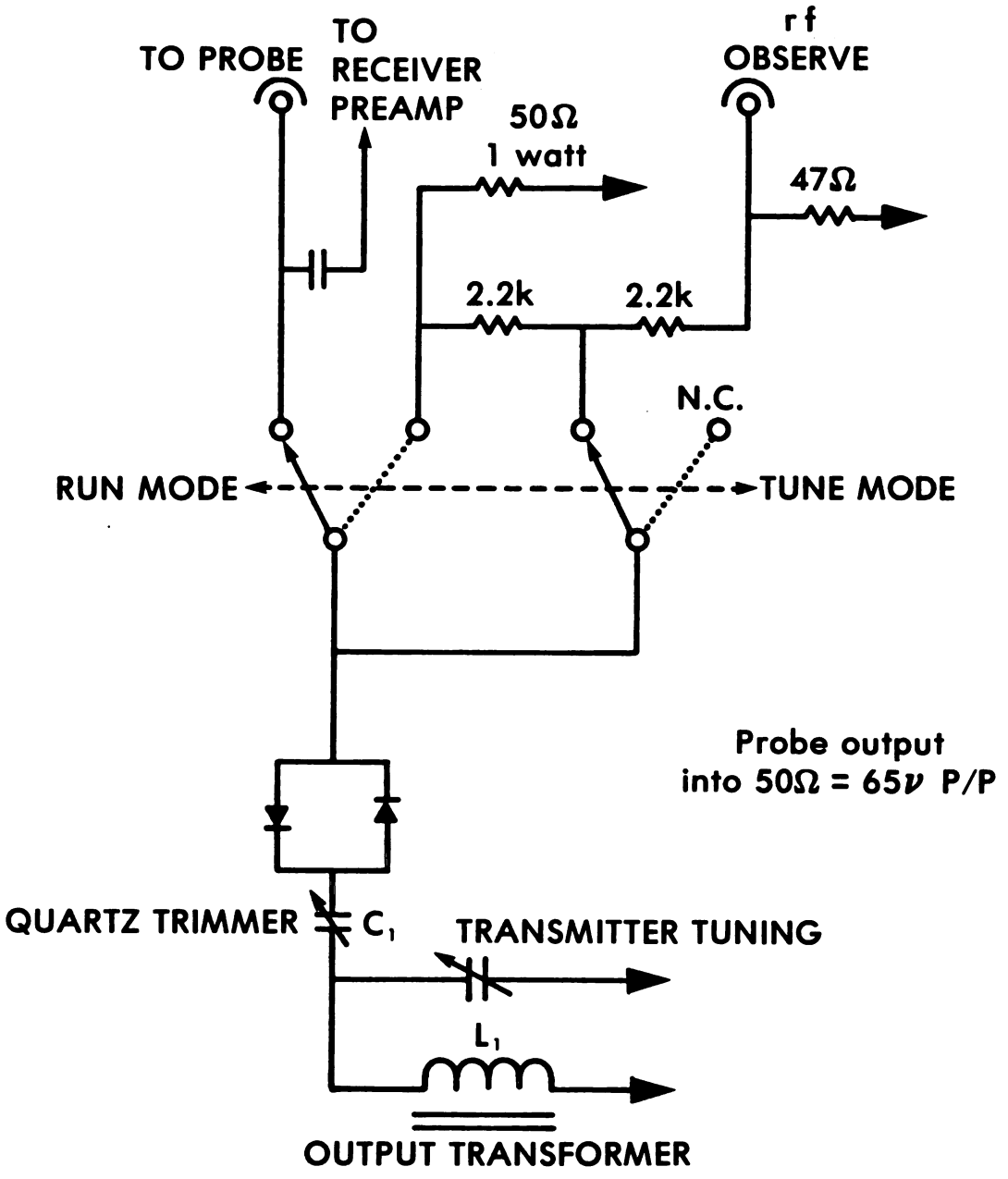

Figure 3-2: Schematic diagram of the modified CPS-2 pulsed NMR spectrometer transmitter output stage.

obtain a maximum amplitude of the radiofrequency pulse. Tuning the transmitter and the probe together when in the operative (or run) mode will be discussed after the probe design is discussed.

3.5.2. Probe design. A single coil probe is used, the coil serving both as the transmitter and receiver. The coil is basically an inductor, one of the "active" components of the resonant tuned probe circuit. The usual properties of an inductor such as wire size and coil dimensions were considered in constructing a coil suitable for the probe circuit. The choice of circuit configuration was a series-parallel resonant tuned circuit giving rise to "tunability" at frequencies mid-range to those offered by a high impedance parallel or low impedance series resonant circuit alone. The schematic diagram for the probe circuit is given in Figure 3-3. The inductor, i.e., the probe coil was designed to have a relatively high Q or quality factor necessary for attainment of a good signal-to-noise ratio (70,71). Wire spacing for the coil was calculated so as to minimize proximity effects (70,71) associated with the conductance of the radiofrequency signal along the surface of the wire (skin effects).

The probe was adjusted to $50\Omega\ \angle 0^{\circ}$ using a vector impedance meter (VIM). A 44.376 MHz signal from the VIM was fed into the probe and the two capacitors, C_2 and C_3, (see Figure 3-3) were adjusted such that a resistance of 50Ω and a phase angle of 0° was read on the VIM.

FIGURE 3-3

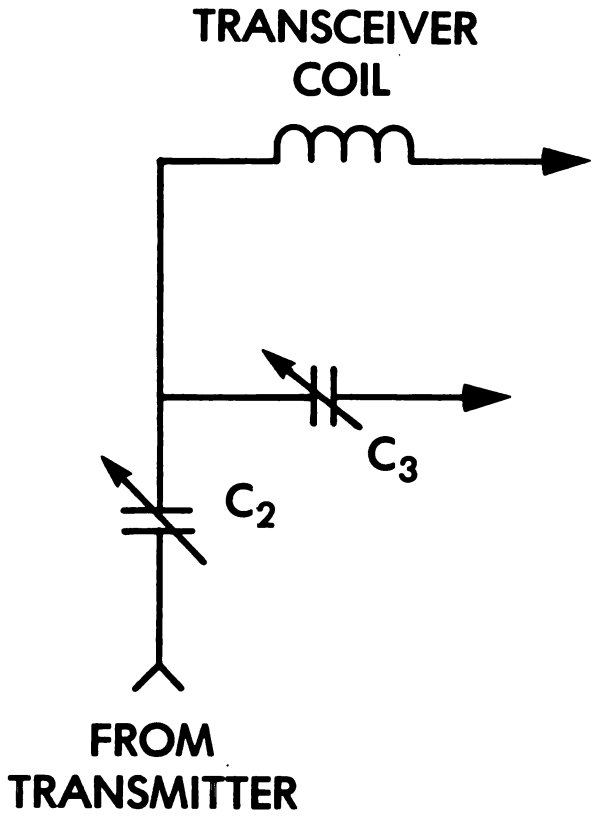

Figure 3-3: Schematic diagram of the probe circuit designed for use with the CPS-2 pulsed NMR spectrometer.

The potential dielectric loss due to the presence of the sample in the probe coil may consequently alter the quality factor and resonant tuning of the probe circuit. Thus, the probe was always tuned with the sample in the coil.

Use of the 50 ohm test circuit, and tuning the probe to 50Ω with the VIM allows impedance matching of the transmitter and probe. It is also possible to monitor the actual radiofrequency signal being transmitted using the "dipstick" method. This method employs a small coil inserted into the NMR probe which serves as an antenna. The signal it receives from the spectrometer radiofrequency pulse can be observed and the tuning can be done by adjusting the transmitter tuning and probe tuning capacitors to find the maximum in the radiofrequency signal received by the dipstick.

The probe design is shown in Figures 3-4 and 3-5. The probe housing was made of machined copper tubing. The coil was positioned inside a section of glass tubing supported in the copper tube by teflon rings. The sample tube support was fashioned from a teflon plug placed over the top of the copper tube. A BNC connector was installed in the side of the probe for connecting the Pomona® box containing the tuning capacitors.

The probe was securely fitted in a teflon block to which the temperature control apparatus was connected. The feed-back thermocouple was inserted in the bottom of the teflon block. A diagram of the air-flow in the probe is

FIGURE 3-4

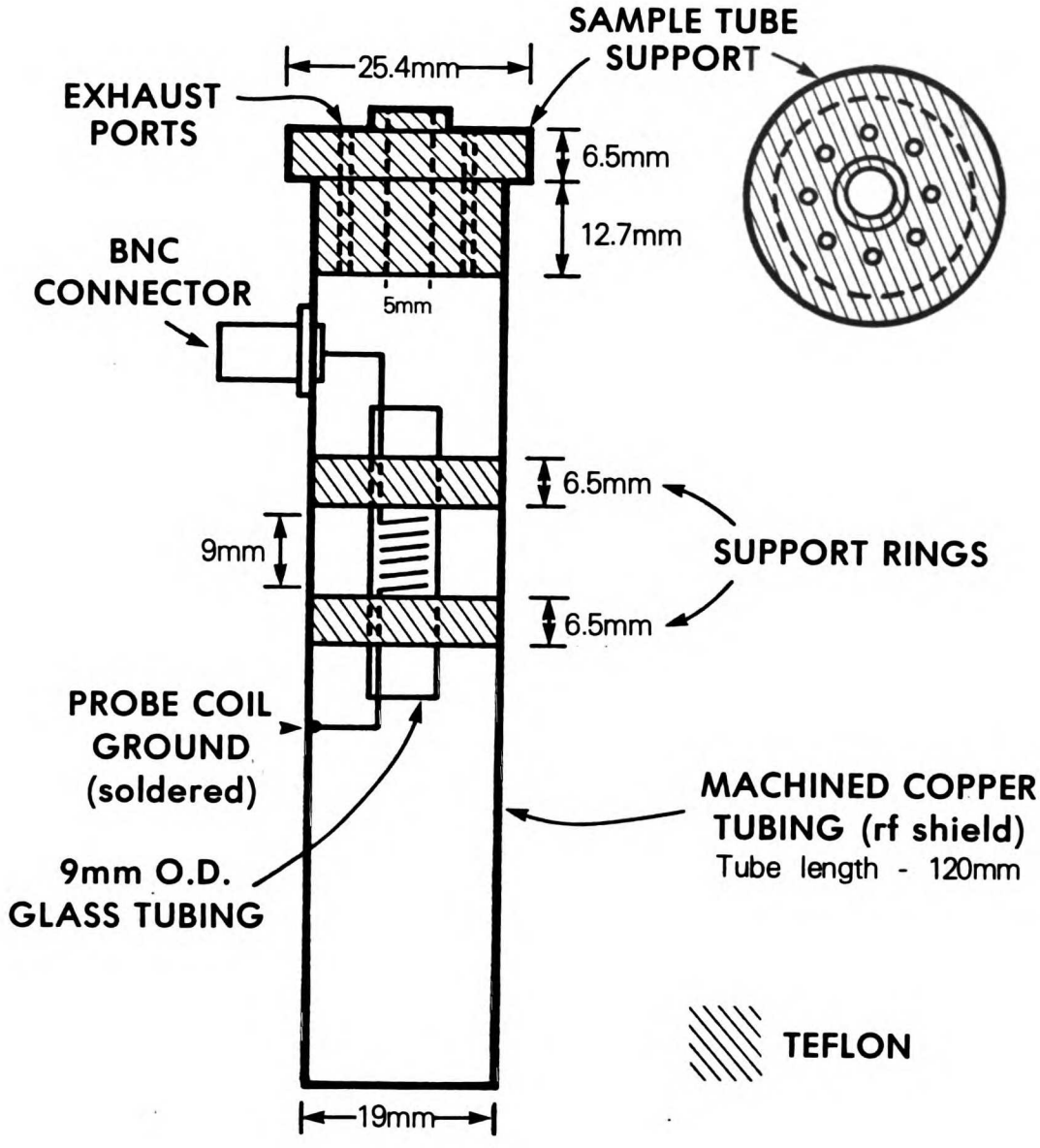

Figure 3-4: Diagram of the probe head constructed for use with the CPS-2 pulsed NMR spectrometer at 44.376 MHz.

FIGURE 3-5

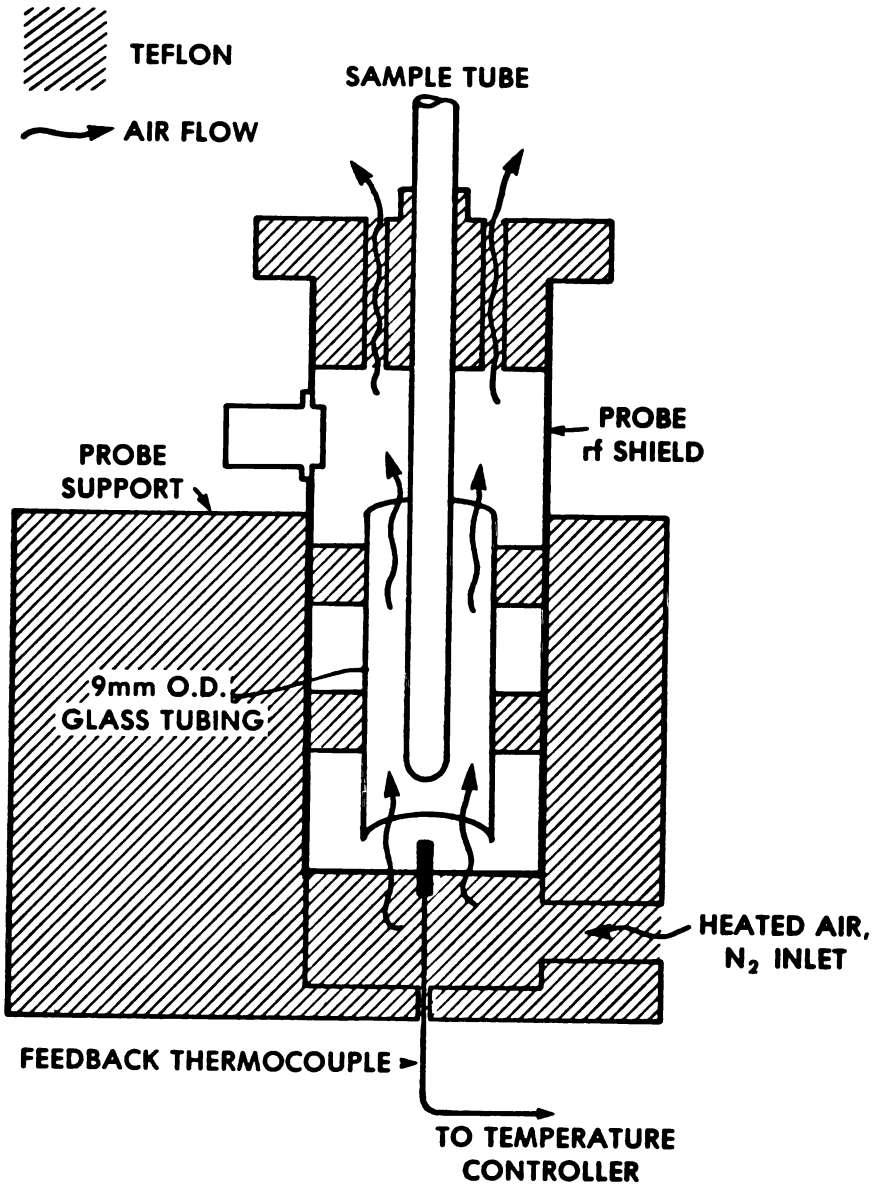

Figure 3-5: Cut-away view of the probe illustrating the temperature control features of the probe.

FIGURE 3-5

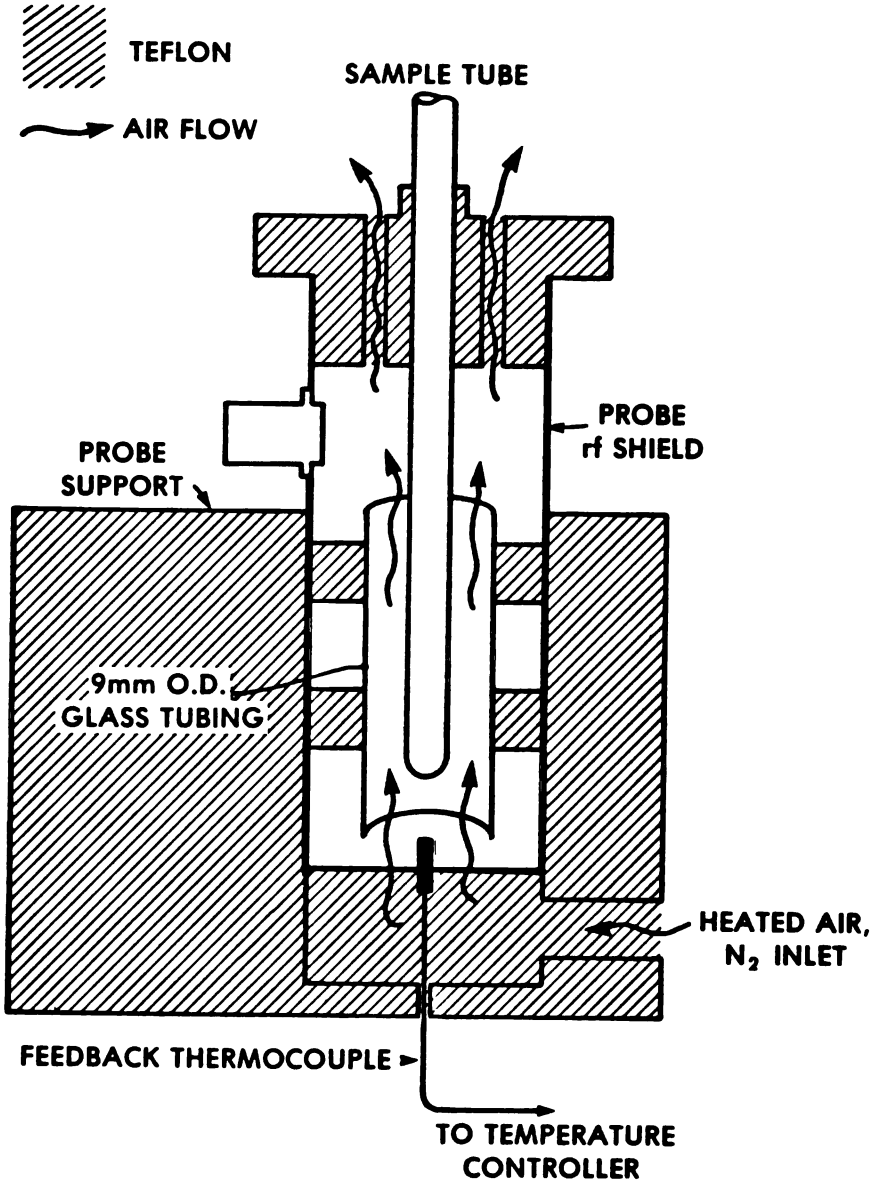

Figure 3-5: Cut-away view of the probe illustrating the temperature control features of the probe.

given in Figure 3-5.

3.6. Detector linearity.

To check whether or not nonlinearity of the spectrometer detection system was a contributing factor to the deviations from single exponential relaxation behavior observed in the phospholipid rotating frame relaxation data (see Figure 4-2), several tests were performed. Coincidently, results of some of these tests provide an indication of the overall accuracy of the relaxation measurements performed with this pulsed NMR instrument.

Proton T_1, $T_{1\rho}$, and T_2 measurements were made on a paramagnetically doped water sample (100 mM $NiCl_2$). T_1 was measured using the inversion recovery method, employing a [π-τ-$\pi/2$] radiofrequency pulse sequence. T_1 is determined by observing the recovery of the initially perturbed magnetization during the time τ, the time between radiofrequency pulses according to

$$(M_\infty - M_\tau) = 2M_\infty \exp\left\{-\frac{\tau}{T_1}\right\} \qquad [1]$$

M_∞ is the FID magnitude after an infinitely long τ spacing in the pulse sequence which is measured simply as the magnitude after a single 90° radiofrequency pulse and M_τ is the FID magnitude following the inversion recovery pulse sequence. T_2 was determined by monitoring the decay in spin

echo amplitude following the application of a Hahn pulse sequence, [$\pi/2$-τ-π-τ-spin echo], as a function of τ, according to

$$M(2\tau) \propto \exp\left\{-\left[2\frac{\tau}{T_2}\right] - \frac{2}{3}\gamma^2 G^2 D \tau^3\right\} \qquad [2]$$

where M(2τ) is the spin echo magnitude, γ the proton gyromagnetic ratio, G the field gradient across the sample due to field inhomogeneities and D is the diffusion coefficient. The $T_{1\rho}$ experiments employed the spin-locking technique described above. Figures 3-6 and 3-7 show the relaxation data from the T_1,T_2 and $T_{1\rho}$ experiments, respectively. The single exponential behavior expected for the water protons is, in fact, observed in all three cases, consequently alleviating the concern as to detector nonlinearity. The linearity of the T_2 data in Figure 3-6 indicates that the diffusion term in eq [2] is apparently insignificant, the transverse relaxation arising predominantly from spin-spin interactions. If this were not the case the T_2 data would begin to "fall away" from the line in Figure 3-6 at the longer tau values. $T_{1\rho}$ measurements on the doped water were done with a relatively low strength spin-locking pulse, H_1, and at the maximum attainable H_1 to determine if the observed frequency dependence in the phospholipid systems arises as some instrumentally-based systematic error. This evidently is not the case, as the values of $T_{1\rho}$ at these two field strengths are identical within the limits of

FIGURE 3-6

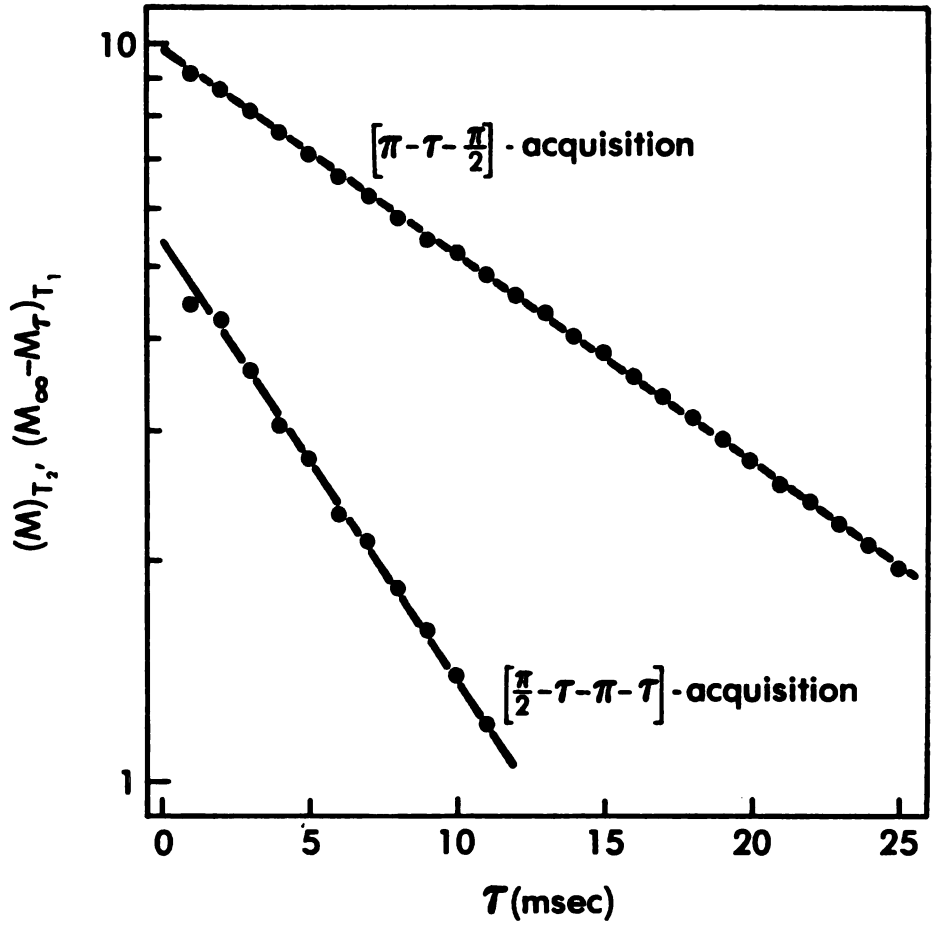

Figure 3-6: T_1 and T_2 relaxation data for water protons in a 100mM $NiCl_2$ solution. Note the single exponential relaxation behavior.

FIGURE 3-7

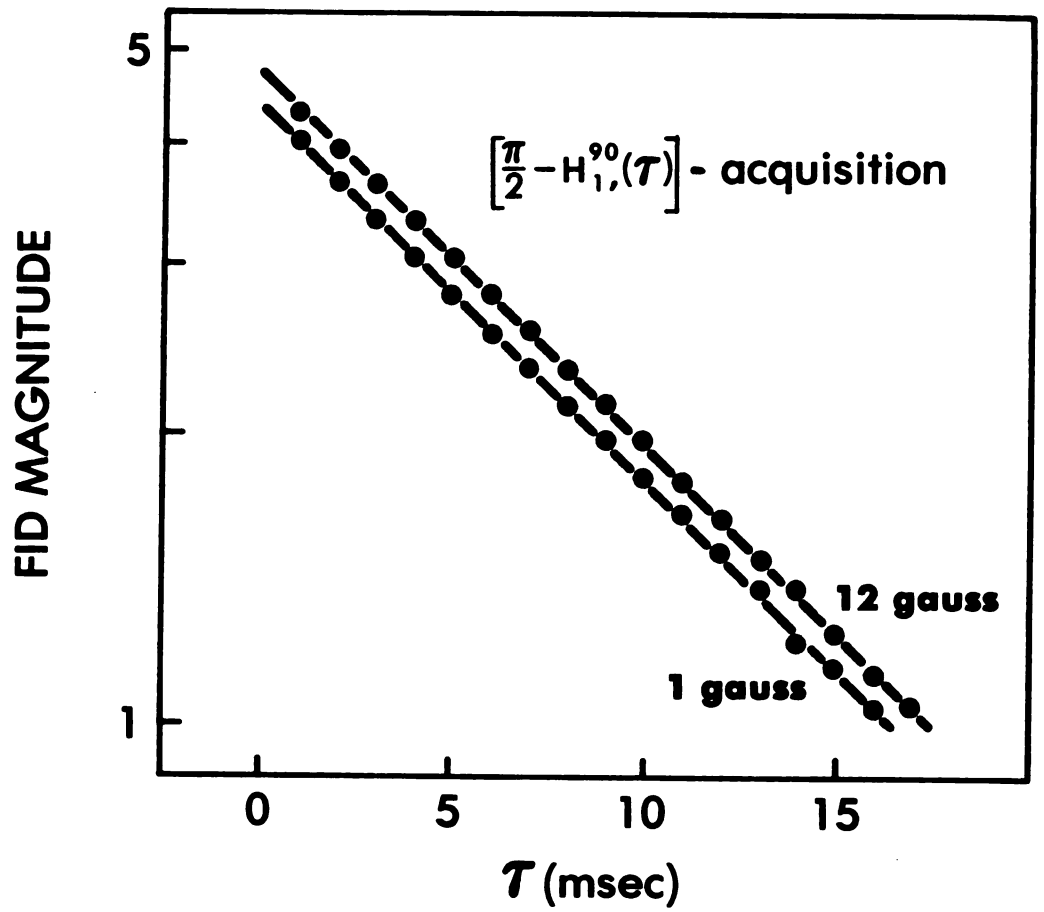

Figure 3-7: Rotating frame spin-lattice relaxation data at a low (1 gauss) and high (12 gauss) spin-locking field strength for water protons in a 100 mM $NiCl_2$ solution. Note the single exponential behavior and the identical slopes of the two sets of relaxation data.

experimental error.

T_1 and T_2 relaxation times were also measured at 100 MHz using the Varian XL-100 FT NMR spectrometer with Nicolet 1080 computer system. Both T_1 and T_2 values determined with the Spin Lock pulsed NMR spectrometer at 44.376 MHz and with the XL-100 FT NMR at 100 MHz show single exponential relaxation, the relaxation times being identical within experimental error, as given in Table 3-1. The results also compare favorably with the values determined by Morgan and Nolle (69).

Another test for detector linearity was performed in the following way. The Spin Lock spectrometer is capable of providing two radiofrequency pulses, A and B. The A pulse length was adjusted to give a FID maximum, i.e., a 90° or $\pi/2$ pulse and the B pulse adjusted such that $t_B < t_A$ (where t_A and t_B are the pulse lengths), i.e., such that the magnitude of the FID following B was small compared to that formed with the A pulse. This gives rise then to a situation in which the receiver is fed a high level and a relatively low level input signal. The ratio of magnitudes $(FID)_B/(FID)_A$ was then determined as a function of spectrometer receiver gain, operating in both phase and diode detection modes. Figure 3-8 reports this data and indicates the linearity of the detector output response with respect to the input signal.

Table 3-1: Experimentally determined values of T_1 and T_2 at 44.376 and 100 MHz for the water protons of a 100 mM $NiCl_2$ solution.

T_1 (msec)	T_2 (msec)	NMR FREQUENCY (MHz)
15.7	15.1	44.376
15.7	15.9	100

FIGURE 3-8

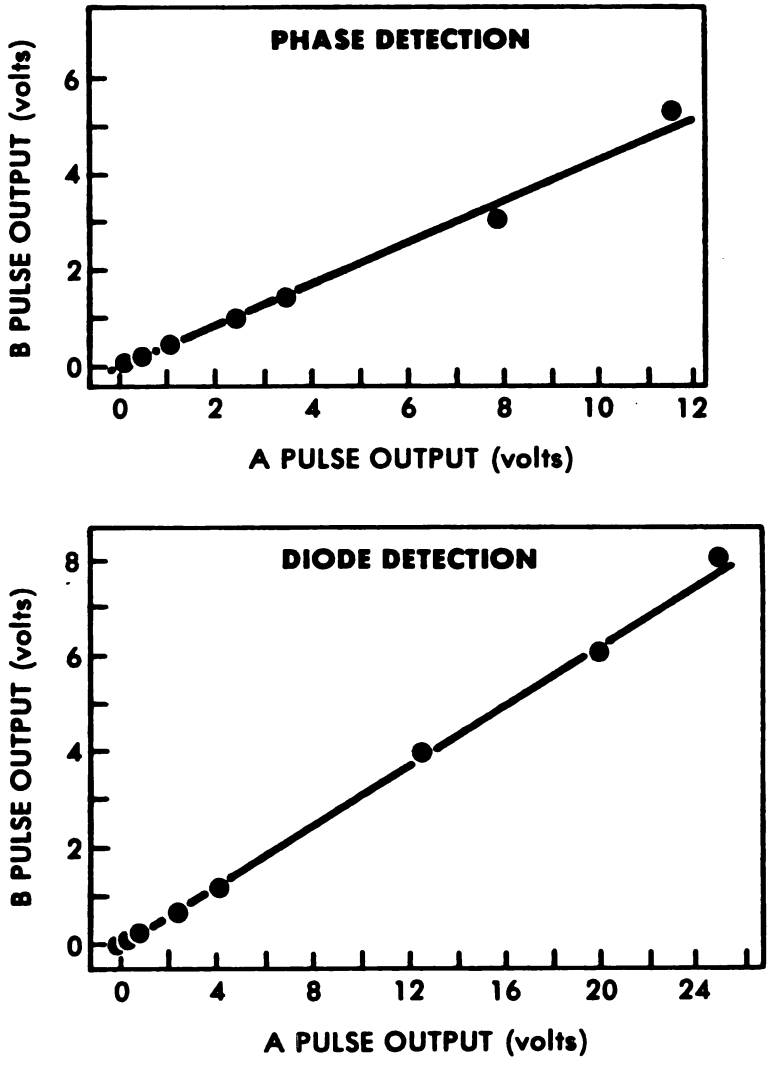

Figure 3-8: Detector output ratios for low-level and high-level input signal to the receiver for increasing receiver gain.

CHAPTER 4

LATERAL DIFFUSION IN PHOSPHOLIPID BILAYERS

4.7. Rotating frame NMR experiment.

Rotating frame spin-lattice relaxation time ($T_{1\rho}$) experiments were performed on the phospholipid and ROS membrane samples according to the spin-locking method described by Solomon (65). Immediately after applying a 90° radiofrequency pulse along the x' axis in the rotating reference frame, a second radiofrequency pulse of magnitude H_1 but phase-shifted by 90° with respect to the initial pulse such that its vector lies along the y' or detector axis, is applied for a time τ. Figure 4-1 illustrates the experimental sequence. The magnitude of the FID is then monitored as a function of τ, the length of time the phase-shifted "spin-locking" pulse is applied. The time constant for the resulting exponential decay of the FID magnitude is $T_{1\rho}$:

$$M(\tau) = M_o \exp\left\{-\frac{\tau}{T_{1\rho}}\right\} \qquad [1]$$

The strength of the "spin-locking" field H_1 was determined

FIGURE 4-1

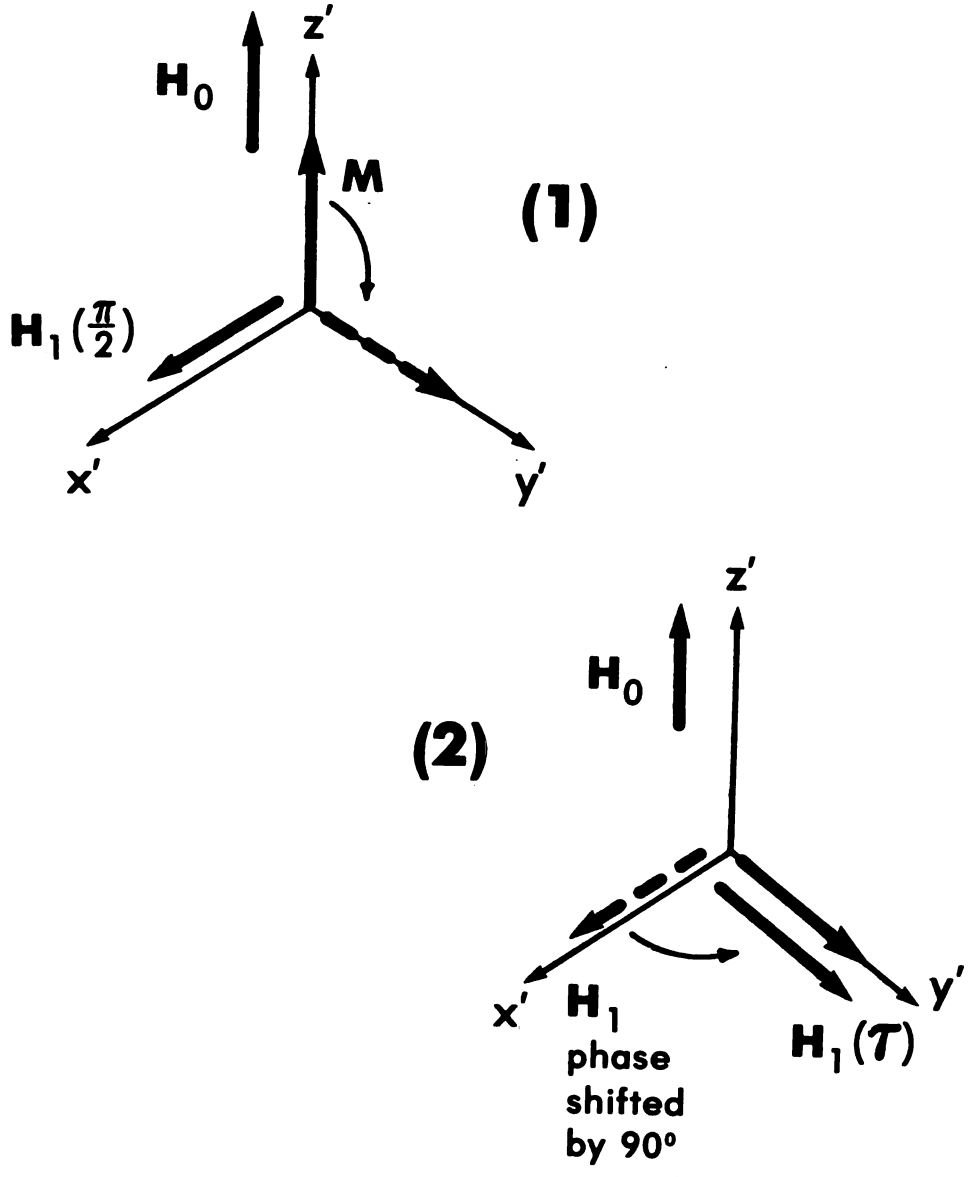

Figure 4-1: Rotating reference frame and the vector representation of the radiofrequency pulses used in the spin-locking experimental sequence.

by measuring the pulse length (t_w) required for a single pulse of magnitude H_1 to produce a null in the FID, the condition for the null being

$$n\,\pi = \gamma H_1 t_w \qquad [2]$$

Successive increments in t_w were measured corresponding to pulse lengths of π, 2π, etc. up to 7π for most cases, and then the average time $\langle t_w \rangle$ was used for calculation of H_1. The uncertainty in H_1 is on the order of 5%, the greatest probable error occurring for small values of H_1. The local dipolar field can be estimated from second moment data such that

$$H_{loc} = \left[\frac{1}{3} M_2\right]^{1/2} \qquad [3]$$

Using the second moment value of 0.4 gauss^2 reported by Veksli *et al* (68), for a 4.0 mole% DPPC/D_2O sample, eq [3] gives a value for H_{loc} of 0.365 gauss. The values of H_1 experimentally employed in this study were approximately a factor of ten larger, ranging from 1 to 15 gauss, than the local dipolar field.

Because of the residual dipolar broadening due to anisotropy of the phospholipid dispersions, T_2 is short and thus the FID for the phospholipids in the smectic liquid crystalline phase decays extremely rapidly. The FID appears to decay with two components; but the $T_{1\rho}$ values determined

from sampling only the fast, only the slow, or at the intermediate composition of the two components of the FID agree to within 5-10%. The rotating frame spin-lattice relaxation rates also exhibited a fast and a slow component. Figure 4-2 offers an example of some data typically obtained from the spin-locking experiment performed on the phospholipid dispersions.

4.8. Spin density determination.

In the second section of Chapter 2 the equation was given which describes how the diffusion coefficient may be determined from the ω_1 frequency dependence of the rotating frame spin-lattice relaxation rate

$$\frac{d\left[\frac{1}{T_{1\rho}}\right]}{d\left[\omega_1^{1/2}\right]} = \frac{-3\sqrt{3}\,\gamma^4 \hbar^2 \pi N}{40\, D^{3/2}} \qquad [4]$$

All the parameters other than ω_1, $T_{1\rho}$ and D are constants except for the resonant spin density N, the number of resonant nuclei per cubic centimeter. Since the densities of the various phospholipids are not available, they must be experimentally determined. Sheetz and Chan (72) have published some apparent molar volume data for an unsonicated DPPC/water dispersion system from which the spin density may be calculated knowing the amount of DPPC present for a given DPPC sample. The spin densities for other phospholipid samples may then be calculated from the ratio of the FID

FIGURE 4-2

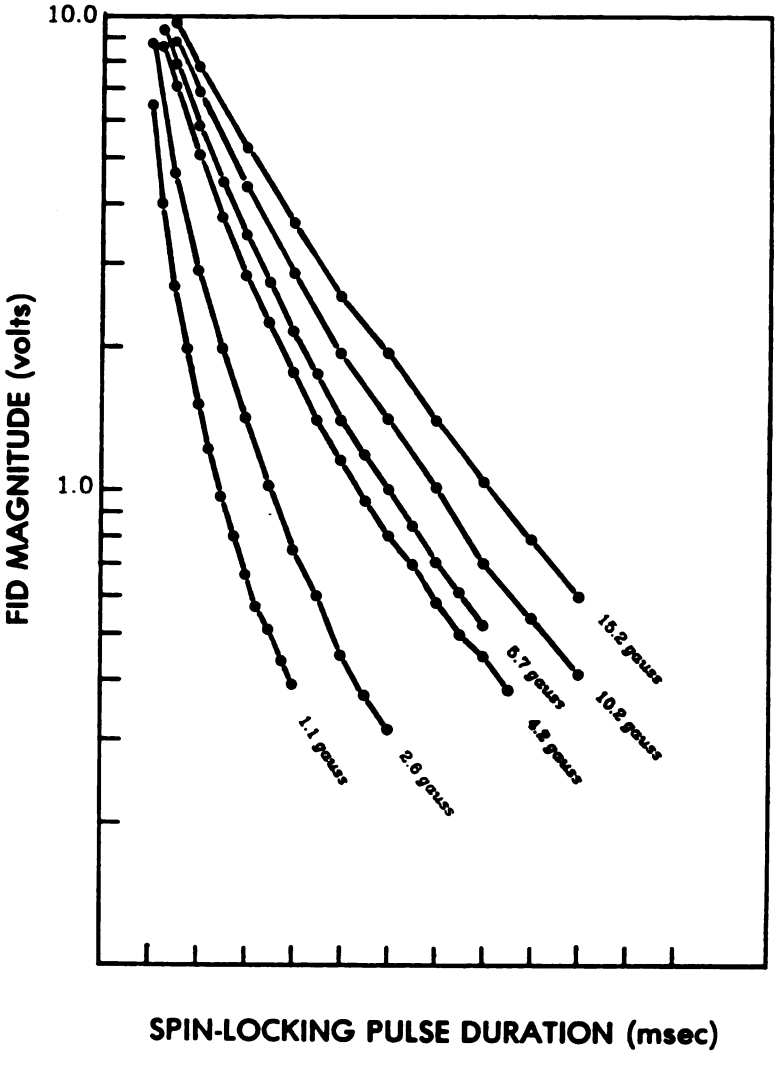

Figure 4-2: Rotating frame spin-lattice relaxation data for DMPC at 30°C. The free induction decay magnitude (FID) is plotted as a function of the spin-locking pulse duration t, in milliseconds.

amplitudes after the application of a 90° radiofrequency pulse.

The nuclear induction signal is proportional to the number of resonant spins in that part of the sample filling the NMR transmitter coil. This may be expressed as

$$M = \kappa\rho \qquad [5]$$

where M is the amplitude of the FID signal, ρ is the spin density in spins per cubic centimeter and k is a proportionality constant which includes information such as the amount of sample present in the coil, i.e., filling factor. Consider then two systems, one which has a known spin density (system A) and one for which the spin density is unknown (system B). The relation between the FID magnitude and spin density for each system can be written as

$$M_A = \kappa\rho^A \qquad [6]$$

$$M_B = \kappa\rho^B \qquad [7]$$

Assuming for the moment that the proportionality constants are identical (consideration of this point is taken up shortly), the unknown spin density is

$$\rho^B = \rho^A \frac{M_B}{M_A} \qquad [8]$$

Thus knowledge of the spin density for one system coupled

with the relative height of the FID for both the known and unknown systems yields the unknown spin density. The spin density in terms of the weight density of a substance is expressed as

$$\rho\left[\frac{spins}{cc}\right] = \rho\left[\frac{gm}{cc}\right] \times \frac{1}{MW}\left[\frac{moles}{gm}\right] \times N_A\left[\frac{molecules}{mole}\right] \times S\left[\frac{spins}{molecule}\right] \quad [9]$$

For the proportionality constants k to be identical for two samples, two conditions must exist. Both samples must have the same filling factor. It is best to carry out the measurements with the sample completely filling the transmitter coil to minimize inhomogeneity effects and eliminate position dependent variations in the absorption of transmitted radiofrequency power by the sample. The other consideration deals with the variation in dielectric loss between the two samples used in any one spin density determination. As the quality factor Q bears a relationship to the amount of stored energy of the probe's total inductance and thus to the tuning of the probe circuit, the samples to be compared as in eq [8] must be chosen such that differences in dielectric loss, if any, must be extremely small; in practice, this means the ionic strength in the two samples must be the same. If this is not the case, the probe tuning may be altered and thus the power transmitted to the two samples may differ (the respective pulse widths for a 90° pulse may be different for the two samples). If this occurs, the relative FID magnitude measurements are no

longer valid for the calculation proposed in eq [8]. For the phospholipid dispersions studied, the DPPC sample was used as the known reference. Before making the NMR FID amplitude measurements necessary for calculating the spin densities of the phospholipid samples, the probe tuning was checked on the VIM with each of the samples inserted in the probe. Variations from 50Ω purely resistive impedance were found to be negligable.

4.9. Intermolecular relaxation.

The theory treating intermolecular dipolar relaxation, due to translational diffusion, shows that a frequency dependence arises in the spectral density for spin-lattice relaxation (34,64). Furthermore, the theory provides an explicit relationship which allows the diffusion coefficient to be calculated from the experimentally measured spin-lattice relaxation rates (44). However, prerequisite to utilizing the frequency dependence of the rotating frame spin-lattice relaxation rate for determining the diffusion coefficient D, it must be demonstrated that a significant contribution to the observed relaxation rate arises from translational diffusion. The rotating frame spin-lattice relaxation rate due to intramolecular dipole-dipole interactions is given by (73)

$$\left[\frac{1}{T_{1\rho}}\right]_{INTRA} = K\left[\frac{3}{2}\frac{\tau}{1+\omega_1^2\tau^2} + \frac{5}{2}\frac{\tau}{1+\omega_o^2\tau^2} + \frac{\tau}{1+4\omega_o^2\tau^2}\right] \qquad [10]$$

in which ω_o is the Larmor frequency ($\omega=\gamma H_1$), ω_1 is the angular frequency of the spin-locking field H_1 ($\omega_1=\gamma H_1$), τ is the correlation time for the rotational motion causing relaxation, and K is a constant that depends on the nucleus being studied. Figure 4-3 gives the functional form of eq [10] for $\omega_o=2\pi x44.376$ rad/sec and several values of ω_1. Of interest is the lack of a dependence on ω_1 in the motional narrowing limit, $\omega_1^2\tau^2<<1$. Because ω_o remains constant, eq [10] becomes, in this region

$$\left[\frac{1}{T_{1\rho}}\right]_{INTER} \approx K\tau \qquad [11]$$

The temperature dependence of the relaxation rate is reflected by the temperature dependence of the correlation time. This relationship may be expressed in terms of the activation energy (E_{act}) for the motion affecting relaxation, in an Arrhenius equation (30)

$$\tau = \tau_o \exp\left\{\frac{E_{act}}{R\,T}\right\} \qquad [12]$$

where T is the absolute temperature in degrees Kelvin.

Experiments were initially performed with dipalmitoylphosphatidylcholine (DPPC) multilayers to: (1) determine if these model membrane systems exhibit a frequency dependence under motional narrowing conditions and (2) estimate the intermolecular contributions (arising from the relative translational motions of the phospholipid molecules) to the

FIGURE 4-3

PROTON ROTATING FRAME SPIN-LATTICE RELAXATION RATES

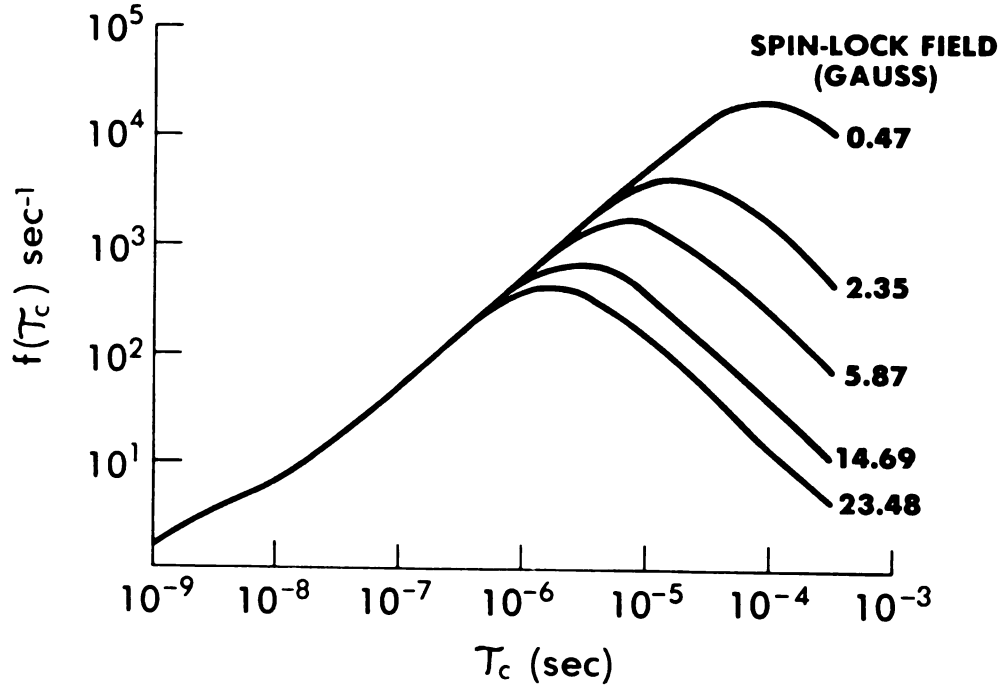

Figure 4-3: Log-log plot of $f(\tau)$, which represents the term in brackets on the right-hand side of eq [10], vs the correlation time τ for intramolecular rotational motions causing relaxation. The Larmor precession frequency, ω_o, is $2\pi(44.376$ MHz), corresponding to the frequency of our pulsed NMR spectrometer, and the family of curves represent various values of ω_1, the spin-locking radiofrequeny field angular frequency ($\omega_1 = \gamma H_1$), representative of those values used in these experiments.

rotating frame spin-lattice relaxation time $T_{1\rho}$.

Figure 4-4 shows the temperature dependence of the Zeeman (at 44.376 MHz) and rotating frame (at various spin-locking field strengths) spin-lattice relaxation rates determined experimentally for the protons of DPPC in the liquid crystalline lamellar mesophase with deuterium oxide. The concentration of the DPPC dispersion is c=72.7%, where c=weight lipid/(weight lipid + weight D_2O). The temperature-dependence is that described by eqs [11] and [12], hence we appear to be observing relaxation in the extreme narrowing limit (also see Figure 4-8). However, a frequency dependence of the relaxation rates is also apparent in Figure 4-4, a result that is inconsistent with the extreme narrowing conditions and eq [11]. A frequency-dependence would be expected if $\omega^2\tau_c^2>1$ according to eq [10], but in that case, the opposite temperature dependence would be expected. Therefore, the intramolecular relaxation picture is incompatible with the observed results and indicates that intermolecular effects may be important.

Further evidence supporting the importance of intermolecular relaxation is given in Figure 4-5. The results are from experiments in which the fully protonated phospholipids have been diluted with phospholipids whose hydrocarbon chains posses only deuterium spins. Samples in which the phospholipid is comprised of 50 (mole %) of DPPC-d_{62} and 50 (mole %) DPPC were studied with the expectation that if,

FIGURE 4-4

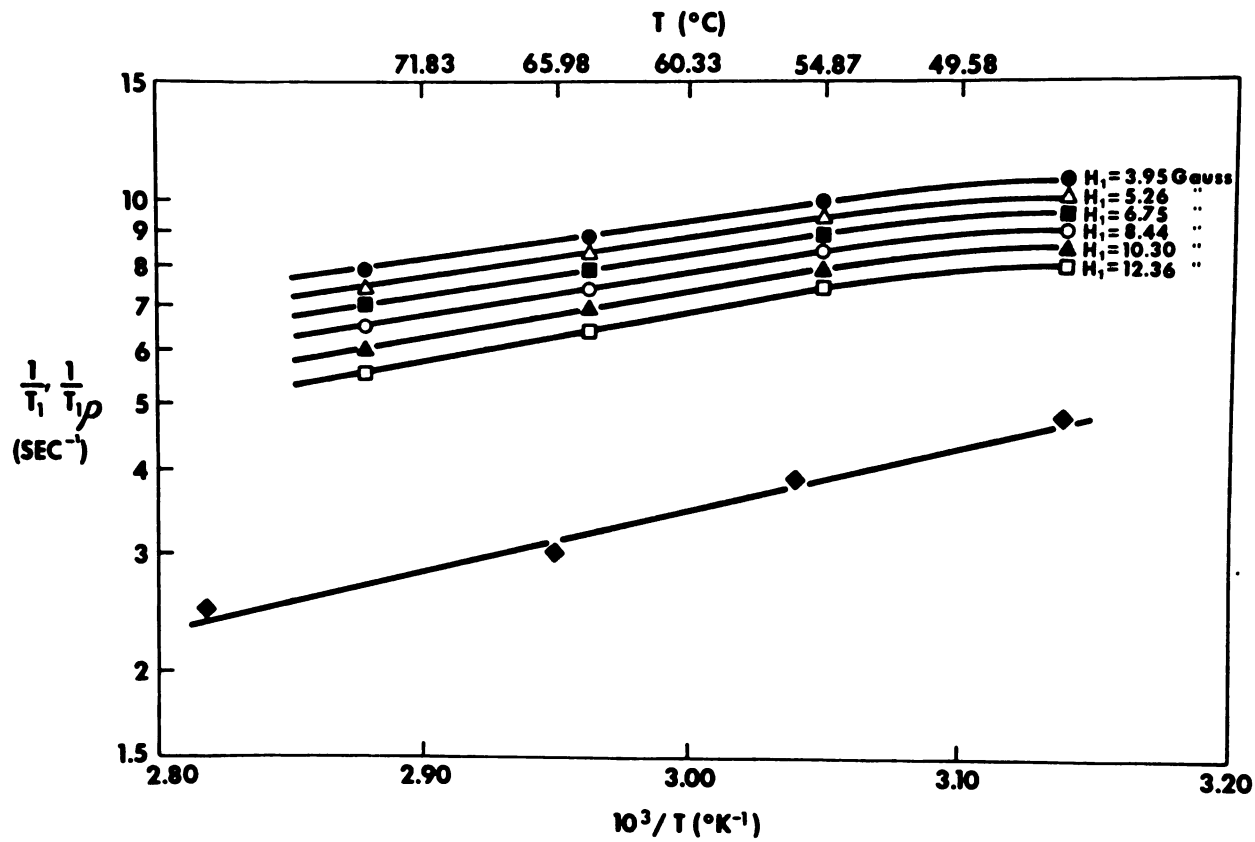

Figure 4-4: Temperature dependence of the proton spin-lattice relaxation rate $1/T_1$ (solid diamonds) and the rotating frame spin-lattice relaxation rate $1/T_{1\rho}$ measured at a Larmor frequency of 44.376 MHz for 72.7% (w/w) dipalmitoylphosphatidylcholine/D_2O. The rotating frame relaxation rate temperature dependence is shown at six different spin-locking field strengths.

FIGURE 4-5

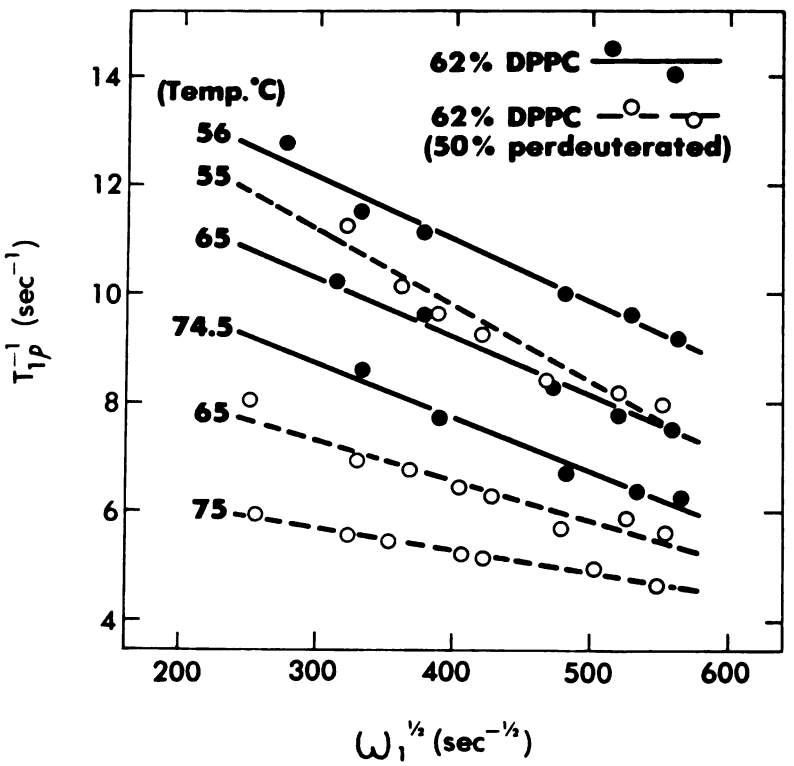

Figure 4-5: Proton rotating frame spin-lattice relaxation rate ($1/T_{1\rho}$) dependence on the spin-locking field angular frequency ω_1, where $\omega_1 = \gamma H_1$, at three temperatures for 62% (w/w) (=4.3 mole %) DPPC and 2.1 mole % DPPC/2.2 mole % DPPC-d_{62} (corresponding to 62% w/w).

in fact, intermolecular relaxation is important, the experimental $T_{1\rho}$ relaxation rates would be diminished with respect to those of the protio-DPPC sample. This is expected because of the weaker dipole-dipole coupling between deuterium and hydgrogen (^2H has a smaller value of γ, the magnetogyric ratio) which means that deuterium is much less proficient than hydrogen in promoting dipolar relaxation. The results in Figure 4-5 show that the $T_{1\rho}$ relaxation rates, for the sample in which half the DPPC molecules are perdeuterated, are 25-35% lower than the relaxation rates for the sample with normal DPPC. The intermolecular contribution to relaxation can be calculated from these results. For the fully protonated sample,

$$\left[\frac{1}{T_{1\rho}}\right]_{OBS} = \left[\frac{1}{T_{1\rho}}\right]_{INTRA} + \left[\frac{1}{T_{1\rho}}\right]_{INTER} \qquad [13]$$

and for the sample in which one half of the phospholipid molecules are perdeuterated in the hydrocarbon chains

$$\left[\frac{1}{T_{1\rho}}\right]'_{OBS} = \left[\frac{1}{T_{1\rho}}\right]_{INTRA} + 0.5\left[\frac{1}{T_{1\rho}}\right]_{INTER} \qquad [14]$$

where the intra- and intermolecular terms themselves remain fixed. Solving these two equations simultaneously yields

$$\left[\frac{1}{T_{1\rho}}\right]_{INTER} = 2\left[\left[\frac{1}{T_{1\rho}}\right]_{OBS} - \left[\frac{1}{T_{1\rho}}\right]'_{OBS}\right] = 2\Delta \qquad [15]$$

from which the contribution to the overall relaxation rate

due to intermolecular effects in these experiments is estimated to be ca. 50%. Thus the relative motion of protons due to translational diffusion of adjacent DPPC molecules in the lamellar mesophase is a significant mechanism for longitudinal nuclear spin relaxation in the rotating frame. The contribution is well-resolved from other relaxation contributions and appears to arise experimentally with a linear dependence of the relaxation rate on $\omega_1^{1/2}$ for the DPPC samples studied, as shown in Figure 4-6.

There remains the possibility that the observed frequency dependence of the $T_{1\rho}$ values arises from mixing of the dipolar and Zeeman fields (74). When the condition for exact resonance is satisfied, the rotating frame spin-lattice relaxation rate may be expressed as

$$\frac{1}{T_{1\rho}} = \frac{1}{T_{1X}}\left[\frac{H_1^2}{H_{loc}^2 + H_1^2}\right] + \frac{1}{T_{1D}}\left[\frac{H_{loc}^2}{H_{loc}^2 + H_1^2}\right] \qquad [16]$$

where T_{1D} is the spin-lattice relaxation time in the local dipolar field and T_{1X} can represent other relaxation terms including those for cross relaxation. Defining H_r^2 as H_1^2/H_{loc}^2 and performing the appropriate algebra on eq [16], a plot of $(1/T_{1\rho})(H_r^2+1)$ vs H_r^2 yields a straight line of slope $1/T_{1X}$. If there exists no frequency dependence in the "other" contributing term (T_{1X}), the intercept is, in fact, $1/T_{1D}$. In this work, nuclear magnetic dipole-dipole relaxation is the mechanism promoting relaxation and the above test is not necessary. However, the extent of a local

FIGURE 4-6

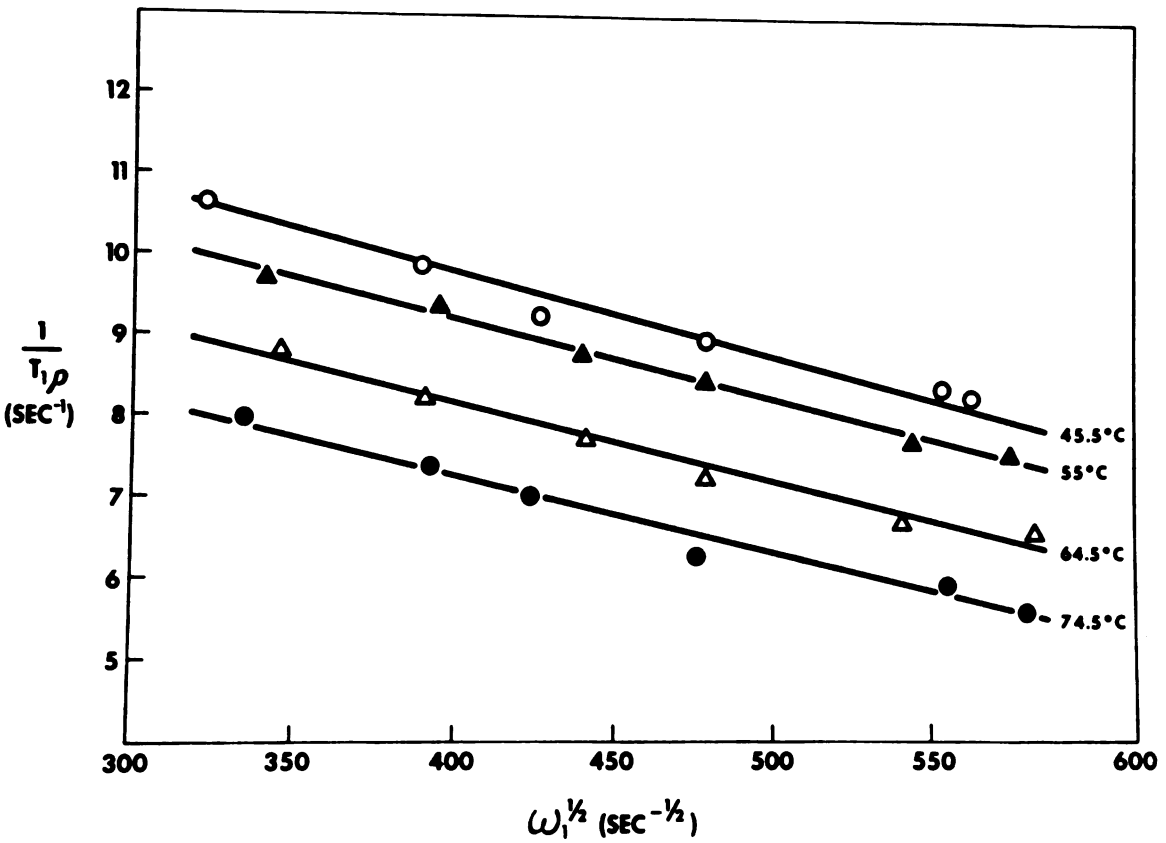

Figure 4-6: The proton spin-lattice relaxation rate in the rotating frame ($1/T_{1\rho}$) for 72.7% (w/w) dipalmitoylphosphatidylcholine/D_2O as a function of the square root of the spin-locking angular frequency ($\omega_1^{1/2}$) at four temperatures. The slope, $d(1/T_{1\rho})/d(\omega_1^{1/2})$, is used in the calculation of the lateral self-diffusion coefficient (D, cm^2/sec). The Larmor frequency is 44.376 MHz.

dipolar field contribution to the frequency dependence of the rotating frame spin-lattice relaxation rate should be evaluated. This may be accomplished by utilizing the value for H_{loc} of 0.365 gauss calculated from the second moment data of Veksli *et al* (68) (see section 1 of this chapter) and the T_{1D} value presented by Valic *et al* (75) of about 25 msec for an unsonicated DPPC dispersion. T_{1X}^{-1} was calculated from the experimentally determined $T_{1\rho}^{-1}$ values at H_1 field strengths of 3.8 gauss and 10.7 gauss and the known values for H_{loc} and T_{1D}^{-1}. $T_{1\rho}^{-1}$ values were then calculated, which included the dipolar contributions, for the limiting H_1 field strengths used. The effect of including the dipolar contribution was evaluated by comparing the calculated and experimentally determined $T_{1\rho}^{-1}$ values. These calculations indicate that approximately 10% or less of the experimentally observed change in $T_{1\rho}^{-1}$ with H_1 variation could be ascribed to the local dipolar source. Consequently, the observed frequency dependence of $T_{1\rho}$ for the protons of the phospholipids in the liquid crystalline lamellar phase is attributed to translational motion.

According to eq [11] of Chapter 2, the ω_1 frequency dependence can be used to calculate the diffusion coefficient. From a plot of $1/T_{1\rho}$ versus $\omega_1^{1/2}$, the least squares slope C of eq [11] of Chapter 2 was evaluated for each experiment and then used to calculate the lateral self-diffusion coefficients *via* eq [4] of this chapter.

The frequency dependence of the relaxation rates yields diffusion coefficients accurate to within 5% if $(\omega_1\sigma^2/D)^{1/2} \leq 2$ (44). Our estimate of σ was obtained using known values of DPPC bilayer dimensions (7,76) and the apparent molar volume of unsonicated DPPC solutions as extrapolated from results given by Sheetz and Chan (33,72). Using an estimate of 8Å for σ and the values of ω_1 corresponding to the weakest and strongest spin-locking field strengths applied, the limiting conditions are

$$\omega_1^{low} : D > 1.4 \times 10^{-10}\ cm^2/sec \qquad [17]$$

$$\omega_1^{high} : D > 5.8 \times 10^{-10}\ cm^2/sec \qquad [18]$$

which are found to be satisfied for all experiments reported in this work.

4.10. Diffusion in model membrane bilayers: Results.

Preliminary experiments were designed to test the feasibility of this novel approach to the study of diffusion in phospholipid model membranes. Diffusion coefficients were then determined from the radiofrequency dependence of the rotating frame spin-lattice relaxation rates for a variety of phospholipid systems in order to investigate several interesting phenomena associated with phospholipid bilayers. The temperature dependence of the diffusion rate was also investigated for each model system allowing the calculation of activation energies for the lateral diffusion

jump process.

Comparison of the lateral diffusion coefficients and diffusion activation energies for the various systems studied should provide some insight into the effects of the changes of various parameters of the model membrane bilayer systems on their dynamic state.

The effects of phospholipid concentration (degree of hydration) and composition (hydrocarbon chain length, presence of unsaturation and polar headgroup composition) on the rate of lateral diffusion of the phospholipid molecules in the lyotropic mesophases were investigated as these particular features are known to have profound effects on the fluidity of membrane bilayers. Lateral diffusion coefficients were determined for DPPC in the gel phase below the transition temperature T_c and experiments were designed to determine the diffusion rates of the headgroup and the hydrocarbon chain portions of the phospholipid molecule.

4.10.1. Concentration effects. Figure 4-7 shows the $\omega_1^{1/2}$ frequency dependence of $T_{1\rho}^{-1}$ for 62%, 80% and 90% (weight %) samples of DPPC in D_2O at several temperatures above the gel-to-liquid crystalline phase transition. Figure 4-8 illustrates this data in a manner that shows, in addition to the frequency dependence, the temperature dependence characteristic of the motional narrowing region. Experimental results obtained with the 50% perdeuterated sample are included. Finally, the lateral diffusion coefficients,

FIGURE 4-7

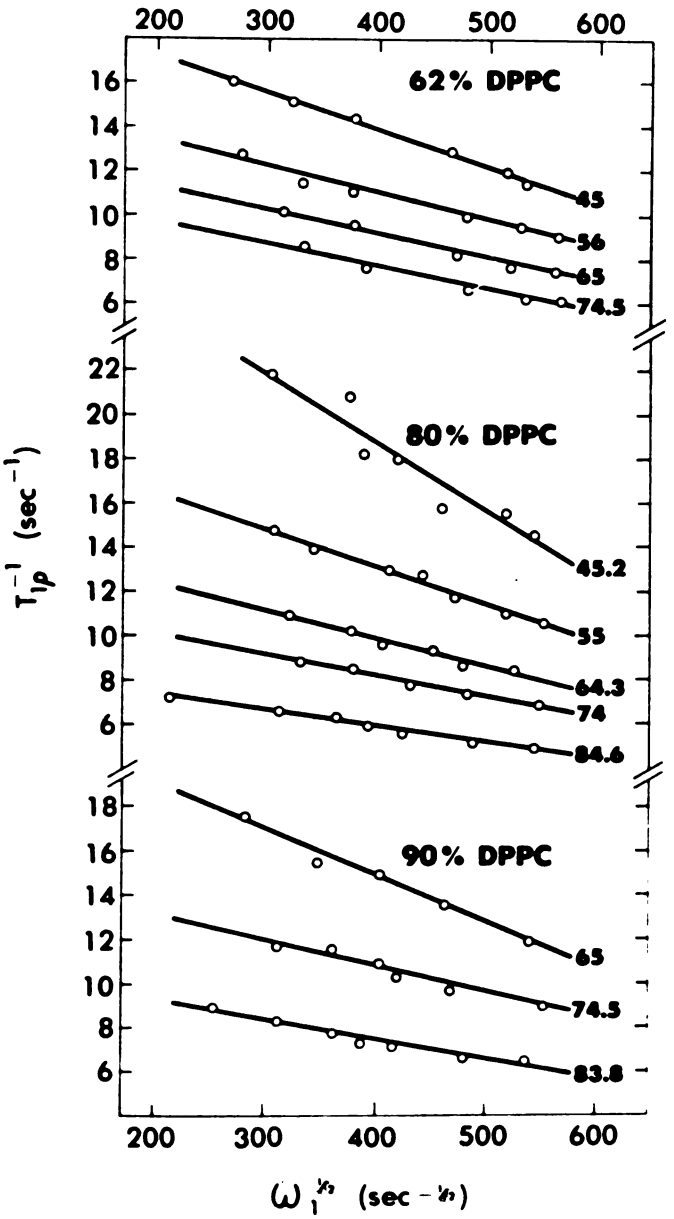

Figure 4-7: Proton rotating frame spin-lattice relaxation rate ($1/T_{1\rho}$) dependence on the spin-locking field angular frequency ($\omega_1 = \gamma H_1$) for 62, 80 and 90% (w/w) DPPC in D_2O. Each sample was examined at several temperatures.

FIGURE 4-8

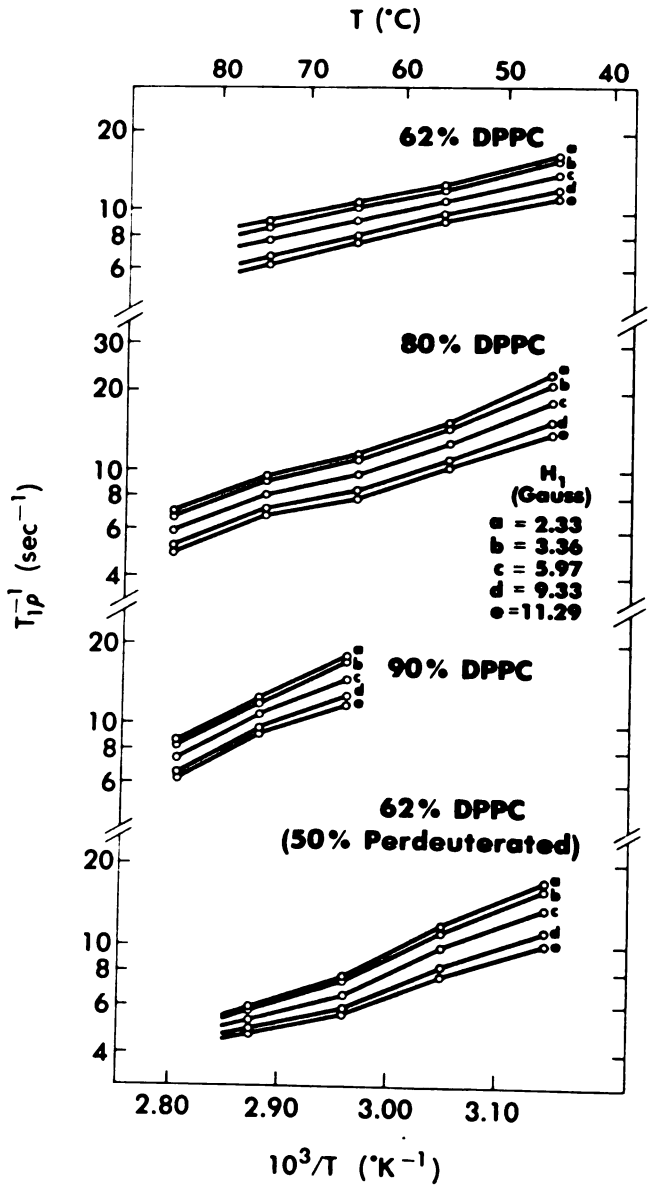

Figure 4-8: Temperature dependence of the proton rotating frame spin-lattice relaxation rate ($1/T_{1\rho}$) showing the variation with spin-locking field strength H_1. The dependence is shown for three normal DPPC samples and one 50% perdeuterated DPPC sample.

calculated from the observed frequency dependence of the rotating frame spin-lattice relaxation rate, are presented in an Arrhenius plot in Figure 4-9 where the behavior may be expressed as (30)

$$D = D_o \exp\left\{\frac{-E_{act}}{R\,T}\right\} \qquad [19]$$

The calculated diffusion data and activation energies are summarized in Table 4-1.

4.10.2. Hydrocarbon chain length. The reciprocal temperature dependence (above T_c for each species) of the diffusion coefficients, calculated from the $\omega_1^{1/2}$ frequency dependence of the rotating frame spin-lattice relaxation rate, for the homologous series of saturated hydrocarbon chain phospholipid dispersions: dilauroylphosphatidylcholine (DLPC), dimyristoylphosphatidylcholine (DMPC), dipalmitoylphosphatidylcholine (DPPC) and distearoylphosphatidylcholine (DSPC) is given in Figure 4-10. The mole ratios of lipid-to-D_2O in the samples were maintained close to 4.3 mole % in order to exclude concentration as a variable factor in the measurement of the diffusion coefficients. The experimentally-derived diffusion coefficients and resulting Arrhenius activation energies are found in Table 4-2.

4.10.3. Unsaturation. To evaluate the effect of unsaturation in the hydrocarbon chains within the bilayer on the rate of lateral diffusion, $T_{1\rho}$ measurements were performed

FIGURE 4-9

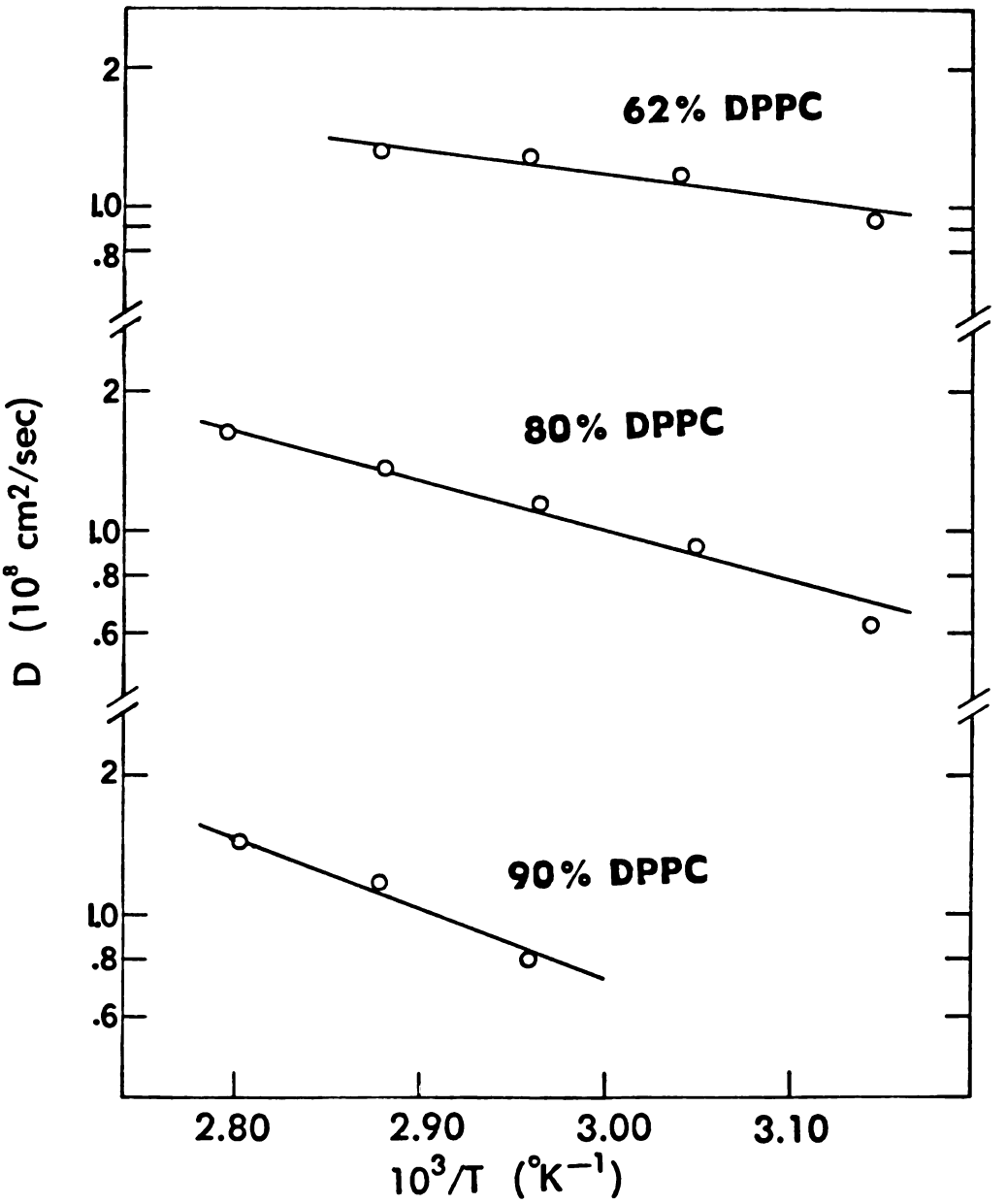

Figure 4-9: Lateral self-diffusion coefficient (D, cm^2/sec) as a function of inverse temperature for 62, 80 and 90% (w/w) dispersed in the lamellar mesophase.

FIGURE 4-10

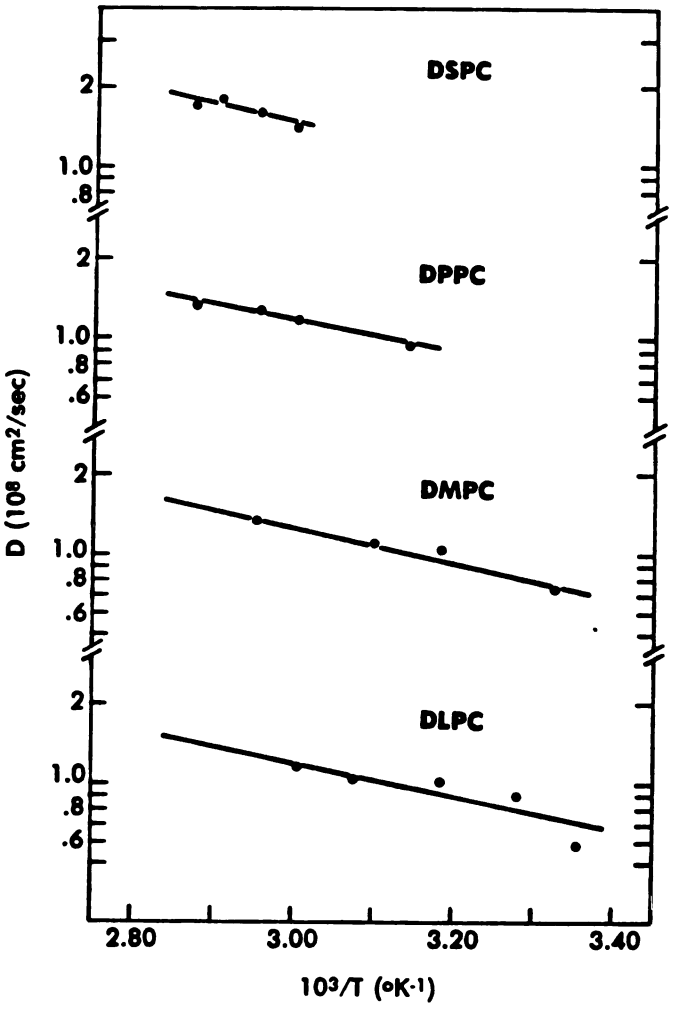

Figure 4-10: Lateral self-diffusion coefficient D as a function of inverse temperature for the homologous series of saturated hydrocarbon chain phosphatidylcholines dispersed in D_2O as the lamellar mesophase: (in weight %) DLPC, 59.29%; DMPC, 59.68%; DPPC, 62.1%; DSPC, 64.62%.

as a function of radiofrequency and temperature on dioleoylphosphatidylcholine (DOPC) which contains a double bond on each of its 18 carbon acyl chains. The diffusion coefficients from these experiments are compared with those for DSPC in Figure 4-11. The activation energies can be compared in Table 4-2.

4.10.4. Headgroup composition. Figure 4-12 provides a comparison of the diffusion coefficients, determined *via* the rotating frame method, for dipalmitoylphosphatidylethanolamine (DPPE) with those found for the 62% DPPC sample. In this case variations in diffusion rates between the two samples (at a given temperature) could arise from the potential changes in headgroup conformation, headgroup hydration or packing arrangement of the phospholipids, as the hydrocarbon chains within the bilayer are identical. Again, the activation energies may be compared in Table 4-2.

4.10.5. Headgroup diffusion-DPPC. Because low resolution pulsed NMR is used in these experiments the NMR signal monitored is the collective proton free induction decay (FID) signal due to all protons present in the phospholipid molecules. The majority of the protons responsible for this NMR signal are attached to the hydrocarbon chains (from 71.9% for DLPC to 79.6% for DSPC). It is therefore of interest to determine the diffusion coefficient for only the headgroup portion of the molecule to verify that the overall molecule is actually moving in the plane of the bilayer at

FIGURE 4-11

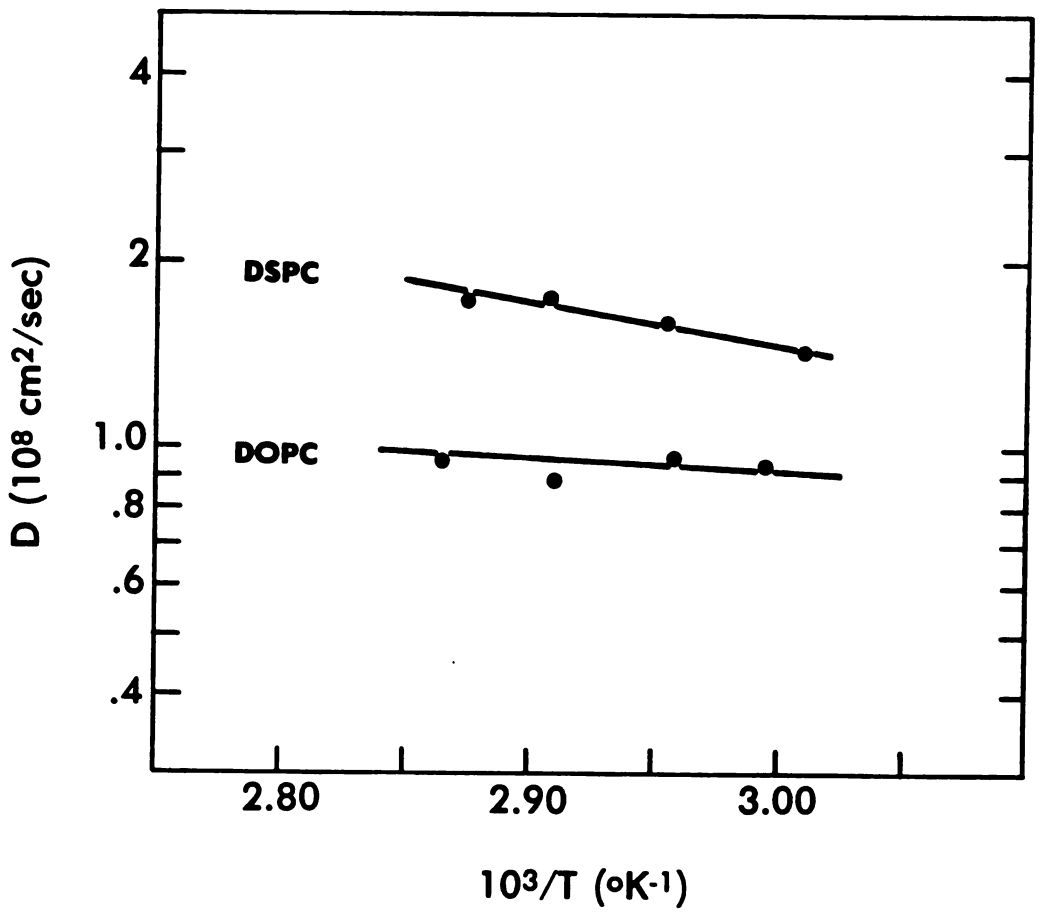

Figure 4-11: Lateral self-diffusion coefficient D as a function of inverse temperature for the 18 carbon saturated hydrocarbon phospholipid DSPC, 64.62% (w/w) and its cis unsaturated analog DOPC, 60.71% (w/w) dispersed in D_2O.

FIGURE 4-12

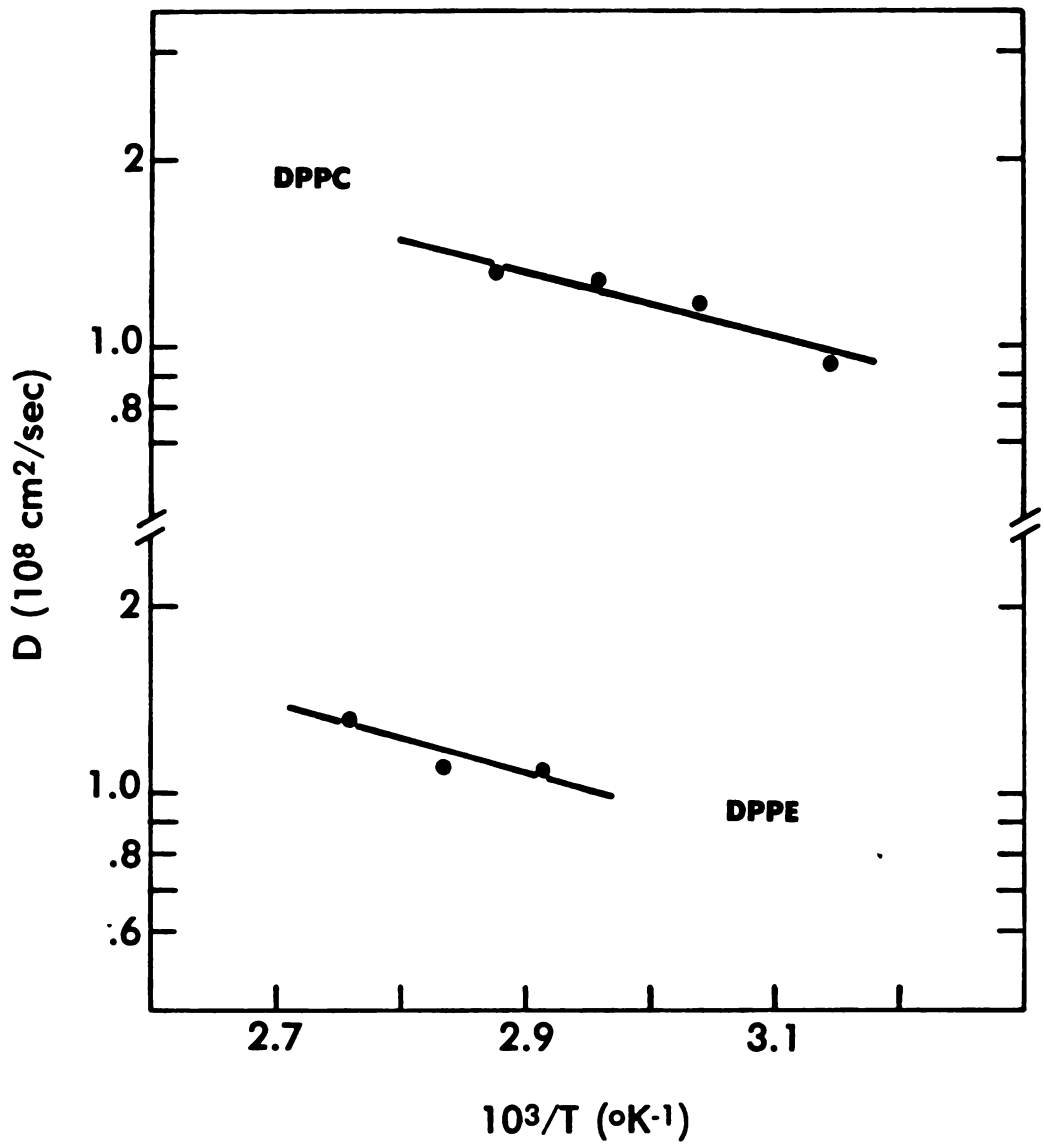

Figure 4-12: Lateral self-diffusion coefficient D as a function of inverse temperature for two types of phospholipid (dispersed in D_2O) with equivalent hydrocarbon chain length but differing hydrophilic portions: DPPC, 62.1% (w/w) and its ethanolamine analog DPPE, 58.7% (w/w).

the rate D as opposed to some collective translational excursions of the hydrocarbon chains. Experiments were performed to determine the diffusion coefficients for a sample in which 100% of the phospholipid DPPC was perdeuterated in the hydrocarbon chains. The resulting diffusion coefficients are shown in relation to those for the fully protonated DPPC sample (with equivalent mole ratio of lipid-to-D_2O) in Figure 4-13. The apparent scatter in the Arrhenius behavior of the deuterated phospholipids' diffusion coefficients gives the calculation of an activation energy no meaning; therefore, a number for the diffusion activation energy is not entered in Table 4-2.

4.10.6. Gel phase diffusion coefficients. Measurement of the diffusion coefficients for phospholipid molecules in the gel phase, i.e., below the gel-to-liquid crystalline phase transition temperature, has eluded most investigative efforts to this date. This certainly has been the case for unsonicated phospholipid dispersions studied with magnetic resonance techniques due to the severe line broadening associated with the solid-like state of these systems in the gel phase. Our technique allows such a study to be undertaken with comparative ease. The diffusion coefficients, determined by the rotating frame method, at temperatures bracketing the phase transition region for DPPC are reported in Figure 4-14, and the activation energies for diffuson above and below the phase transition temperature can be compared

FIGURE 4-13

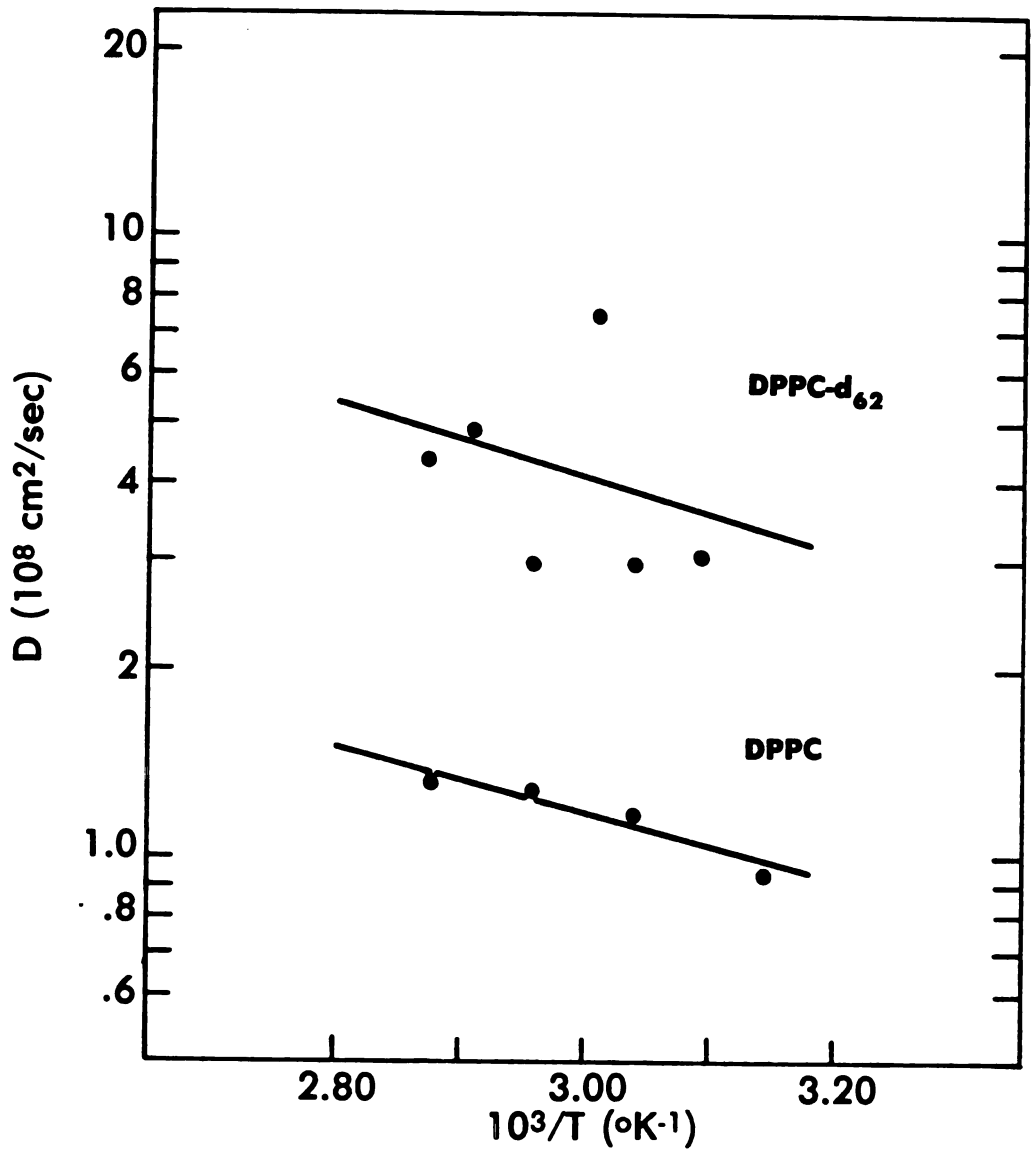

Figure 4-13: Lateral self-diffusion coefficient D as a function of inverse temperature for DPPC, 62.1% (w/w) and DPPC-d_{62}, 65.4% (w/w) dispersed in D_2O, in which the hydrocarbon chains are perdeuterated leaving the headgroup protons as the sole contributing spins for the NMR signal.

FIGURE 4-14

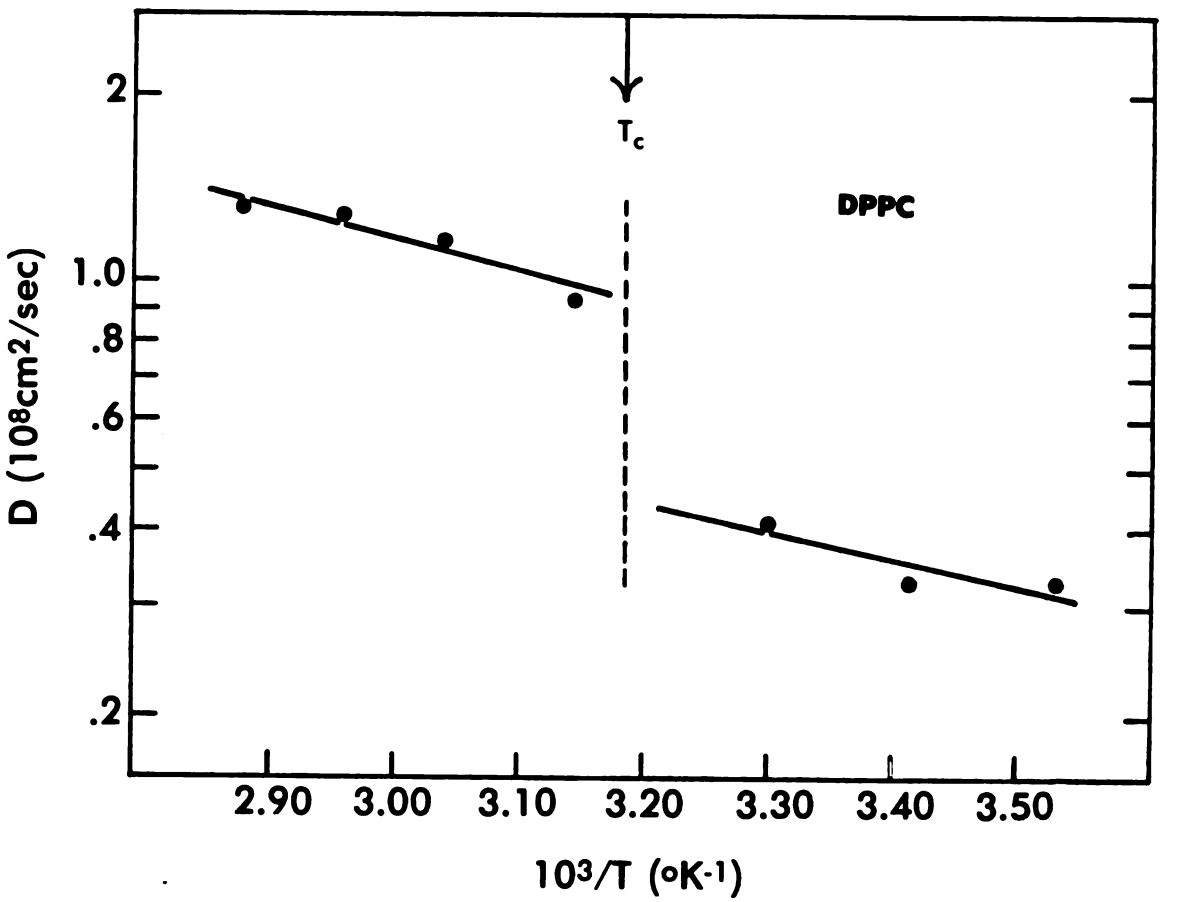

Figure 4-14: Lateral self-diffusion coefficient D as a function of inverse temperature for DPPC, 62.1% (w/w) above the gel-to-liquid crystalline phase transition temperature and DPPC, 62.82% (w/w) below the transition temperature. The results below T_C are one of the few sets of data available for phospholipid diffusion in the gel phase.

in Table 4-2.

4.11. Diffusion in a biological membrane (Retinal rod outer segment membrane): Results.

The ultimate goal for any series of experiments on a model membrane system is to either extrapolate results to or actually obtain results from a natural membrane system. Diffusion studies were made utilizing the rotating frame technique on a sample of bovine rod outer segment (ROS) membranes and on the lipids extracted from these membranes. The resulting diffusion coefficients are shown on an Arrhenius plot in Figure 4-15. This is an attractive system for study as the biochemistry, physiology and chemical composition of the ROS system have been well characterized (78-80). This is an attractive system for study also because it is relatively free of cholesterol, in contrast to most natural membranes.

4.12. Discussion of results.

The lateral diffusion coefficient is a physically measurable parameter representing the overall molecular mobility of phospholipid molecules in a membrane system. The fluidity of a bilayer is more a composite description, than a physical parameter, of the effects from all determinants contributing to the dynamic state of the membrane system. Studies of diffusion coefficients in artificial and natural membranes have proven useful in providing insight

FIGURE 4-15

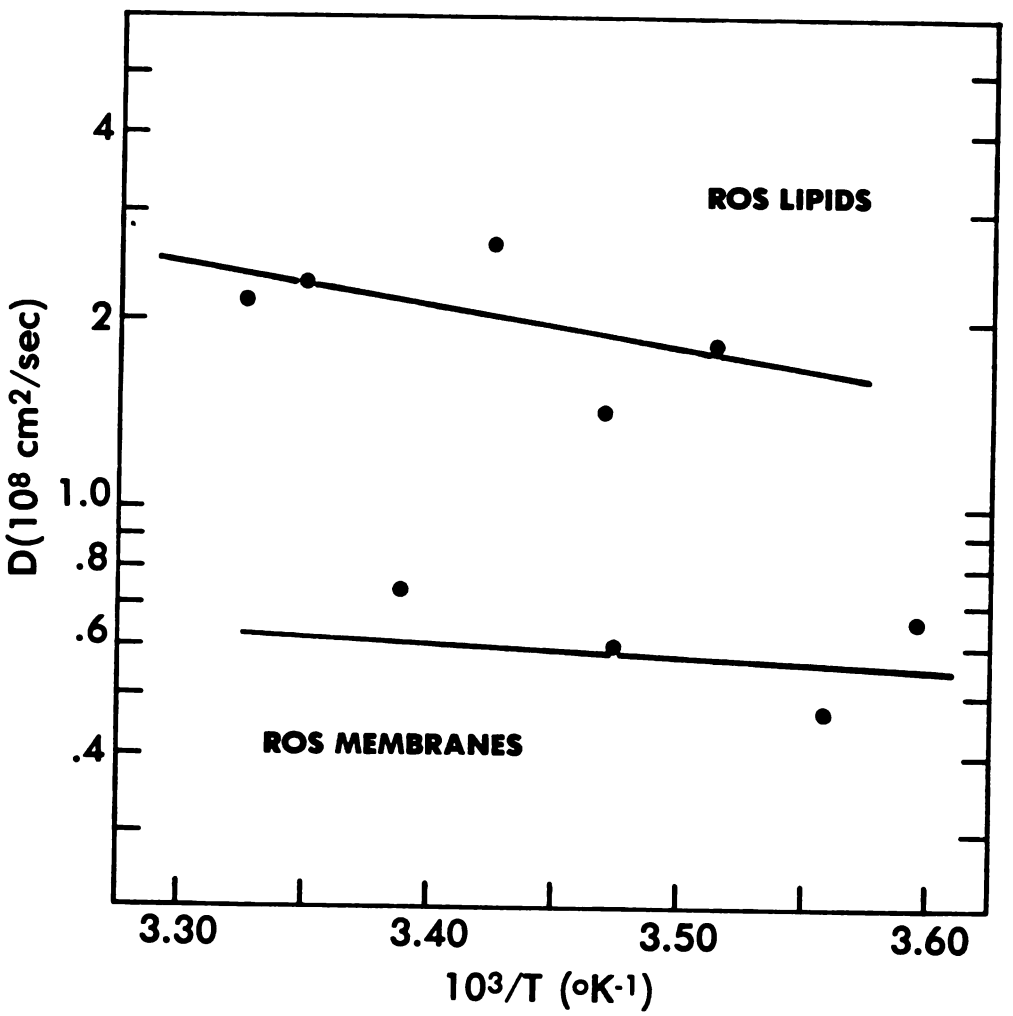

Figure 4-15: Lateral diffusion coefficient D for phospholipids in bovine rod outer segment (ROS) membranes and for the lipids extracted from ROS membranes.

into the dynamics of molecular events contributing to the fluidity of these systems. Diffusion coefficients have been determined for lecithin and other related molecules distributed in natural membrane bilayers and for proteins residing on the surface of cell membranes (18,21,24,77). This information itself may be useful in understanding the mechanisms by which these cell-surface molecules act and allows more detail to be assigned to membrane model theories. There is also, provided that a suitable model is chosen to describe the system's behavior, information contained within the diffusion coefficient pertaining to the microscopic events of translational motions, which yield on the macroscopic level the process of translational diffusion. The basis of the rotating frame spin-lattice relaxation rate technique for obtaining diffusion coefficients, in fact, dwells in the microscopic detail of the diffusion process.

The significance here is that we are able to extract the lateral self-diffusion coefficient directly from the experimental NMR data without making any *a priori* assumptions about molecular geometries or motional time scales. For the most part, diffusion studies by ESR spin-label methods, the usual NMR relaxation time measurements or observation of the fluorescence of optically excited probes involve estimations and assumptions about correlation times, molecular geometries and which electromagnetic interactions dominate the observed spectral results (42).[6] In fact, with

[6] See Chapter 1.

these techniques, the estimated correlation time is used in conjunction with eq [6] of Chapter 1 to estimate the diffusion coefficient. Values calculated for the diffusion coefficient are then only estimates or are limiting values.

With the implementation of our technique for the direct determination of lateral diffusion coefficients in a model membrane system, it is of interest to consider how bilayer fluidity and molecular dynamics are reflected in the diffusion coefficient when physical changes take place within a bilayer. Experiments, from which the results of section 4.4 were derived, were designed in an attempt to evaluate how changes in the lateral diffusion coefficient may relate to changes in bilayer dynamics and to the factors which affect membrane fluidity.

The initial investigations into this matter deal with the temperature dependence and concentration dependence of the diffusion coefficient for DPPC bilayers above the phase transition temperature (see Figures 4-7 through 4-9). Over the temperature range studied, a moderate dependence of the diffusion coefficient on temperature does exist (see Figure 4-9) as one would intuitively expect.

It is also evident that over the temperature range examined the diffusive mechanism does not change as only a single Arrhenius activation energy is obtained from the plots of D <u>vs</u> 1/T (see Table 4-1). The phase transition temperature increases at concentrations above 62% (weight %) (see Figure 2-5) and the air delivery tube to the probe

becomes susceptible to melting at temperatures greater than 95°C. Thus the temperature range for doing experiments on DPPC in the lamellar liquid crystalline phase becomes extremely limited with samples possessing increasing amounts of water. The data does suggest a slight trend towards decreasing diffusion coefficients with increasing concentration of phospholipid, at least for temperatures approaching the phase transition temperature. The small differences between diffusion coefficients at various temperatures is contrasted by the striking changes in the Arrhenius activation energies calculated for the three different concentrations of DPPC (see Table 4-1). The dependence of the activation energy on concentration, more so than the concentration dependence of the diffusion coefficients, indicates that the relative amount of water involved with headgroup hydration in the inter-lamellar channels affects the molecular dynamics to a large extent. This is certainly consistent with the phase transition behavior shown in Figure 2-5. As the amount of solvent around the headgroups decreases (below the point of maximum hydration), the phase transition temperature begins to rise and approaches the first thermotropic phase transition temperature in the limit of 100% phospholipid. Thus as the affect of water, in loosening the gel phase and crystalline solid phase lattice structure by weakening the intermolecular forces, is reflected in the transition temperature behavior, it is reflected as well in one of the parameters associated with

molecular dynamics. The degree of hydration appears then to determine the height of the potential energy barrier which must be overcome for a diffusive jump to occur. The results imply that this effect is large (for concentrations involving amounts of water less than or equal to the amount of water at maximum hydration) while, once the diffusive jump occurs, the extent of that jump varies only slightly as a function of concentration.

The results of the diffusion experiments for the homologous series of saturated hydrocarbon chain phosphatidylcholines as shown in Figure 4-10 and Table 4-2 indicate that hydrocarbon chain length is relatively unimportant in terms of translational molecular dynamics (at least over the range of chain lengths studied, C_{12}-C_{18}). The diffusion coefficients at any given temperature all agree within a factor of 1.5 for the series. The activation energies for diffusion also appear to be in very close agreement, the one exception being the activation energy found for the 4.3 mole % DPPC sample. The disparity of 600 cal (about 20%) between the value reported and that which would be anticipated from the results for DLPC, DMPC and DSPC, i.e., approximately 3 kcal, is a little too large to be completely attributed to experimental error. The exact source of this deviation is not clear. Even if an activation energy of about 3 kcal is assumed for the 4.3 mole % DPPC sample, this value would still indicate an appreciable concentration dependence of the activation energies as observed in the DPPC experiments.

The chain length apparently affects only the phase transition temperature and neither the diffusion coefficient nor the activation energy for diffusion. In view of the concentration studies discussed above, the phase transition differences must be a hydrocarbon region phenomenon. The increase in T_C with each additional pair of methylene groups in the hydrocarbon chains indeed acknowledges the requirement for additional thermal energy in order to cross the gel-to-liquid crystalline phase boundary. Once in the liquid crystalline state the phospholipid molecules become "unaware" of their chain length and the diffusive jumps occur with the same dependence on temperature, each jump producing the same result (at a given temperature) for each of the molecules in the series DLPC, DMPC, DPPC and DSPC.

No significant variations are observed on comparing the diffusion coefficients and activation energies determined for DPPC and DPPE (see Figure 4-12 and Table 4-2). The diffusion coefficients agree (at a given temperature) to within a factor of 1.5 and the activation energies for diffusion are nearly the same. Again in this case, thermodynamic considerations are of interest as opposed to parameters describing the molecular dynamics of the systems being compared, i.e., T_C is 22° higher for DPPE than for DPPC whereas the diffusion rates and diffusion activation energies are quite similar for the two systems (at the concentration and temperatures studied). Because the hydrocarbon chains are of equal length, the transition temperature must be a head-

group or inter-lamellar channel phenomenon due either to the manner in which the hydrophilic portion of the molecules pack together at the surface of the bilayers or to electrostatic interactions and the particular way in which the hydration "dilutes" these intermolecular forces.

Unfortunately, the information gained from these diffusion experiments is not sufficient to differentiate the importance of these effects. It can be speculated, however, that stronger electrostatic interactions due to different hydration mechanisms are not the principal cause of the higher transition temperature because, once above T_C, the activation energy for DPPE is about the same as with the 4.3 mole % DPPC sample. From the hydration dependence of the diffusion rate and diffusion activation energy, it may be inferred that the potential energy barriers, which must be overcome for a diffusive jump to occur, are equivalent for the two samples DPPC and DPPE (of equivalent concentration). Consequently, the headgroups' intermolecular forces as modified by the state of hydration must be equivalent or variations, if any, must be negligible.

The results given in Figure 4-11 and Table 4-2 compare the temperature dependence of the lateral diffusion coefficients and activation energies for diffusion, respectively, for DSPC and its unsaturated analog DOPC. These results are extremely interesting and strikingly peculiar at first glance. In ESR and NMR experiments investigating membrane fluidity or the order parameter corresponding to some region

in the bilayer's hydrocarbon core, unsaturation is found to increase the fluidity and give a decrease in the order parameter when compared to phospholipids with completely saturated lipid chains. Here the diffusion coefficient is observed to be smaller by a factor of 2 for the unsaturated *vs* the saturated phospholipid molecules in a bilayer. The overall entropy is greater within the hydrocarbon region (*i.e.*, increased fluidity and smaller order parameter) but in terms of translational motion the final outcome seems to be a more restricted motion. Accompanying the motional restrictions, however, is a lowering of the potential energy barrier to a diffusive step. Thus the inherent thermal energy required to promote a diffusive step is considerably less for the unsaturated phospholipid DOPC, but once this jump is able to occur the effective "amount" or extent of diffusion has been reduced by the disorder of the system.

The experimental investigation of diffusion with the DPPC sample 100% perdeuterated in the fatty acid chains does not provide a strong case for comparison with the fully protonated DPPC sample. The DPPC-d_{62} diffusion coefficients, representing the diffusion of the polar headgroup (glycerol backbone and phosphocholine group), plotted with those of normal DPPC against reciprocal temperature in Figure 4-13 give an extremely small correlation to a linear relationship. The line in Figure 4-13 is drawn only to illustrate the relative sizes of the diffusion coefficients determined. The diffusion coefficients measured for the headgroup por-

tion of the phospholipid molecule at the interlamellar interface as determined with the rotating frame method range from a factor of 2.3 to an extreme of 6 times greater than the diffusion coefficients determined from the proton NMR signal of the fully protonated molecules. A detailed evaluation of the headgroup diffusion results is not pursued at this time because of the poor data. A more complete NMR study of the headgroup protons is necessary to determine the relative importance of intra- and intermolecular relaxation contributions in order to verify the validity of using eq [4] for calculating the headgroup's diffusion coefficient. This work does not include such a study.

Some of the more exciting aspects of this work lie in the last two sets of experiments to be discussed: diffusion in the gel phase of a model membrane system and diffusion in a biomembrane.

The results which compare the diffusion values for DPPC at temperatures above and below the gel-to-liquid crystalline phase transition are given in Figure 4-14 and in Table 4-2. There have been few reports to date of diffusion coefficients in the gel phase. The results in Figure 4-14 illustrate the applicability of the $T_{1\rho}$ technique to such measurements, which have otherwise proven difficult. Except for the work reported by Cullis (37), the utility of the conventional magnetic resonance techniques used to study diffusion in model membrane systems is diminished due to the residual dipolar line broadening produced in the gel phase.

That diffusion in the gel phase is about an order of magnitude slower than in the liquid crystalline phase is indicated by our results and by a few other investigators (37,81). These measurements are significant. The application of our technique to the gel phase of a model membrane system represents a powerful extension of its applicability. Even though the highly unsaturated natural membrane lipids probably exist in the liquid crystalline state at physiological temperatures, lipid clustering may occur such that homogeneous pools of identical phospholipids are segregated from the bulk lipid phase. Depending upon the chemical composition of the particular phospholipids, this lateral phase separation could result in regions of lipid maintained in the gel phase, i.e., the particular physiological temperature would be greater than the gel-to-liquid crystalline phase transition temperature of the phospholipids within one of these homogenious pools. The rotating frame technique may well prove to be one of the more elegant probes of the potentially significant biological phenomenon of lateral phase separation.

It is somewhat surprising that the activation energy for diffusion in the gel phase is slightly smaller than that calculated for the liquid crystalline phase. It is possible, however, that the greater degree of order in the the hydrocarbon core provides a lesser impedance to each diffusive jump.

As an initial attempt at monitoring the rate of lateral diffusion of phospholipids in a natural membrane, the rotating frame method was applied to bovine rod outer segment membranes. The results from these experiments, given in Figure 4-15, must be understood to be only semi-quantitative at this point as the complexity of the system brings in a multitude of factors to consider in interpreting the results. It should also be pointed out that the integrity of the ROS membranes as used in these experiments is questionable. Freeze-drying can disrupt natural membranes. The final state, of the membrane sample used in these experiments, may actually be more like aggregates of membrane fragments rather than intact membranes. However, monitoring the collective proton FID due to all the protons in the sample, as is done for these experiments, necessitates minimizing the water proton contribution to the FID. Thus, the freeze-drying procedure was unfortunately necessary in order to perform the experiments on the ROS membrane sample. The outcome of these preliminary experiments is none-the-less encouraging. Figure 4-15 demonstrates a definite difference in phospholipid diffusion rate in the whole membrane preparation as opposed to the extracted lipids alone. An interpretation of the change in activation energy calculated, of 2.2 kcal for the whole ROS membrane preparation to 3.1 kcal for the extracted ROS lipids, is not in order since a major portion of the difference could lie in the scatter of the data. The significance of these results is seen to

be in the slower (by a factor of 3) diffusion rate of the lipids in the whole membrane preparation.

The diffusion coefficients for the ROS membrane and membrane extracted lipid samples were calculated using the radiofrequency dependence of the rotating frame spin-lattice relaxation rate and thus eq [4]. The spin density, N, in eq [4] deserves special consideration for the ROS membrane sample. The spin densities of both the ROS membrane and extracted lipid samples were determined as described in section 4.2. Incorporation of a correction factor in the spin density for the ROS sample, in recognition of the presence of protein, would most probably introduce a greater uncertainty into the outcome of the diffusion coefficient calculations than arises from using the uncorrected spin density.

Consideration of two special cases in addition to the results reported in Figure 4-15 should indicate that, in fact, an inherent difference between the diffusion rates of the extracted and membrane lipids exists and does not result as an artifact from using uncorrected spin densities. The spin densities, obtained directly from eq [8] in section 4.2, for the ROS membranes were greater on the average by a factor of 1.8 than those for the extracted lipids. Inspection of eq [4] shows that N is proportional to D as the two thirds power. If the spin density of the lipids in the ROS membrane sample is less than or equal to the density of the extracted lipids, then the resulting diffusion coefficients would be even smaller than those in Figure 4-15 for the ROS

membranes. If the spin density of the ROS membrane lipids is greater by even a factor of 3 than for the extracted lipids, the diffusion rates calculated for the membrane sample would still be less by a factor of at least 1.6. Thus it is evident that the diffusion of the lipids in the membrane sample in the presence of protein is slower by at least a factor of 1.6 than for the extracted lipid sample.

Slower phospholipid diffusion in the intact membrane is not unreasonable. Two supportive arguments may be made in analogy with the reasons suggested for the smaller self-diffusion coefficients of water in protein solutions (30,82). The obstruction effect arises from the large size of the protein in the membrane bilayer with respect to the phospholipids. As the protein constitutes about 60% by weight of the ROS membrane the influence of the protein will be appreciable. In order for diffusion of a phospholipid molecule from point A to point B to take place it may have to circumnavigate one or more protein molecules as opposed to a straight line between A and B for the protein-free extracted lipids. The solvation effect may also impede the diffusional progress of a phospholipid molecule. If a passing phospholipid wanders from the bulk lipid phase into the "boundary layer" of phospholipids surrounding a protein molecule, its motion may be retarded due to lipid-protein interactions. These speculative reasons for slower phospholipid diffusion in the presence of proteins remain to be proven, but these experiments have certainly given evidence

of the applicability of the rotating frame method for diffusion coefficient determination in a biomembrane system. As mentioned earlier, cholesterol is a minor component of the ROS membrane. Cholesterol is therefore probably not instrumental in the observed decrease in the diffusion rates of the ROS membrane sample.

Molecular dynamics have been emphasized in this discussion. The diffusion coefficient is related to the mean time between diffusive jumps (see eq [7] in Chapter 1) or the diffusive jump frequency ν_j:

$$\nu_{jump} = \frac{4D}{\sigma^2} \qquad [20]$$

assuming the phospholipid molecules in the bilayer are arranged in a hexagonal lattice (76,83). As an example of this calculation, mean jump times were calculated for DPPC molecules in the multilamellar dispersions above the phase transition temperature using the estimated value of 8Å for σ (see above) and the experimentally determined diffusion coefficients; the values range from 1.2×10^{-7} sec to 1.7×10^{-7} sec. Thus, the DPPC molecules will be exchanging lattice sites, on the average, at a rate $\geq 5.9 \times 10^{6}$ sec^{-1}.

The investigations and their results reported in this dissertation explore the versatility of a novel new technique for measuring lateral diffusion coefficients in model membrane systems and demonstrate its potential for studying diffusion in biological membranes. Several advantages

accompany the employment of this technique. Diffusion of the phospholipid molecules in a membrane may be studied without the use of potentially perturbing foreign probes (spin-labeled probes for ESR experiments and fluorescent probes for optical spectroscopic investigations) because the naturally abundant spins of the native bilayer constituents act as intrinsic probes (the phospholipid protons in this study). This method is unique, allowing the direct calculation of the diffusion coefficient from the experimental NMR relaxation data. The diffusion coefficients determined *via* the radiofrequency dependence of the rotating frame spin-lattice relaxation rate generally agree very well with those of other investigations (see Chapter 1).

Of particular interest at this stage of development is to apply FT NMR techniques to this experiment. The capability for this will shortly be available in our lab. Successful completion of such experiments should resolve the major shortcoming of the method as currently used, *i.e.*, the isolation of NMR signals from the individual membrane components.

Table 4-1: Sample composition and activation energies for diffusion of DPPC/D_2O dispersions at three different concentrations.

Composition with D_2O			
SAMPLE	(W/W)%	(MOLE)%	$E_{act}\left[\frac{kcal}{mole}\right]$
DPPC A	62.1	4.3	2.4
DPPC B	80.0	10.0	4.9
DPPC C	90.0	19.7	7.1

Table 4-2: Sample composition and activation energies for diffusion from experiments investigating the effects of chain length, unsaturation and headgroup composition. Values are also given for diffusion in the gel phase.

Composition with D_2O			
SAMPLE	**(W/W)%**	**(MOLE)%**	$E_{act}\left[\frac{kcal}{mole}\right]$
DLPC	59.3	4.4	2.9
DMPC	59.7	4.2	3.1
DPPC A	62.1	4.3	2.4
DSPC	64.6	4.3	3.1
DOPC	60.7	3.8	0.9
DPPE	58.7	4.0	2.6
DPPC-d_{62}	65.4	4.5	
DPPC (gel)	62.8	4.4	1.9

REFERENCES

(1) Gorter, E., and Grendel, F. (1925), J. Exp. Med. 41, 439.

(2) Danielli, J. F., and Davson, H. (1935), J. Cell. Comp. Physiol. 5, 495.

(3) Singer, S. J., and Nicolson, G. L. (1972), Science 175, 720.

(4) Weissmann, G., and Claiborne, R., ed. (1975), in Cell Membranes; Biochemistry, Cell Biology and Pathology, New York, N. Y., HP Publishing Co., Inc., p 37.

(5) Levine, Y. K., and Wilkins, M. H. F. (1971), Nature New Biology 230, 72.

(6) Wilkins, M. H. F., Blaurock, A. E., and Engleman, D. M. (1971), Nature New Biology 230, 72.

(7) Schoenborn, B. P. (1976), Biochim. Biophys. Acta 457, 41.

(8) Schoenborn, B. P. (1977), Chem. and Eng. News Jan. 24, 31.

(9) Reinert, J. C., and Steim, J. M. (1970), Science 168, 1580.

(10) Hubbell, W. L., and McConnell, H. M. (1971), J. Am.

Chem. Soc. 93 (2), 314.

(11) Tanford, C. (1973), in The Hydrophibic Effect, New York, N. Y., Wiley, p 169.

(12) De Gier, J., Mandersloot, J. G., and Van Deenan, L. L. M. (1968), Biochim. Biophys. Acta 150, 666.

(13) Vanderkooi, J. M., Landesberg, R., Selick II, H., and McDonald, G. G. (1977), Biochim. Biophys. Acta 464, 1.

(14) Hubbell, W. L., and McConnell, H. M. (1968), Proc. Natl. Acad. Sci. U. S. 61, 12.

(15) Johnson, F. H., and Flagler, E. A. (1950), Science 112, 91.

(16) Johnson, S. M., and Miller, K. W. (1970), Nature 228, 75.

(17) Seeman, P., and Roth, S. (1972), Biochim. Biophys. Acta 255, 171.

(18) Lee, A. G., Birdsall, N. J. M., and Metcalfe, J. C. (1973), Biochemistry 12 (8), 1650.

(19) Wade, C. G. (1977), Personal communication.

(20) Träuble, H., and Sackmann, E. (1972), J. Am. Chem. Soc. 94 (13), 4499.

(21) Devaux, P., and McConnell, H. M. (1972), J. Am.

Chem. Soc. 94 (13), 4475.

(22) Scandella, C. J., Devaux, P., and McConnell, H. M. (1972), Proc. Natl. Acad. Sci. U. S. 69 (8), 2056.

(23) Fahey, P. F., Koppel, D. E., Barak, L. S., Wolf, D. E., Elson, E. L., and Webb, W. W. (1977), Science 195, 305.

(24) Schlessinger, J., Axelrod, D., Koppel, D. E., Webb, W. W., and Elson, E. L. (1977), Science 195, 307.

(25) Wu, E., Jacobson, K., and Papahadjopoulos, D. (1977), Biochemistry 16 (17), 3936.

(26) Devaux, P., and McConnell, H. M. (1973), Annals of the New York Academy of Science 222, 489.

(27) Abragam, A. (1961), in The Principles of Nuclear Magnetism, Oxford, Clarendon Press.

(28) Carrington, A., and McLachlan, A. D. (1967), in Introduction to Magnetic Resonance, New York, N. Y., Harper and Row.

(29) Slichter, C. P. (1963), in Principles of Magnetic Resonance, New York, N. Y., Harper and Row.

(30) James, T. L. (1975), in Nuclear Magnetic Resonance in Biochemistry, New York, N. Y., Academic Press.

(31) Bloembergen, N., Purcell, E. M., and Pound, R. V. (1948), Phys. Rev. 73 (7), 679.

(32) Kornberg, R. D., and McConnell, H. M. (1971), Proc. Natl. Acad. Sci. U. S. 68 (10), 2564.

(33) Fisher, R. W., and James, T. L. (1978), Biochemistry 17 (7), 1177.

(34) Torrey, H. C. (1953), Phys. Rev. 22, 962.

(35) Kruger, G. J. (1969), Z. Naturforsch 24A, 560.

(36) Horwitz, A. F., Horsley, W. J., and Klein, M. P. (1972), Proc. Natl. Acad. Sci. U. S. 69, 590.

(37) Cullis, P. R. (1976), FEBS LETT. 70 (1), 223.

(38) McDonald, G. G., and Vanderkooi, J. M. (1975), Biochemistry 14 (10), 2125.

(39) Lindblom, G., Wennerstrom, H., Arvidson, G., and Lindman, B. (1976), Biophysical Journal 16, 1287.

(40) Lindblom, G., and Wennerström, H. (1977), Biophysical Chemistry 6, 167.

(41) Azzi, A. (1975), Quarterly Reviews of Biophysics 8 (2), 237.

(42) Edidin, M. (1974), Ann. Rev. Biophys. Bioeng. 3, 179.

(43) Seelig, A., and Seelig, J. (1974), Biochemistry 13 (23), 4839.

(44) Burnett, L. J., and Harmon, J. F. (1972), J. Chem. Phys. 57, 1293.

(45) Brown, G., Doane, J., and Neff, V. (1971), in A Review of the Structure and Physical Properties of Liquid Crystals, CRC Press.

(46) Shipley, G. G. (1974), in Fundamentals of Lipid Chemistry, Burton, R. M., and Guerra, F. C., Ed., Webster Groves, Mo., BI-Science International, Chapter 24.

(47) Saupe, A. (1969), in Liquid Crystals 2, Part I, Brown, G. H., Ed., New York, N. Y., Gordon and Breach Science Publishers, p 59 ff.

(48) Luzzati, V., and Husson, F. (1962), J. Cell Biol. 12, 207.

(49) Small, D. M. (1967), J. Lipid Res. 8, 551.

(50) Luzzati, V., and Tardieu, A. (1974), Ann. Rev. Phys. Chem. 25, 79.

(51) Lawrence, A. S. C. (1969), in Liquid Crystals 2, Part I, Brown, G. H., Ed., New York, N. Y., Gordon and Breach Science Publishers, p 1 ff.

(52) Reiss-Husson, F. (1967), J. Mol. Biol. 25, 363.

(53) Chapman, D. (1974), Pure Appl. Chem. 38, 59.

(54) Chapman, D., (1973), in Form and Function of Phospholipids, Ansell, G. B., Hawthorne, J. N., and Dawson, R. M. C., Ed., New York, N. Y., Elsevier Scientific Publishing Co., Chapter 6.

(55) Chapman, D. (1968), in Membrane Models and the Formation of Biological Membranes, Bolis, L., and Pethica, B. A., Ed., New York, N. Y., John Wiley and Sons, Inc.

(56) Chapman, D., Williams, R. M., and Ladbrooke, B. D. (1967), Chem. Phys. Lipids 1, 445.

(57) Phillips, M. C., Williams, R. M, and Chapman, D. (1969), Chem. Phys. Lipids 3, 234.

(58) Sackman, H., and Demus, D. (1966), Mol. Cryst. 2, 81.

(59) Rand, R. P., Chapman, D., and Larsson, K. (1975), Biophys. J. 15, 1117.

(60) Brown, M. F., and Seelig, J. (1978), Biochemistry 17, 381.

(61) Papahadjopoulos, D. (1973), in Form and Function of Phospholipids, Ansell, G. B., Hawthorne, J. N., and Dawson, R. M. C., Ed., New York,N. Y., Elsevier Scientific Publishing Co., Chapter 7.

(62) Seiter, C. H. A., and Chan, S. I. (1973), J. Am.

Chem. Soc. 95, 7541.

(63) Lichtenberg, D., Petersen, N. O., Girardet, J., Kainosho, M., Kroon, P. A., Seiter, C. H. A., Feigenson, G. W., and Chan, S. I. (1975), Biochim. Biophys. Acta 382, 10.

(64) Harmon, J. F., and Muller, B. H. (1969), Phys. Rev. 182(2), 400.

(65) Solomon, I. (1959), C. R. Acad. Sci. 248, 92.

(66) Ailion, D. C. (1971), in Advances in Magnetic Resonance, Vol. 5, Waugh, J. S., Ed., New York, N. Y., Academic Press, p 177 ff.

(67) Harmon, J. F., Personal Communication.

(68) Veksli, Z., Salsbury, N. J., and Chapman, D. (1969), Biochim. Biophys. Acta 183, 434.

(69) Morgan, L. O., and Nolle, A. W. (1959), J. Chem. Phys. 31 (2), 365.

(70) Welsby, V. G. (1950), in Theory and Design of Inductive Coils, London, MacDonald Pub. Co.

(71) Hoult, D. I., and Richards, R. E. (1976), J. Mag. Res. 24, 71.

(72) Sheetz, M. P., and Chan, S. I. (1972), Biochemistry 11 (24), 4573.

(73) Jones, G. P. (1966), Phys. Rev. 148, 332.

(74) Thompson, R. T. and Kydon, D. W. (1974), J. Chem. Phys. 61, 1813.

(75) Valic, M. I., McKay, A., and Bloom, M. (1976), Int. Congr. Magn. Reson. Biol. Syst., 7th, St. Jovite, Sept. 19-24.

(76) Levine, Y. K., Bailey, A. I., and Wilkins, M. H. F. (1968), Nature (London) 220, 577.

(77) Stier, A., and Sackmann, E. (1973), Biochim. Biophys. Acta 311, 400.

(78) Korenbrot, J. I., and Montal, M. (1976), in The Enzymes of Biological Membranes vol. 4, Martinosi, A., Ed., New York, N. Y., Plenum Publishing Corporation, p 365 ff.

(79) Brown, M. F., Miljanich, G. P., and Dratz, E. A. (1977), Proc. Natl. Acad. Sci. USA 74 (5), 1978.

(80) Brown, M. F., Miljanich, G. P., and Dratz, E. A. (1977), Biochemistry 16 (2), 2640.

(81) Silva-Crawford, M., Gerstein, B. C., Kuo, A., and Wade, C. G. (1979), Poster B-26, 20 th Experimental NMR Conference, Asilomar, California, February 19-23.

(82) Wang, J. H. (1954), J. Am. Chem. Soc. 76, 4755.

(83) Devaux, P., Scandella, C. J., and McConnell, H. M. (1973), J. Magn. Reson. 9, 474.